ANNUAL REPORT

SUBMITTED TO: National Aeronautics and Space Administration Langley Research Center Hampton, Virginia 23665

INSTITUTION: Department of Physics and Engineering Studies Hampton Institute Hampton, Virginia 23668

TITLE OF GRANT: Local Effects of Partly-Cloudy Skies on Solar and Emitted Radiation

GRANT NUMBER: NAG 1-87

PERIOD COVERED BY THIS REPORT: August 1, 1981 to July 31, 1982

CO-PRINCIPAL INVESTIGATORS: D. A. Whitney
D. D. Venable

RESEARCH ASSOCIATE: T. J. Griffin

RESEARCH ASSISTANT: J. R. Foreman

(NASA-CR-169272) LOCAL EFFECTS OF PARTLY-CLOUDY SKIES ON SOLAR AND EMITTED RADIATION Annual Report, 1 Aug. 1981 - 31 Jul. 1982 (Hampton Inst.) 100 p HC A05/MF A01 CSCL 04A G3/46

N82-31849

Unclas 27772

LOCAL EFFECTS OF PARTLY-CLOUDY SKIES ON SOLAR AND EMITTED RADIATIONS

D. A. Whitney
T. J. Griffin
Department of Physics and
Engineering Studies

ABSTRACT

The second year of the proposed three year research project has now elapsed. The computer automated data acquisition system for atmospheric emittance, and global solar, downwelled diffuse solar, and direct solar irradiances are now fully operational. Hourly-integrated global solar and atmospheric emitted radiances have been measured continuously from February 1981 and hourly-integrated diffuse solar and direct solar irradiances have been measured continuously from October 1981. One-minute integrated data are available for each of these components from February 1982. All Phase II objectives related to the data acquisition system have been attained. The results of the correlation of global insolation with fractional cloud cover for the first year's data set have been completed. A theoretical model has been developed for correlation of satellite radiometric data with insolation measurements at the ground. A February data set, composed of one-minute integrated global insolation and direct solar irradiance, cloud cover fractions, meteorological data from nearby weather stations, and GOES East satellite radiometric data, has been collected to test the model and develop the cloud dependence for the local measurement site.

TABLE OF CONTENTS

INTRODUCTION

A solar energy measurement station was established at Hampton Institute, February 15, 1981. Routine measurements are being made of global, diffuse, and direct solar irradiances and of atmospheric emittance. Data acquisition was computer automated in February 1982 and, since then, one-minute integrated radiometric data, as well as one-hour integrated data, have been recorded.

Work has continued on the correlation of global insolation with cloud cover fractions using the ARL model. The results for the first complete year of data are discussed in part III-C of this report. A theoretical model has been developed and a data set has been accumulated to test this model which is used to estimate global insolation from satellite radiometric data. Detailed information about the model is provided in section IV of this report.

I. SOLAR RADIATION MEASUREMENT PROGRAM

An observation platform for solar and atmospheric radiation measurements was established on the roof of Turner Hall (latitude 37.02°N, longitude 76.34°W, and elevation 24 meters) February 15, 1981. A radio tower and a smokestack are the only two obstructions greater than ten degrees above the horizon. Routine measurements are made of global solar irradiance, diffuse solar irradiance, direct solar irradiance, and atmospheric emittance. Information (Griffin, 1982) about the solar radiation measurement program was presented at the April 20-23, 1982 meeting of the Virginia Academy of Science held in Blacksburg, VA. The Abstract of the presentation by T. J. Griffin is attached as Appendix I. A summary of the solar and atmospheric data available at the time of this report is provided in TABLE I.

A. Instrumentation

Since detailed descriptions of the radiometric instrumentation are available in the first Annual Report (Whitney, 1981) for this grant, only a summary of our measurement capabilities is presented here. The global solar irradiance on a horizontal surface is measured by an Eppley Precision Spectral Pyranometer (PSP) with a hemispherical WG7 Schott glass dome. Diffuse solar irradiance on a horizontal surface is measured by an Eppley PSP with a WG7 dome that is mounted on an Eppley Solar Tracker and Occulting Disk System. Direct solar irradiance is measured by an Eppley Normal Incidence Pyrheliometer (NIP) mounted on a Solar Tracker. An Eppley Hickey-Frieden Absolute Cavity Pyrheliometer is used to calibrate the NIP regularly. Atmospheric emittance is measured with an Eppley Precision Infrared Radiometer (PIR). In addition, turbidity (Volz, 1974) measurements are made approximately hourly for clear sky conditions using a Volz Sunphotometer.

The all-sky camera system was modified in order to allow computer activation of the camera. The Aetna fisheye adaptor lens and previous Ricoh XR-2 lens system were mounted on a Pentex ME-II camera body with an electronic shutter and an autowind system. The camera is mounted on an Eppley Shadow Band Stand and aimed at the zenith in order to eliminate the need for frequent adjustment of the sunshade. A clock and a date card are placed on the inside face of the shadow band to document the time of day and date that each photograph is taken. Whole-sky photographs (color slides) are taken every one-half hour on weekdays when clouds are present without precipitation. Color slides are used in order to aid in the distinction between clear sky patches and dark cloud bottoms. The image of the sky is projected directly onto an analysis grid to obtain the fractional cloud cover. Processing and analysis times for whole-sky photographs have been greatly reduced from the previous black-and-white enlargement method.

The wavelength range of each of these instruments is listed in TABLE II. Information about the measurement frequency and about the time periods that insolation data are available is presented in TABLE I.

B. Calibration

Each radiometer was calibrated prior to delivery by the manufacturer. Subsequent calibrations have been performed by comparison to secondary or primary standards at Hampton Institute or at Eppley Laboratory. The NIP was calibrated by comparison to the Hickey-Frieden Absolute Cavity Pyrheliometer which is considered to be a primary standard. The pyrgeometer (PIR) and the older pyranometer (PSP # 20022F3) were recently recalibrated at Eppley Laboratory. The other pyranometer was then recalibrated by comparison with the calibrated pyranometer by operating side-by-side for a period of two days and comparing the two-day integrated global irradiance totals. Calibration data are presented in TABLE III by listing each instrument, the date and site of

each calibration, the sensitivity factor, and the percent change in each instrument's sensitivity factor. Comparisons between the two pyranometers indicate a consistent difference of about one percent which is within the two percent accuracy of each instrument. The rather large change in sensitivity of the older instrument implies either that both instruments have changed sensitivity at the same rate, or that an error exists in the 8-July-82 calibration. Discussions with Eppley Laboratory about this matter are currently being pursued and correction factors for each instrument will be calculated for each month of operation since the sensitivity factors for these two pyranometers apparently changed by more than two percent. A change in calibration standards at Eppley Laboratory in October 1981 accounts for 2.5% of the sensitivity factor changes. The second pyranometer is being sent back to Eppley Laboratory for recalibration to verify this apparent change in sensitivity factors.

The recorder systems were calibrated at least every six months by using a stable millivolt source and adjusting the integrator and strip chart recorder gains to give the proper readings. The maximum adjustment made for any of the integrators has been 0.4% while larger adjustments were occasionally needed for the recorders. The radiometric data are obtained from the integrator LED display BCD panels and are only rarely supplemented from the strip chart recorder trace.

The Volz Sunphotometer is calibrated by checking for linearity of the sensor on a Langley Plot of readings versus air mass.

C. Meteorological Data

Standard hourly meteorological observations taken at nearby Langley Air Force Base (LAFB) are picked up on a monthly basis from Detachement 7, Third Weather Squadron. These data include information about cloud height, cloud type, fractional sky cover, precipitation, sea level pressure, and temperature. These data are supplemented by whole-sky photographs and visual cloud obser-

vations at Hampton Institute. Additional meteorological data and ozone data are purchased from the National Climatic Center archives in Asheville, North Carolina and The World Ozone Center, Environment Canada, Toronto, Canada for use in the data analysis.

D. Data Handling and Quality Control

A data storage procedure for the radiation data has been devised to efficiently handle the data and ensure quality control. First, the integrated radiometric data and times are stored on a Tektronix 4051 microcomputer's internal magnetic tape unit. Then on a weekly basis these raw data files are transferred via computer hookup from the Tektronix 4051 to the PDP 11/34 minicomputer where the data are permanently stored on 1600 bpi magnetic tape. All preliminary processing is done on the Tektronix 4051, while data analysis routines and application programs are performed on the PDP 11/34 system. The data are examined for errors by a computer program that locates the gaps in the data and identifies errors to be corrected.

The automated data acquisition system for global and direct solar irradiances was fully operational February 1, 1982, and since then, integrated radiometric data for one-minute intervals have been obtained directly from the Eppley integrators and stored on magnetic tape. Specific data handling procedures and quality control for these data are discussed in more detail in the next section of this report.

Prior to the installation of the automated data acquisition system, only one-hour integrated measurements were recorded on magnetic tape. Printed data from the integrators were scanned on a daily basis for missing or problem data and incorrect timing caused by power failures or other electrical and mechanical malfunctions. Missing data were supplemented by the strip chart record when available. On a weekly basis, these data were manually entered into the Tektronix 4051 microcomputer, inspected for operator errors, and then transferred to the PDP 11/34 data storage tape.

II. AUTOMATED DATA ACQUISITION SYSTEM

One of the major objectives of the second year of this research project was to develop and implement an automated data acquisition system. This system reduces the manpower requirements, and the number of operator induced errors, involved with data transferral from the integrator-recording system to final permanent magnetic tape storage. The hardware requirements, operating procedures, features, and performance of the system are discussed below.

A. System Overview

The automated data acquisition system connects the radiometric sensor-integrator recording system with the microcomputer I/O capabilities via an interface box. The microcomputer reads the integrated radiometric values from the BCD interface panels at a preset time interval and records these data on the internal magnetic tape unit. Whole-sky photographs are triggered by computer command at preset times and a record of time and picture number is recorded on the magnetic tape. Integrated atmospheric emittance, and global, direct, and diffuse solar irradiances are measured at one-minute intervals from 0400 EST to 2000 EST and at ten-minute intervals for the rest of the night. The data for each month are transferred to separate 1600 bpi magnetic tape for permanent storage.

B. System Description

The data acquisition system can be separated into three subsystems:

(1) the radiometric sensor-integrator system;

(2) the integrated data sampling and recording system; and

(3) the data storage system.

A flow chart of the data acquisition system is presented in Figure 1. The radiometric sensor-integrator system is located at the top half of the chart and includes the following five components:

(1) the Eppley radiometers;

(2) the Eppley integrators that sum the instantaneous readings from the radiometers;

(3) the Digitec printers that provide a hard copy printout of one-hour radiance values;

(4) the X-Y strip chart recorders that provide a hard copy of instantaneous radiances; and,

(5) the camera system that takes the whole-sky photographs.

The integrated data sampling and recording system located at the lower left-hand side of the chart includes:

(1) the integrator signals that are provided at the BCD interface on the Eppley integrators;

(2) the interface box that centralizes the data for computer access;

(3) the ROMs that interface the BCD data to the Tektronix 4051;

(4) the Tektronix 4051 microcomputer that reads the ROMs and activates the camera photocounter; and,

(5) the magnetic tape cartridge where the computer stores the data.

The data storage system is located at the lower right-hand side of the chart and consists of three components:

(1) another Tektronix 4051 microcomputer with a RS232 interface that acts as a link between the PDP minicomputer and the internal tape of the Tektronix computer;

(2) the PDP 11/34 minicomputer system that reads the data from the Tektronix 4051; and

(3) the 1600 bpi, 9 track magnetic tape for permanent storage of the data.

The hardware used in the integrated data acquisition and storage systems are listed in TABLE IV along with two other devices that were used in the development and testing of the interface box and software programs. Detailed information about the operation of these devices and about the construction of the interface box is kept in a documentation file in the Solar Energy Measurement Laboratory.

C. Operating Procedure

The data acquisition system operates on the Tektronix 4051 microcomputer using the computer program SOLAUTO written in BASIC by D. D. Venable. The program works by comparison of the time provided by the Real Time Clock ROM

Pack with times that are calculated from fixed time intervals entered into the program. At the proper times the computer reads each ROM for the radiometric data, or activates the camera shutter and autowind system. A flow chart for the SOLAUTO program is presented in Figure 2 in order to represent the logic used in this part of the program. A copy of the program listing is kept in the documentation file in the Solar Energy Measurement Laboratory.

The correct time, date, selected sampling times for the radiometric data and for camera activation, and also, user messages can be entered into the computer by using the User Defined Keys (UDK) on the computer. The radiometric data are recorded on the magnetic tape in 72 character records. The first two-digit flag (Ø#) of the data record indicates the type of data string using: Ø1 for radiometric data, Ø2 for a photograph record, Ø3 for a user message, and Ø4 for a system message. The next characters indicate the day of the week (three letter abbreviation) separated by two spaces from the date in the form: day-month-year (DD-MMM-YY). The date is represented by two digits each for the day and for the year, and by the three letter abbreviation for the month. The next set of numbers (HH:MM:SS) in the data string are the time (EST) represented by two digits each for the hour, minute, and second, and the remaining characters are either a message or data. A radiometric data record has the form:

Ø1, DDD DD-MMM-YY HH:MM:SS, GL#,NNNNN,DF#,NNNNN,IR#,NNNNN,DR#,NNNNN

The radiometric data are recorded as integrated totals starting from zero at midnight using the two letter abbreviation for each radiation component, a single digit activation code (1 for on, Ø for off), and five digits for each reading (NNNNN). Global solar irradiance is abbreviated by GL: diffuse solar by DF: infrared (atmospheric emittance) by IR: and direct solar by DR.

The system is initially operated by loading the SOLAUTO program into the memory of the Tektronix 4051 computer and then inserting the data tape cartridge.

After entering "RUN", the parameters are set to indicate which ROMs should be read, the frequency for sampling data and activating the camera, the proper date and time, and the data storage/display locations. TABLE V lists the program features by identifying the function of each key, while the most frequently used keys are discussed below. UDK 1 - "Note to Tape" is used to make comments about sensor cleaning, tape changes, or other important messages. UDK 2 - "Read ROMs" is used to check the ROM readings by comparison with the LED displays on the integrators. The camera is manually activated by UDK 3 - "Photograph" and is frequently used to check the electronic shutter operation and to verify the photograph number. The photograph or sensor reading time intervals are changed by using UDK 5 - "Intervals" and the Photograph number can be reset or corrected by using UDK 10 - "Photocount". In order to interrupt the operation of any instrument for maintenance or calibration without causing a fatal program error, the corresponding ROM can be turned off (or on) by using UDK 7. Program execution can be stopped completely by using UDK 20 - "Stop" and resumed by using UDK 19 - "Continue". The use of UDK 13 "Status" provides a quick check of the I/O status, sampling rates, photograph numbers, the data, and the time that are currently stored in memory.

In addition, several operations can be performed with the data during the sampling operation. Because of the time required to rewind and read the magnetic tape cartridge, the data strings are internally stored by the 4051 computer when using UDK 15, 16, or 17 in order not to lose any data. The function of UDK 15 - "Tape Dump" is to read the tape and display the data for a certain day, or to list all photograph times, user messages, or system messages. By using UDK 17 - "Graph" a plot of global, direct, infrared, or diffuse irradiances can be obtained on the Tektronix 4051 Graphics Display Screen. New data tape cartridges are installed approximately once a week.

D. System Performance

The performance of the computer automated data acquisition can be measured by calculation of the amount of data lost in comparison with the data recovered on magnetic tape. The performance record of the previous data acquisition system must also be considered since both systems have some of same causes for loss of data. For example, diffuse solar radiometric data are not collected during calibration periods for either pyranometer. Intercomparison of the two pyranometers are made for the horizontal global solar orientation, which means that no diffuse solar data are available during the calibration periods. Electrical storms can interfere with computer program execution and can stop data collection until the system is restored to normal operation. Electrical storms, which also affect the printers and integrators, reset the printer times and the integrator count values, an effect that destroys the printer data during the time period of the storm. The strip chart recorders can be used to retrieve most of the lost data and have been used to obtain hourly integrated data. Mechanical solar tracking failures can destroy the direct or diffuse solar data obtained by either system.

One-hourly integrated data availability is presented by month in the DATA RECOVERY RECORD TABLES (VI-IX) for the full period of the insolation measurement program at Hampton Institute. TABLE X contains the one and ten minute integrated data recovery information specifically related to the automated data acquisition system. The measurement interval for global and direct solar irradiances was set at one-minute starting at 0942 EST February 1, 1982. One-minute integrated data sampling for the diffuse solar and atmospheric emittance began at 2038 EST, March 1, 1982 when the second half of the interface box was completed. On March 13, 1982 the sampling interval at night was changed to ten minutes (from 2000 EST to 0400 EST) in order to reduce computer tape storage requirements. One Tektronix Data Tape Cartridge is used to store approximately six and one-half

(6½) days of insolation data.

Two measures of the performance of the automated data acquisition system are to calculate the average time period between failures and the average length of time lost for each error. These measures are referred to as Meantime to Fail and Downtime per Error, respectively. The Mean Time to Fail can be calculated by dividing the total possible number of data records by the number of failures and by the data record sampling rate, as long as the sampling rate is constant. The Downtime per Error can be calculated by dividing the number of data records lost by the number of errors and by the sampling rate. The results of these measures of performance were reported (Blakey, 1982) at the 39th Joint Annual Meeting of the National Institute of Science and Beta Kappa Chi Scientific Society held in Washington, DC, March 17-20, 1982. Rody Blakey, an undergraduate assistant on this project, used the data obtained during the first month of computer automated data acquisition to calculate the Meantime to Fail and Downtime per Error. The results of his analysis were an average of 8.7 days between failures and an average of 6.7 hours downtime per error. The large downtime per error was caused by the two nightime failures that stopped program execution for several hours until the system could be returned to normal the following working day. (Mr. Blakey received a Third Place Award for his paper in the Mathematics and Computer Science Section of the Meeting and, also, one of two general awards given.) A copy of the abstract of his paper is attached to this report as Appendix II.

III. RADIOMETRIC AND METEOROLOGICAL DATA ANALYSIS

Several types of data analysis have been completed using the radiometric and meteorological data collected at Hampton Institute. The first type of analysis is to present average values for the various measurements in graphical form. A second type of analysis is required to treat the raw turbidity measurements in order to obtain useful parameters such as optical depths and precipitable water. Correlation of data with empirical formulae is a third type of analysis performed. At this time, satellite-derived radiometric data have not been analyzed by any of these methods but are expected to be completed within the next few months. The results of the analysis methods used are discussed below.

A. Radiometric Data Presentation

Diurnal variability in the various solar insolation components are observed by comparison of the average hourly values for afternoons with values for mornings. Average hourly global, diffuse, and direct solar irradiances and atmospheric emittance are plotted for each month from July 1981 through June 1982 in Figure 3 through Figure 14. Diurnal variability is indicated by the lack of symmetry in these graphs. Seasonal variability can be seen by plotting global solar irradiance for clear sky days selected from each season such as is done in Figure 15. Plots can also be made for values averaged over shorter time intervals (one minute to sixty minutes). Five minute integrated values are plotted routinely for each day to verify the computer system data.

B. Turbidity Data Results

The Volz Sunphotometer is used to obtain atmospheric turbidity parameters α and β, the aerosol extinction coefficients or optical depths at 500, 875, and 390 nanometers, and precipitable water concentrations. The instrument operates by generating a dc voltage proportional to the direct normal solar irradiance measured through narrow band transmission filters centered

on 390, 500, 875, and 945 nm. Measurements are made under cloud free sky conditions. Calculations are then required to convert voltages into the turbidity parameters.

Aerosol optical depths at the wavelengths measured are calculated using the following equation from Volz (1974):

$\tau_A = \frac{1}{M} \ln (F I_0/I) - K (\tau_R + \tau_0)$; where,

τ_A = aerosol optical depth,

I_0 = extraterrestrial irradiance at mean polar distance,

I = irradiance measured with the Sunphotometer,

F = correction factor for mean sun-earth distance

M = optical air mass,

τ_R = Rayleigh optical depth,

τ_0 = ozone optical depth, and

K = correction for differing optical path at $M > 2.5$.

Monthly average aerosol extinction coefficients at 390, 500, and 875 nm for the measurement period March 1981 through June 1982 are graphed in Figures 16-18, respectively. Turbidity parameters α and β are calculated from the aerosol extinction coefficients using the Ångström (1961) empirical expression:

$\tau_A (\lambda) = \beta\lambda^{-\alpha}$; where,

λ = the wavelength in microns,

$\tau_A (\lambda)$ = the aerosol optical depth at wavelength λ,

β = Ångström turbidity coefficient, and

α = Ångström wavelength coefficient.

The turbidity coefficient β is a measure of the quantity of aerosol particles in the atmosphere. Large values of β indicates that a high aerosol concentration exists in the local air mass. Small β values indicate a clear air mass with low aerosol concentrations. For the measurement period, the largest clear sky daily average β value was 0.48 obtained on July 28, 1981 when atmospheric conditions were extremely hazy. The smallest daily average

was 0.05, obtained on February 28, 1981.

Figure 19 graphs monthly average β values for the measurement period. The graph shows that local aerosol concentrations of dust, smoke, sea salts, and other particles peak in the midsummer.

The Ångström exponent α is a measure of aerosol size distribution. A large α value indicates small particles dominate the aerosol population, while a small α means that large particles dominate. Ångström states that a typical value for α is 1.3. At Hampton Institute we have obtained a range of daily average α values from 1.73 to - .89, with an average value of 0.72.

Figure 20 plots monthly average values of α and, as shown by the graph, the values are highly variable. This variability may be due to the fact that local aerosol distribution is a function of the type of air mass over the measurement site. Further study into the variations of α will focus on the particle distribution under different air mass conditions.

C. Correlations with Cloud Cover Fractions

An empirical model developed by the Air Resources Laboratory (ARL) of the National Oceanic and Atmospheric Administration was initially selected for correlation of the global solar irradiance data with fractional cloud cover values. This is an established model used by meteorological stations, and is used to correlate hourly average global solar irradiance with opaque cloud cover fractions which makes it particularly compatible with our solar energy and cloud cover measurement program. The results of the correlation can be used for comparison with other measurement sites in order to characterize the measurement site at Hampton Institute.

The major factors that affect the amount of global solar energy received at the ground on a flat surface are solar zenith angle and opaque cloud cover. The ARL empirical equations selected for use with our measurements are:

(1) $SRC = A_0 + A_1 \cos ZA + A_2 \cos^2 ZA + A_3 \cos^3 ZA$, and

(2) $SR = SRC\ (B_0 + B_1\ OPQ + B_2\ OPQ^2 + B_3\ OPQ^3 + B_4\ RN)$

SRC is the solar radiation hourly value for clear sky conditions;

ZA is the zenith angle at the midpoint of each one-hour interval;

OPQ is the average opaque cloud cover fraction; and

RN is a rain term that is equal to one if some form of precipitation is reported, otherwise it is zero.

The coefficients for the first regression equation are calculated separately for mornings, and afternoons, for each month of the year in order to partially account for diurnal and seasonal changes in atmospheric turbidity, water vapor, and other such factors. The first and last partial hours of the day are not included in the regression calculation. The coefficients for the second equation are normally calculated for mornings plus afternoons using a full year of data at a time.

1. Clear Sky ARL Model Results

The clear sky data have to be analyzed before the cloudy sky data can be normalized by the solar zenith angle dependence. Determination of clear sky hours was made using the LAFB cloud observation data set. A plot of hourly values of clear sky global solar for mornings and for afternoons are shown in Figures 21 to 33 for the months of June 1981 through June 1982. The line plotted through the data was obtained by the Marquardt's nonlinear least-squares method (Marquardt, 1963) using Equation 1. The regression coefficients and number of points used in each correlation are listed for each month in TABLE XI. The number of totally clear sky hours was insufficient for meaningful analysis for most months and, therefore, were supplemented with "nearly clear" points for which the cloud cover fraction was less than 0.2 and the strip chart trace showed no indication of clouds. These nearly clear points are added in order to increase the number of points in the data set used in the regression, and to extend the meaningful range of the curve fit to zenith angles for which totally clear sky points are not available. Nearly clear sky data points were selected from hours which were coded as clear at the beginning or end of the

hour, and also from hours which were coded as having low fractions of transparent or semitransparent clouds. In Figure 21 to 33 the clear sky data points are plotted with open circles and the nearly clear sky points with plus signs. Results for the data prior to June 1981 were reported in the first Annual Report (Whitney, 1981)

2. Cloudy Sky ARL Model Results

The regression coefficients for clear sky mornings and for clear sky afternoons, were used in Equation 1 to estimate the clear sky irradiance for each one-hour interval. The cloudy sky data were then normalized and fit to Equation 2 by using the Marquardt's nonlinear least-squares method. The data for mornings and afternoons are plotted for each month from June 1981 to June 1982 in Figures 34 to 46. The cloud cover fractions obtained from whole sky photographs are represented in these plots by plus signs and satellite photoprint-derived fractions are represented by open circles.

The correlation coefficients for each month of combined morning and afternoon data are listed in TABLE XII. The cloud cover fractions used in these correlations are averages of the LAFB visual observations made at the beginning and end of each hour. Coefficients for data sets with more than 230 points, the limiting number of data points in the analysis program, were obtained by calculating the average normalized irradiance for clear sky conditions and for overcast sky with and without precipitation. The first coefficient B_0 was assigned the mean SR/SRC value for clear and nearly clear sky conditions since B_0 is the value of Equation 2 at the point OPQ=0, i. e. for clear sky. The fifth coefficient B_4 was assigned the mean difference between values with precipitation and values without precipitation at total cloud cover, since the rain term RN nearly always equals one for overcast sky conditions (OPQ=1) and is rarely non-zero for partly-cloudy sky conditions.

ARL coefficients for Equation 2 are normally reported for a complete

calendar year of data. The results for the first year of data, March 1981 through February 1982 are presented in TABLE XIII for both the clear-sky and cloudy-sky equations. Since the cloud fractions obtained from the LAFB visual observations were too numerous for the computer program used, the average normalized global irradiance values (SR/SRC) were calculated for each 0.05 cloud fraction step. The mean values and points one standard deviation above and below these means were used to calculate the correlation coefficients. All the data points for partly-cloudy sky with precipitation were also included in the calculation. The correlations were repeated with fractions obtained from satellite photoprints and with the whole sky photograph values using the mean values for clear, overcast without precipitation, and overcast with precipitation for the endpoints. The results are given in TABLE XIII and the data are plotted in Figures 47 and 48.

The large scatter of the data in Figures 47 and 48 imply that the correlation coefficients are not defined well enough to draw many meaningful conclusions. The results for the cloudy sky model are similar to those from other meteorological recording stations along the East Coast but the clear sky coefficients are not. The probable error in each coefficient is calculated in the analysis program used and the errors in A_2 and A_3 for the clear sky data are frequently much larger that the coefficients themselves. Thus a comparison between the measurement site at Hampton Institute with other sites would require a much larger data set before the ARL model could distinguish between sites with similar climates. The scatter in the data indicated that fractional cloud cover and precipitation are not the only parameters that affect hourly global insolation at a given location. Additional factors involving cloud geometry, locations, altitude, and thickness are significant. Perhaps, the method of calculating fractional cloud cover is flawed, and a single fraction for an hour should be calculated from some type of time averaged set of fractions. These fractions should not be just the cloud cover fraction directly

over the site, but rather, the fraction between the site and the sun. Normalized global irradiance is plotted versus whole-sky photo fractions in Figure 49 and versus Satellite photoprint fractions in Figure 50. The error bars indicate the mean values for overcast sky, plus/minus one standard deviation.

The frequency of occurrence for certain average cloud cover fractions is plotted in Figures 51, 52, and 53, from the three different cloud cover fraction sources used in the correlations with the ARL model. There were 2,926 fractions used from the LAFB visual observations, 53 fractions from the satellite photoprint analysis, and 95 fractions from the whole-sky photograph analysis. The 0.05 interval in cloud fraction is the result of averaging two fractions provided in tenths from the LAFB data set, and from rounding the fractions from the other data sets to the nearest 0.05. The actual number of whole-sky photographs is much larger than 95 since only hourly averages were used.

The normal bimodal distribution of cloud cover fractions is indicated in Figure 49, but is not observed in Figures 50 and 51 since photoprints and photographs were not used for either clear sky or overcast sky conditions. The slight peak at small fractions for the satellite photoprint data set is probably due to the inability to distinguish very low level and very small clouds from the ground in the photoprints. The whole-sky photograph data set indicates that the cloud cover fractions for partly-cloudy sky are distributed uniformly for the small region of view (of the order of a few kilometers in radius) as well as for the much larger region used in the LAFB visual observations (horizon to horizon).

IV. THEORETICAL MODELING

The theoretical model developed by J. R. Foreman, was selected for use with our data and this method is presented below in detail. The clear sky part of this model is being applied to a March 1979, Michigan regional data set as a PhD. in Atmospheric Science dissertation project. Our local data set is being used to test and develop the model on a small scale and to expand the model to partly cloudy sky conditions. The month of February 1982 was selected as the first month to apply this model for the following reasons: (1) the ground albedo was expected to remain nearly constant throughout the month providing that there was no snow and that there was little change in the amount of ice in the tidal basin (2) the automated data acquisition system provided short-time interval (one minute) integrated data; and (3) clear sky conditions were sufficiently common to provide a data base for characterization of ground albedo and normal atmospheric absorption and scattering.

A. Summary of the Model

The method of estimation of global solar irradiance on a horizontal surface is an extension of the short wavelength energy balance equation developed by Ellis and Vonder Haar (1978)

$$I_{hg} = \frac{1}{(1 - \alpha)}(I_o - I_r - I_a) \quad \text{where:}$$

I_{hg} equals the horizontal global shortwave irradiance at the earth's surface;

α equals the local ground albedo;

I_o equals the horizontal extraterrestrial solar irradiance weighted by the spectral response of the satellite imaging device;

I_r equals the total shortwave irradiance reflected to space by the earth's atmospheric system;

and, I_a equals the total (incident and reflected) shortwave radiation absorbed by the various components of the atmosphere.

The term I_r is calculated from the satellite measured brightness of a line element and an appropriate angular reflectance model, which is being selected from the recent survey by Davis and Cox (1981).

The portions of I_a due to absorption by ozone and water vapor can be found to high accuracy from parameterizations developed by Lacis and Hansen (1974) and the absorption by permanent gasses can be calculated using a model presented by Yamamoto (1962). The absorption of light by dry and semi-wet aerosols will be parameterized to the mean low level relative humidity, $\bar{f}$, as found from a weighted average of the mean surface to 500 mb, the 850 mb, and the 700 mb relative humidities. The weighting will be done in accordance with some mean vertical distribution of aerosols in the low levels, according to a formula suggested by Hänel (1976): $I_{ad} = I_{od}\exp\{ -C_1 m(\frac{p}{p_o}) (1 - \bar{f})^{C_2} \}$;

where I_{ad} is the total radiation absorbed by atmospheric aerosols;

I_{od} is the incident radiation with ozone absorption accounted for;

p is the unreduced surface pressure (p_o equals 1013.25 mb);

m is the relative optical air mass of Kasten (1966); and

C_1 and C_2 are empirical coefficients.

The fourth absorption portion of I_a is caused by clouds and is the least understood of the various absorption mechanisms. Several relationships between absorption by clouds and the total short-wave radiation reflected upward by the clouds, the presence or absence of precipitation in the clouds (as revealed by radar reports) and the presence or absence of ice crystals in the cloud top (as inferred from the infrared estimated cloud top temperature) will be investigated during the next year.

B. Data Sets

The meteorological data needed for this model have been purchased from various sources. Most of the airways reports and weather data were purchased through the Environmental Data Services, National Climatic Center, Asheville,

NC. Some of these data are available in August and were not received at the time of the report. The local study region is indicated in Figure 54. by the dotted lines and with the Hampton Institute measurement site indicated by an X. As noted in the legend, each meteorological site is represented by a separate number. The sources of data outside the study region are used to establish parameters at the boundaries of the study region and as back-up data sets since several data sources are not regular one-hourly reporting stations. A summary of the data sets needed in the analysis is given below in outline form.

1. Satellite Data

   a. Source: GOES-East visible and infrared digitized brightness values.

   b. Resolution: 0.9 km x 0.9 km visible, 3.7 km x 3.7 km infrared.

   c. Data Array Coordinates:

Point	Satellite line x element	Geographical latitude x longitude
Center -	2992 x 7517	37.019°N x 76.338°W
NW Corner -	2942 x 7567	37.587°N x 76.884°W
NE Corner -	3042 x 7567	37.584°N x 75.801°W
SE Corner -	3042 x 7467	36.470°N x 75.798°W
SW Corner -	2942 x 7467	36.473°N x 76.858°W

   d. Period: Clear Sky Hours for Feb. 7,8,10,11,22 and 28, 1982;
   Cloudy Sky Hours for Feb. 4,13,17,18,21, and 24, 1982;

2. Meteorological

   a. Insolation:

      i. Type: horizontal global - 0.3 μm to 2.8 μm.
      ii. Frequency: ten-minute totals centered on satellite scan time (GMT).
      iii. Source: Eppley PSP one-minute integrated data at Hampton Institute.

   b. Humidity
      i. Hourly surface airways reports of temperature, dew point, and altimeter settings from local airport, Coast Guard, Air Force, Navy, and Army weather data sources for low level data.
      ii. Radiosonde data from Wallops Island and Sterling VA and from Cape Hatteras and Greensboro NC for upper level data.

   c. Cloud Parameters
      i. Cloud fraction: HI photographs and satellite brightness readings.
      ii. Cloud type and height: Langley Air Force Base observations.
      iii. Water content: radar reports (facsimile charts) from local airports.
      iv. Cloud top temperature: Infrared satellite data.

d. Ozone and Aerosols

i. Turbidity readings at Hampton Institute
ii. Dobson spectrophotometer readings of total ozone column over Nashville, TN, Tallahassee, FL, Wallops Island, VA, and Washington, DC. obtained from the World Ozone Data Center, Environment Canada, Toronto, Canada.

3. Miscellaneous
a. Ground albedo: calculated from clear sky satellite brightness values using an equation developed by Otterman and others (Otterman, 1980).
b. Elevation: most points within the study region are treated as being at sea level but use of United States Geological Survey Maps is being made to ascertain elevations throughout the study region.
c. Cloud shadows; use of photoprint and calculation of shadow positions from sun-cloud-satellite geometery.

C. Progress

The first group of steps in the theoretical modeling have been completed; i.e., a model has been selected and a data set has been accumulated for comparison with the model. Satellite radiometric imagery has been obtained from the Environmental Data Services of NOAA for the Hampton Institute study region for selected times within the month of February 1982. Meteorological data have been ordered from the National Climatic Center for local observation sites for the same time period. The ozone data has already been obtained and the horizontal global irradiance values are readily available. The procedure for the application of J. R. Foreman's model is outlined below to give an indication of the steps that must be performed.

1. Assemble Data Set

a) select times and dates;

b) order satellite imagery (visible and infrared brightness values);

c) request meteorological data (ozone and relative humidity data);

d) calculate satellite scan times for insolation intervals;

e) assemble horizontal global insolation values;

f) calculate relative humidity for surface to 500 mb, 700 mb, and 850 mb;

g) divide data set into clear and cloudy data sets.

2. Use Clear Data Set to:

a) calculate ground albedo (α) from I_{hg}, I_r and angular reflectance model;

b) characterize absorption by permanent gasses;

c) calculate absorption by ozone from spectrophotometer or Volz sunphotometer data;

d) obtain coefficients for absorption by aerosols from I_a, $\bar{T}$, and absorption by ozone and permanent gasses.

3. Use Cloudy Data Set to:

a) separate cloud effects from clear sky effects;

b) determine dependence on cloud type, height, transmittance and amount.

Since the data set has not been completely assembled, we have not progressed to the ground albedo and model parameter calculations. The complete data set should be assembled within the next month and then work can commence on the application of the model.

LIST OF TABLES

TABLE I

HAMPTON INSTITUTE SOLAR MEASUREMENT SUMMARY

Measurement	Instrumentation	Data Frequency	Starting Date
SOLAR IRRADIANCES			
Global	Eppley PSP with WG7 clear glass dome	One-hour integrated and continuous chart	February 17, 1981
		One-minute integrated*	February 1, 1982
Direct	Eppley NIP with quartz glass and solar tracker	One-hour integrated and continuous chart	October 1, 1981
		One-minute integrated*	February 1, 1982
Diffuse	Eppley PSP with WG7 clear glass dome	One-hour integrated and continuous chart	October 1, 1981
		One-minute integrated*	March 1, 1982
ATMOSPHERIC EMITTANCE	Eppley PIP	One-hour integrated and continuous chart	March 18, 1981
		One-minute integrated*	March 1, 1982
ATMOSPHERIC PROPERTIES			
Aerosol Extinction @ 380 and 875 nm Turbidity @ 500 nm Precipitable Water	Volz Sunphotometer	Approximately one hour intervals for clear sky	March 24, 1981

* After March 13, 1982 the radiometer sampling rate was set at one-minute from 0400 EST to 2000 EST and at ten-minutes from 2000 EST to 0400 EST.

TABLE II

RADIOMETRIC INSTRUMENTATION AND WAVELENGTH CAPABILITIES

Instrument	Normal Observation Wavelength Range
Eppley Precision Spectral Pyranometer	0.285 to 2.8 microns
Eppley Precision Infrared Radiometer	4.0 to 50.0 microns
Eppley Normal Incidence Pyrheliometer	0.285 to 4.5 microns
Eppley Hickey-Frieden Absolute Cavity Pyrheliometer	0.2 to 50 microns
Additional Wavelength Ranges for the Pyranometers and Pyrheliometers	0.53 to 2.8 microns
	0.63 to 2.8 microns
	0.70 to 2.8 microns
Volz Sunphotometer	Center of Band - Halfwidth
	380 nm - 11 nm
	500 nm - 40 nm
	875 nm - 17 nm
	940 nm - 16 nm

TABLE III RADIOMETER CALIBRATION SUMMARY

Radiometer	Calibration Information			Sensitivity Factor ($\frac{\mu V}{W/m2}$)	Change in Sensitivity
	Date	Comparison With	Performed By		
Precision Spectral Pyranometer					
Eppley PSP # 20022F3	10/1/80	Standard References	Eppley Laboratory	10.55	-
	4/30/81	PSP # 20613F3	Hampton Institute	*	-1.7%
	6/24/81	PSP # 20613F3	Hampton Institute	*	-1.1%
	6/21/82	PSP # 20613F3	Hampton Institute	*	-1.0%
	7/8/82	Standard References	Eppley Laboratory	10.00 †	-5.5%
Eppley PSP # 20613F3	2/28/81	Standard References	Eppley Laboratory	11.10	-
	7/15/82	PSP # 20022F3	Hampton Institute	10.62 †	-4.5%
Normal Incidence Pyrheliometer					
Eppley NIP # 20254E6	3/4/81	Standard References	Eppley Laboratory	9.21	-
	5/12/82	H-F Absolute Cavity Pyrheliometer	Hampton Institute	9.21**	0%
Precision Infrared Radiometer					
Eppley PIR # 20078F3	10/6/80	Standard References	Eppley Laboratory	4.95	-
	7/7/82	Standard References	Eppley Laboratory	4.86	-1.8%

* Since these sensitivity factors are unchanged within the $\pm$ 2 % accuracy of the instruments, the data were not adjusted prior to 7/16/82.

** The sensitivity factor was unchanged within the accuracy of the calibration instruments($\approx$1 %).

† Eppley Laboratory changed calibration standards October 1981, which represents 2.5 % of the sensitivity change.

TABLE IV DATA ACQUISITION AND STORAGE HARDWARE

ITEM DESCRIPTION	QUANTITY	MANUFACTURER & MODEL NUMBER
Integrator with BCD Interface	4	Eppley Laboratory, Model 411-6140
Microcomputer System with RS232 Interface	2	Tektronix, Inc., Model 4051
Microcomputer ROM Expander	1	Tektronix, Inc., Model 4051E01
Real Time Clock ROM Pack	1	Trans Era, Model 641-RTC
Binary/BCD I/O Interfaces - Interconnected - User Supplied Interface Box	5	Trans Era, Model 632 BCD with Options 1 and 2
Minicomputer with 9 Track Tape Drive	1	Digital Equipment, PDP 11/34
Interface Box with LED Photo Count Display	1	Designed and Built by D. D. Venable & R. D. Blakey
2 Channel - 12 Bit D/A Converter *	1	Trans Era, Model 620 DAC
12 Bit 16 Channel Data Acquisition System *	1	Trans Era, Model 652 ADC

* These two devices were used in the design and testing stages.

TABLE V SOLAUTO PROGRAM (UDK) FEATURES

USER DEFINED KEY #	NAME AND FUNCTION OF KEY
1	"Note to Tape" - Enter a user's note to be stored on tape.
2	"Read ROMs" - Read all active ROMs, prompts for tape storage.
3	"Photograph" - Activates camera, prompts for tape storage.
4	"D to A" - Controls Digital to Analog feature of ROMs.
5	"Intervals" - Sets photograph and ROM reading intervals.
6	"Reset" - Resets all ROM and user defined functions.
7	"ROMs On/Off" - Controls readings of ROMs two through five.
8	"Time" - Displays time and prompts for reset.
9	"Output Control" - Selects if records are to be written to tape and/or screen.
10	"Photocount" - Lists current photo count and prompts for reset (36 maximum).
11	"EOT" - Locates end of data on tape and leaves tape positioned for writing.
12	"A to D" - Controls Analog to Digital feature of ROMs.
13	"Status" - Prints out list of current parameters in the form listed below: ROM_i, i=2-5, 1 - enabled; Ø - disabled ROM DEL - interrupt interval (minutes) for reading ROMs PIC DEL - interrupt interval (minutes) for photographs ROM/TAPE - 1 - write records to tape; Ø - suppress ROM/DIS - 1 - write records to screen; Ø - not displayed PIC/TAPE - 1 - write records to tape; Ø - suppress Last ROM - Last ROM record Last PHOTO - Last photograph record PHOTO CNT - current photograph count TAPE REC - number of records written to tape Time - current time DELAY - current delay time to next interrupt $FLAG_i$ - values of flags: 1 - ROM record; 2 - Photo record; 3 - User message; 4 - System messages
14	Pin 5 CONTROL - Output is high, low, low—high—low, high-low-high, minimum pulse width is 0.01 sec.
15	"TAPE DUMP" - Reads tape by date and/or flag.
16	"NEW TAPE" - Runs sequence for installing new data tape.
17	"GRAPH" - Plots ROM data differentials vs. time by date.
18	- Reserved for future use
19	"Continue" - Resumes data acquisition after stopping program with UDK 20.
20	"Stop" - Stops program execution until resumed by the use of UDK 19.

TABLE VI DATA RECOVERY RECORD: HOURLY INTEGRATED GLOBAL SOLAR IRRADIANCE

Year	Month	Number of Hour-Values Stored on Tape	Data Recovery Rate (%)	Number of Hour-Values Missing			
				System Failure	Calibrations	Solar Tracker Misalignment	Other
1981							
	February	300	44.6	-	-	-	372 *
	March	744	100	-	-	-	-
	April	720	100	-	-	-	-
	May	744	100	-	-	-	-
	June	719	99.9	1	-	-	-
	July	741	99.6	3	-	-	-
	August	740	99.5	4	-	-	-
	September	720	100	-	-	-	-
	October	743	99.9	-	-	-	1†
	November	720	100	-	-	-	-
	December	742	99.7	-	2	-	-
1982							
	January	744	100	-	-	-	-
	February	672	100	-	-	-	-
	March	743	99.9	-	-	-	1†
	April	720	100	-	-	-	-
	May	740	99.5	-	-	-	4†
	June	720	100	-	-	-	-

* Continuous global insolation measurements began at 1200 EST February 16, 1981.

† The strip chart record was too variable to allow recovery of these values.

TABLE VII DATA RECOVERY RECORD: HOURLY INTEGRATED ATMOSPHERIC EMITTANCE

Year	Month	Number of Hour-Values Stored on Tape	Data Recovery Rate (%)	Number of Hour-Values Missing			
				System Failure	Calibrations	Solar Tracker Misalignment	Other
1981							
	February	120	17.9	-	-	-	552 *
	March	664	89.2	80†	-	-	-
	April	718	99.7	2	-	-	-
	May	744	100	-	-	-	-
	June	720	100	-	-	-	-
	July	741	99.6	3	-	-	-
	August	741	99.6	3	-	-	-
	September	720	100	-	-	-	-
	October	742	99.7	-	-	-	2
	November	720	100	-	-	-	-
	December	740	99.5	-	4	-	-
1982							
	January	722	97.0	-	-	-	22**
	February	672	100	-	-	-	-
	March	658	88.4	86†	-	-	-
	April	720	100	-	-	-	-
	May	744	100	-	-	-	-
	June	512	71.1	-	208	-	-

* Continuous atmospheric emittance measurements began 00 EST February 24, 1981.

** Ice coated the silicon hemisphere of the sensor.

† The battery had to be changed.

TABLE VIII DATA RECOVERY RECORD: HOURLY INTEGRATED DIFFUSE SOLAR IRRADIANCE

Year	Month	Number of Hour-Values Stored on Tape	Data Recovery Rate (%)	Number of Hour-Values Missing			
				System Failure	Calibrations	Solar Tracker Misalignment	Other
1981							
	June	37	5.1	-	-	-	683 *
	July	117	15.7	-	-	-	627 *
	August	0	0	-	-	-	744 †
	September	43	6.0	-	-	-	677 *
	October	712	95.7	-	-	9	23 *
	November	716	99.4	-	-	4	-
	December	732	98.4	-	4	8	-
1982							
	January	639	85.9	-	-	105 **	-
	February	672	100	-	-	-	-
	March	744	100	-	-	-	-
	April	716	99.4	-	-	4	-
	May	721	96.9	-	-	23	-
	June	479	66.5	-	241	-	-

* Data were obtained for midday hours intermittantly due to temporary electrical power for solar tracker operation prior to October 19, 1981. All data prior to October 3, 1981 are available on printer tape only.

† The strip chart recorder was inoperative during August and September.

** The motor on the solar tracker burned out.

TABLE IX DATA RECOVERY RECORD: HOURLY INTEGRATED DIRECT SOLAR IRRADIANCE

Year	Month	Number of Hour-Values Stored on Tape	Data Recovery Rate (%)	Number of Hour-Values Missing			
				System Failure	Calibrations	Solar Tracker Misalignment	Other
1981							
	September	13	1.8	-	-	-	707 *
	October	529	71.1	105	-	103	7 *†
	November	615	85.4	-	2	6	97 *†
	December	611	82.1	-	-	9	100 *†
1982							
	January	676	90.9	-	-	10	58 †
	February	668	99.4	-	-	3	1
	March	738	99.2	-	-	5	1
	April	692	96.1	-	-	28	-
	May	715	96.1	-	2	27	-
	June	720	100	-	-	-	-

* Continuous measurements during midday hours started September 28, 1981 but are only available on printer tape from September 28 to October 3, and on strip chart recorder trace to December 28, 1981. The integrator was inoperative from October 3 to December 27 and the strip chart recorder was inoperative before September 28, 1981. The recorder is necessary to ensure proper solar tracking and the integrator is necessary to handle the large variability in the direct irradiance signal.

† This sensor, integrator and printer system was used for testing and development of the automated data acquisition system.

TABLE X DATA RECOVERY RECORD FOR AUTOMATED DATA ACQUISITON SYSTEM
ONE AND TEN MINUTE INTEGRATED IRRADIANCES

Month - Insolation Component	Maximum Possible Number of Data Records	Amount Recovered by Computer Number - Percent	Number of Missing Data Records			
			User Interrupt	System Crash	System Calibration	Other
February - 1982						
Global*	40,320	36,326 - 90.1	2,205	1,190	-	599
Direct*	"	35,163 - 87.2	3,358	1,200	-	599
March						
Global	36,648	35,369 - 96.5	446	678	-	155
Direct	"	35,381 - 96.5	433	679	-	155
Diffuse**	"	34,434 - 94.0	263	679	-	1,272
Infrared**	"	26,470 - 72.2	257	679	-	9,242
April						
Global	30,240	29,673 - 98.1	61	407	-	99
Direct	"	29,708 - 98.2	26	407	-	99
Diffuse	"	29,708 - 98.2	26	407	-	99
Infrared	"	29,708 - 98.2	26	407	-	99
May						
Global	31,248	29,519 - 94.5	17	1,712	-	-
Direct	"	29,519 - 94.5	17	1,712	-	-
Diffuse	"	29,519 - 94.5	17	1,712	-	-
Infrared	"	29,519 - 94.5	17	1,712	-	-
June						
Global	30,240	28,232 - 93.4	181	1,827	-	-
Direct	"	28,232 - 93.4	181	1,827	-	-
Diffuse	"	16,112 - 53.3	181	1,827	12,120	-
Infrared	"	19,453 - 64.3	181	1,827	8,779	-

* One-minute readings only from 0942 February 1, 1982 to 2000 EST March 13, 1982 and ten-minute readings at night after March 13.

** One-minute readings only from 2038 EST March 1, 1982 to 2000 EST March 13, 1982 and ten-minute readings at night after March 13.

TABLE XI ARL REGRESSION COEFFICIENTS FOR CLEAR SKY GLOBAL SOLAR IRRADIANCE

Time of Day - Month	Number of Points		Regression Coefficients (Wh/m^2)			
	Clear Only	Nearly Clear	A_0	A_1	A_2	A_3
Mornings -						
March, 1981	10	0	- 59	935	349	- 180
April	8	11	- 29	758	578	- 267
May	9	23	12	395	1109	- 533
June	5	8	- 28	604	317	100
July	6	5	- 26	673	284	40
August	20	5	-119	1329	-1130	927
September	35	5	- 24	630	777	- 423
October	9	0	-111	1558	-1570	1530
November	10	10	-151	786	503	- 134
December	1	18	- 49	1053	5	242
January, 1982	11	1	6	482	1935	-1747
February	1	6	- 40	951	306	- 21
March	19	0	- 94	1326	- 497	393
April	29	3	- 4	638	958	- 549
May	5	17	- 21	657	723	- 341
June	3	6	6	294	1373	- 684
Afternoons -						
March, 1981	14	0	- 52	1071	- 233	314
April	5	12	- 14	672	761	- 379
May	0	12	48	166	1844	-1065
June	5	2	- 2	329	1502	- 873
July	0	6	- 24	472	878	- 335
August	4	2	17	181	1455	- 653
September	17	4	15	210	1594	- 800
October	1	8	- 9	482	1718	-1501
November	8	2	- 75	1097	53	41
December	5	4	-135	1712	-1854	2041
January, 1982	12	2	15	260	2435	-1937
February	1	8	- 3	600	1046	- 527
March	14	4	- 29	819	434	- 100
April	14	9	- 70	1047	- 24	105
May	10	17	- 15	573	765	- 293
June	3	9	- 38	746	189	109

TABLE XII ARL REGRESSION COEFFICIENTS FOR NORMALIZED CLOUDY SKY GLOBAL SOLAR IRRADIANCE

Year	Month	Number of Data Points			Regression Coefficients				
		LAFB Visuals	Satellite Photoprints	Whole-Sky Photographs	B_0	B_1	B_2	B_3	B_4
1981									
	March	126	13	2	1.017	- 0.282	- 1.126	0.721	- 0.168
	April	92	9	12	1.001	0.160	- 1.493	0.620	- 0.112
	May	161	16	10	1.006	- 0.499	- 0.523	0.370	- 0.184
	June	331	10	9	0.999	- 0.618	1.084	- 0.919	- 0.409
	July	356	0	2	0.996	- 0.302	0.885	1.151	- 0.240
	August	332	0	0	1.006	- 0.266	1.006	- 1.262	- 0.297
	September	295	0	2	1.001	0.060	- 0.284	- 0.237	- 0.330
	October	258	0	10	0.998	- 0.390	0.664	- 0.906	- 0.217
	November	218	0	5	1.007	- 0.974	2.224	- 1.793	- 0.331
	December	266	0	7	1.000	- 0.353	0.717	- 0.973	- 0.202
1982									
	January	260	0	4	1.000	- 0.266	0.528	- 0.836	- 0.286
	February	231	5	32	1.004	- 0.966	2.087	- 1.720	- 0.251
	March	291	0	20	1.000	- 0.570	1.421	- 1.393	- 0.245
	April	271	0	0	1.000	- 0.430	0.677	- 0.889	- 0.230
	May	328	0	40	0.998	- 0.668	1.179	- 0.970	- 0.349
	June	411	0	27	1.001	- 0.752	1.494	- 1.309	- 0.187

TABLE XIII ARL COEFFICIENTS FOR THE FIRST YEAR DATA SET

(March 1981 Through February 1982)

Clear Sky Global

Data Fit to Equation 1	Number of Points	Regression Coefficients (Wh/m^2) A_0	A_1	A_2	A_3	Standard Deviation (Sigma in Wh/m^2)
Mornings						
Clear Sky Only	125	- 39	847	316	- 171	45
Clear & Nearly Clear	217	- 58	1030	- 84	86	44
Afternoons						
Clear Sky Only	72	- 70	1089	- 126	154	37
Clear & Nearly Clear	135	- 36	765	649	- 369	34

Normalized Cloudy Sky Global

Data Fit to Equation 2	Number of Points	Regression Coefficients B_0	B_1	B_2	B_3	B_4	Standard Deviation
Reduced LAFB Data Set	92	1.004	- 0.353	0.789	- 1.089	- 0.215	0.14
Satellite Photoprints	62	1.017	- 0.468	- 0.182	0.033	- 0.253	0.13
Whole-Sky Photographs	104	0.955	- 0.615	0.975	- 0.850	- 0.319	0.14

LIST OF FIGURES

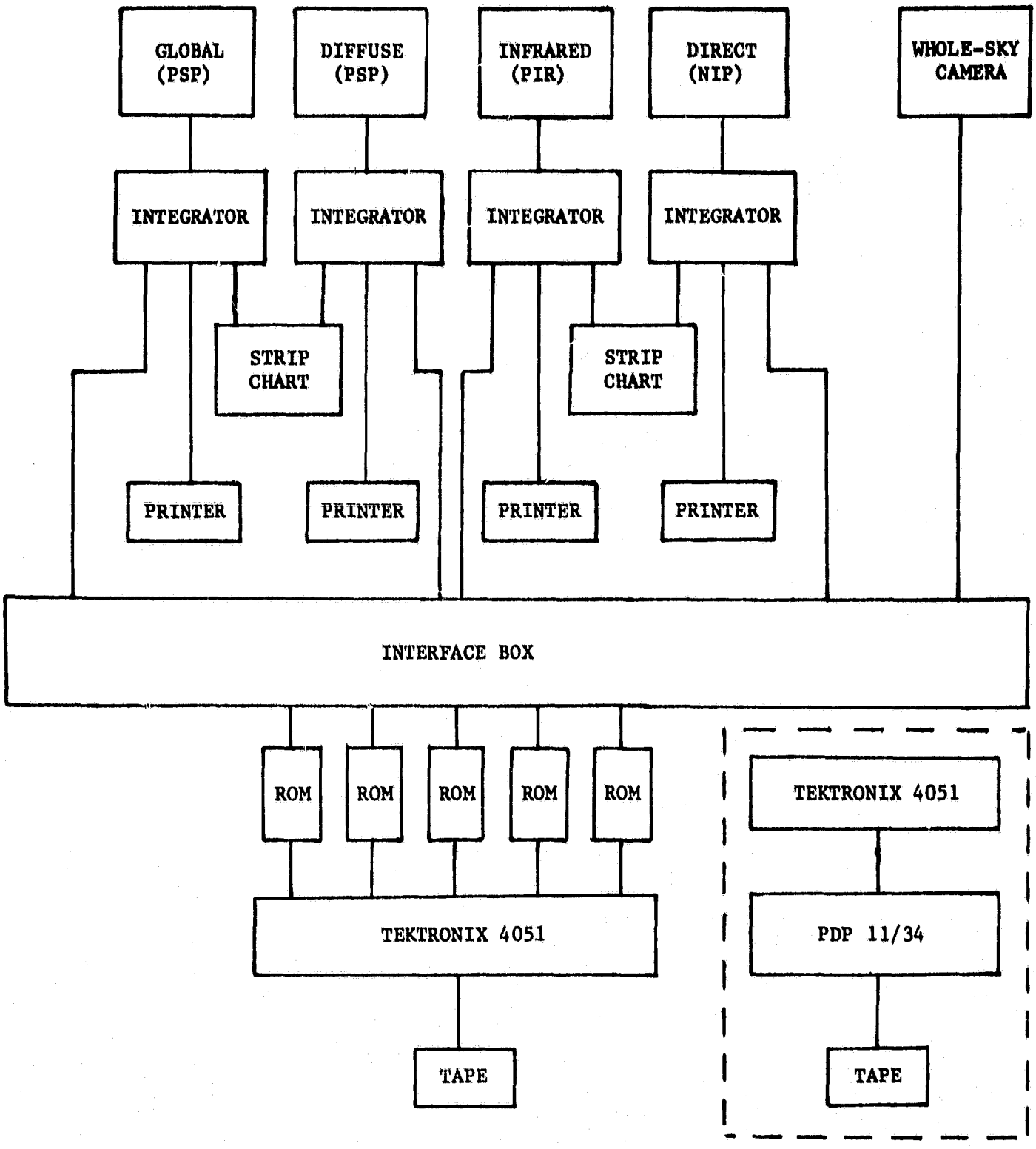

Figure 1. Automated Data Acquisition System Flow Chart

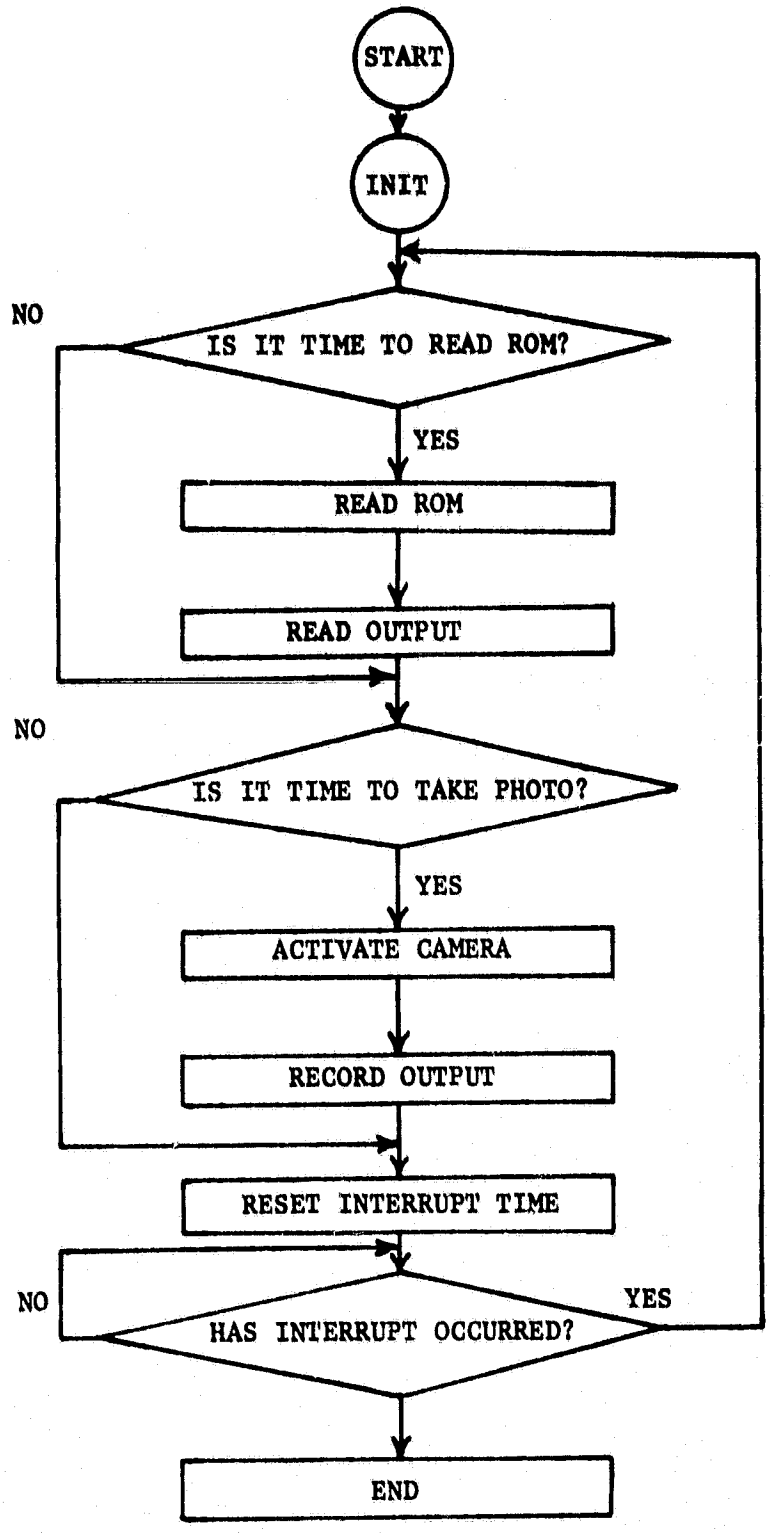

Figure 2. SOLAUTO Program Data Acquisition Logic

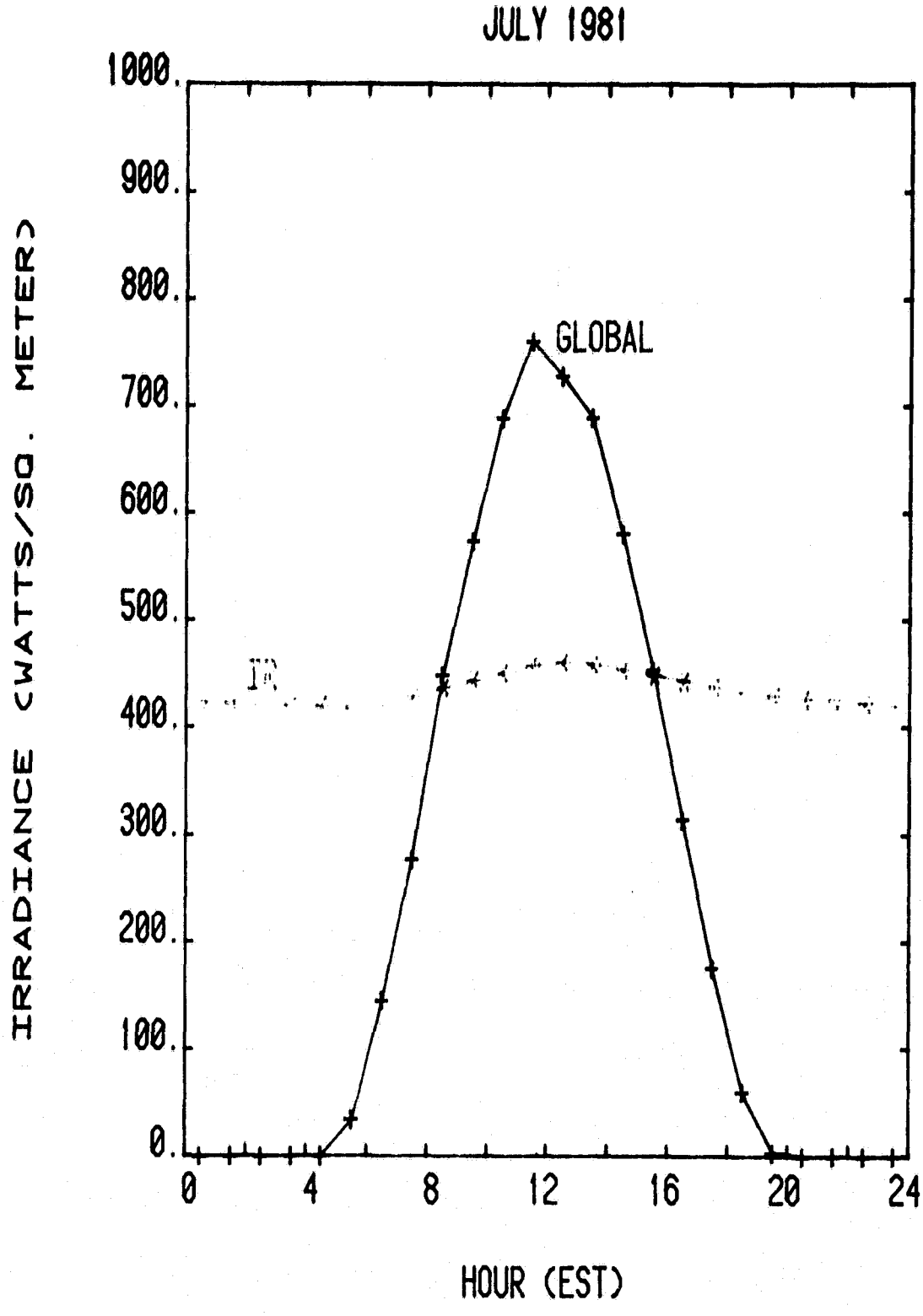

Figure 3. Average Diurnal Variation of Global Solar Irradiance and Atmospheric (IR) Emittance for July 1981.

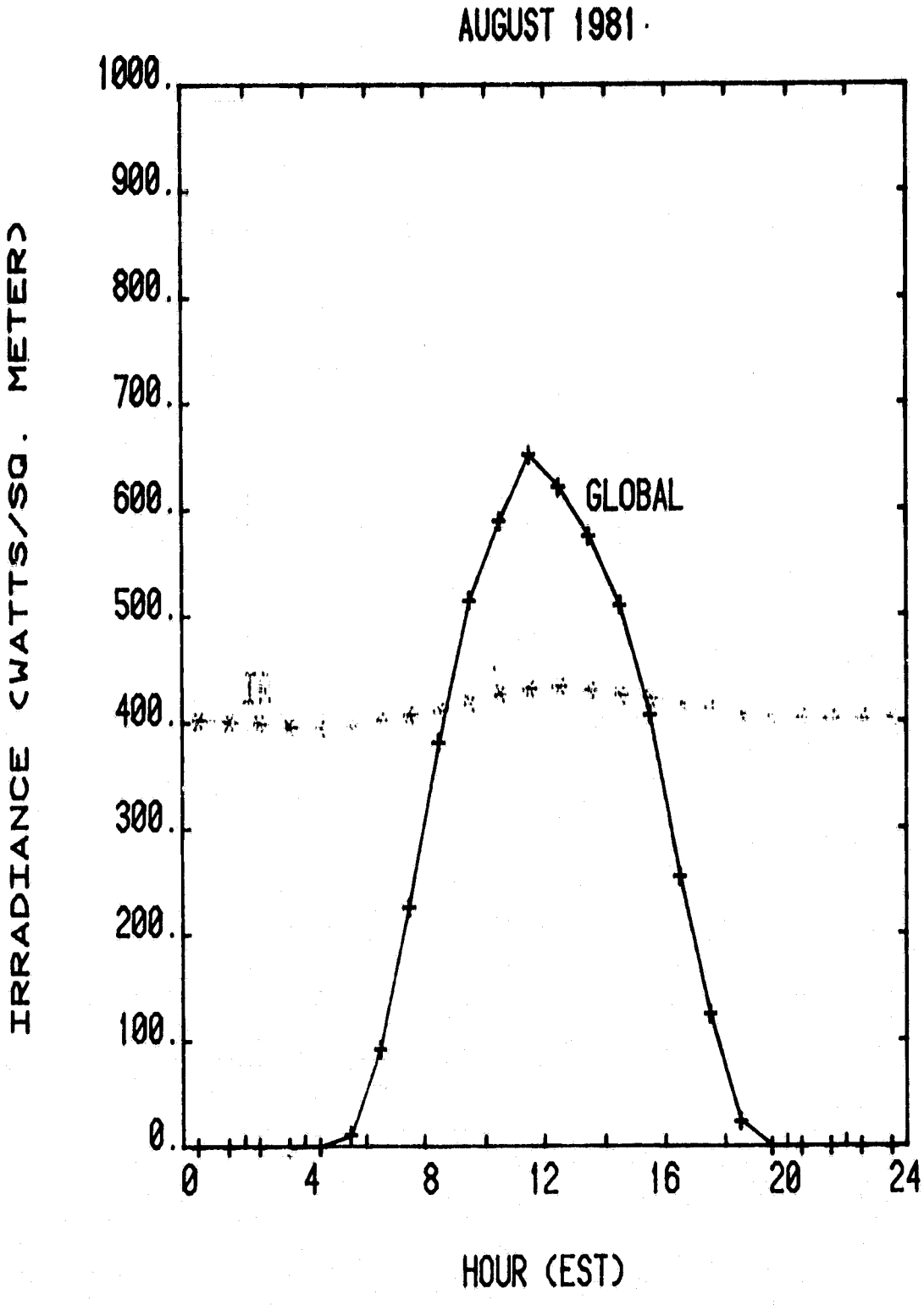

Figure 4. Average Diurnal Variation of Global Solar Irradiance and Atmospheric (IR) Emittance for August 1981.

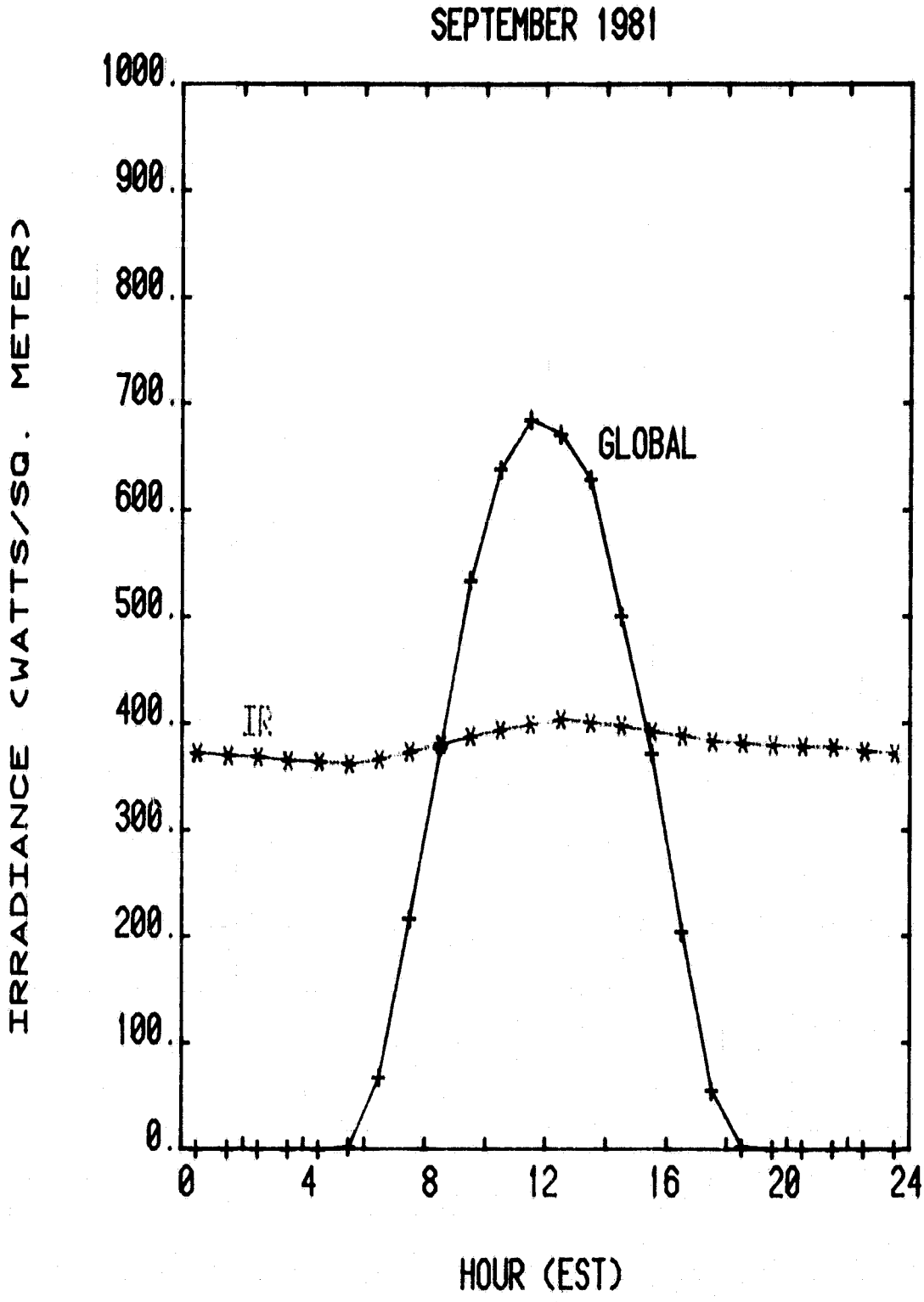

Figure 5. Average Diurnal Variation of Global Solar Irradiance and Atmospheric (IR) Emittance for September 1981.

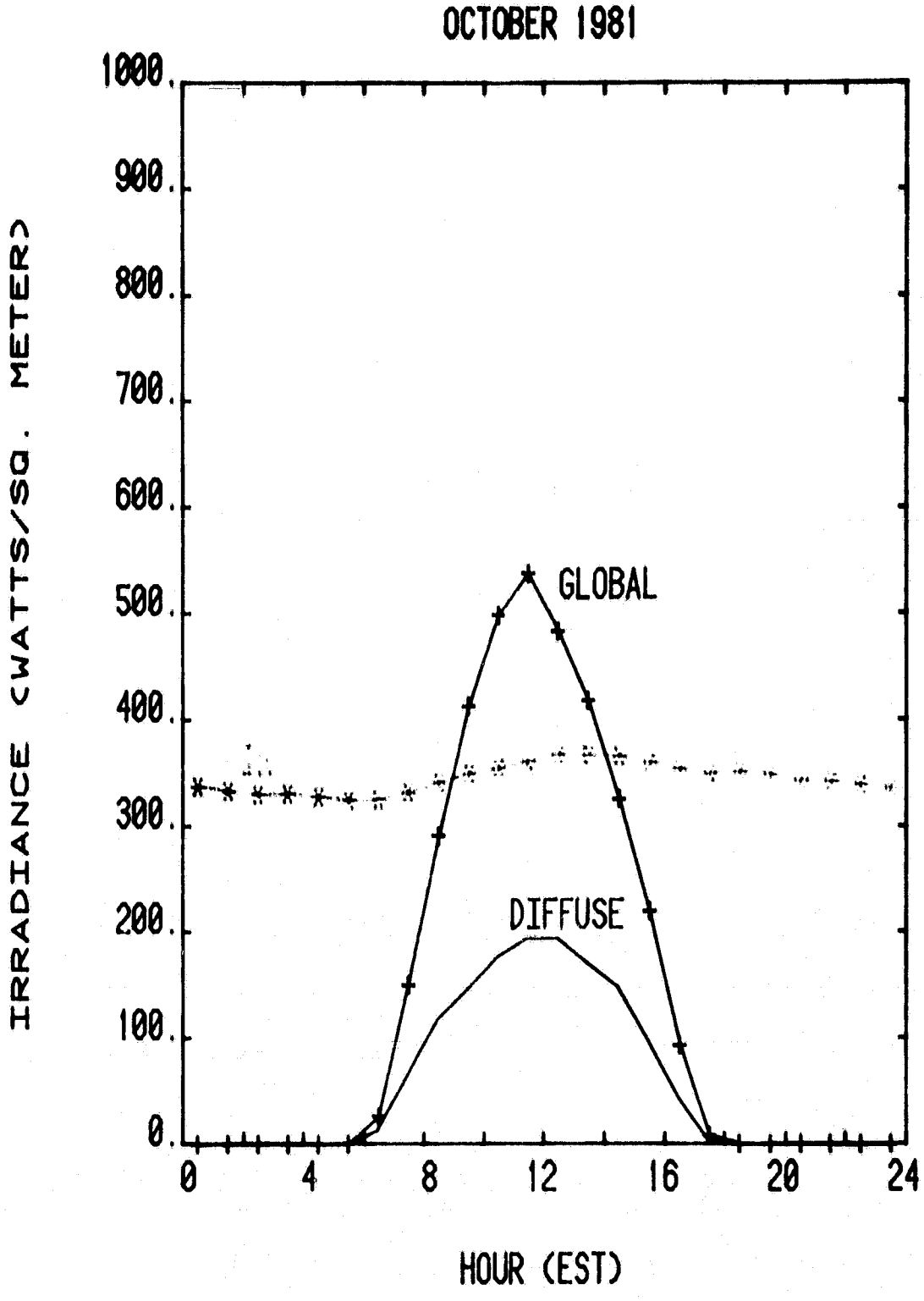

Figure 6. Average Diurnal Variation of Global and Diffuse Solar Irradiances and Atmospheric (IR) Emittance for October 1981.

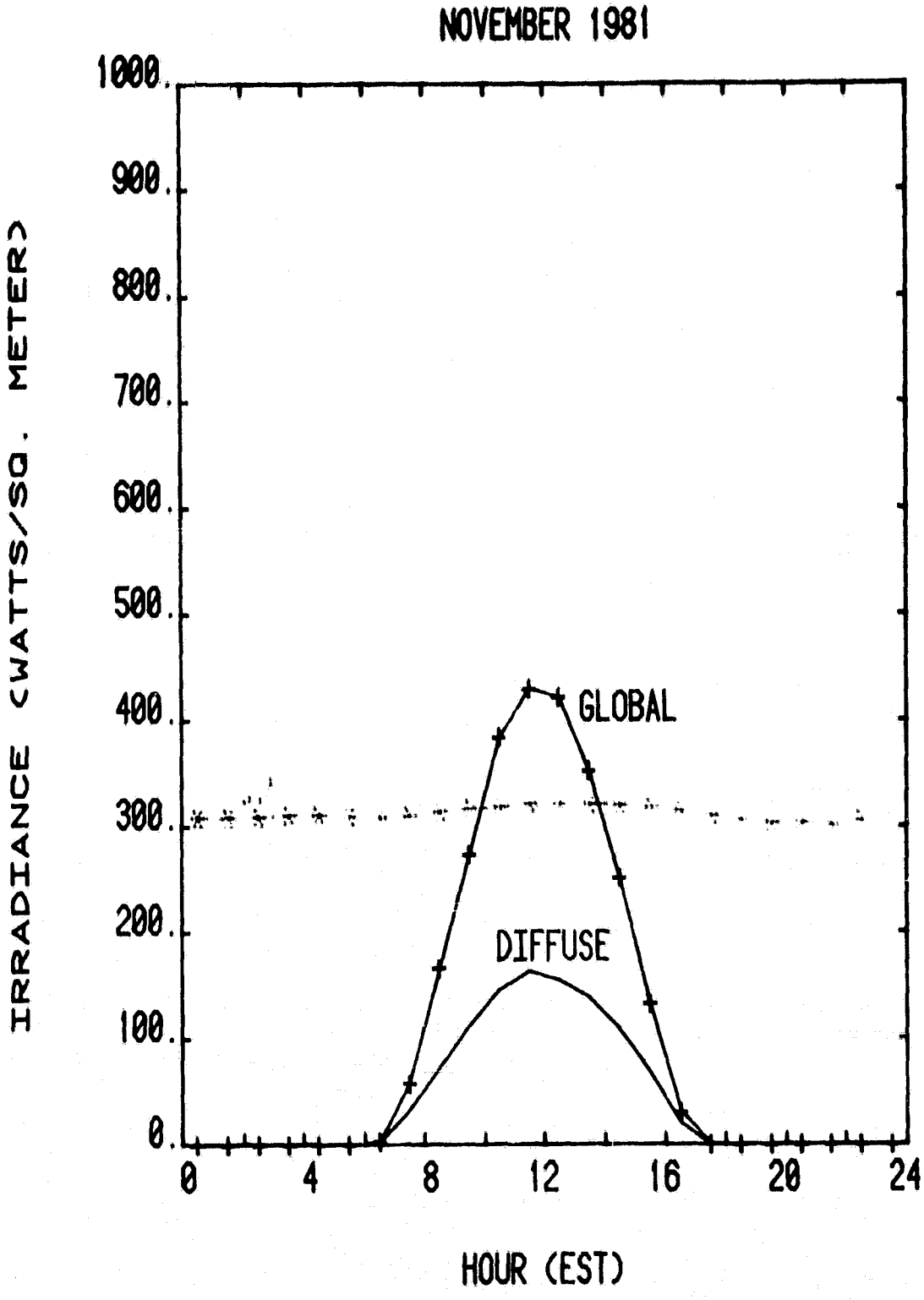

Figure 7. Hourly Average Global and Diffuse Solar Irradiances and Atmospheric (IR) Emittance for November 1981.

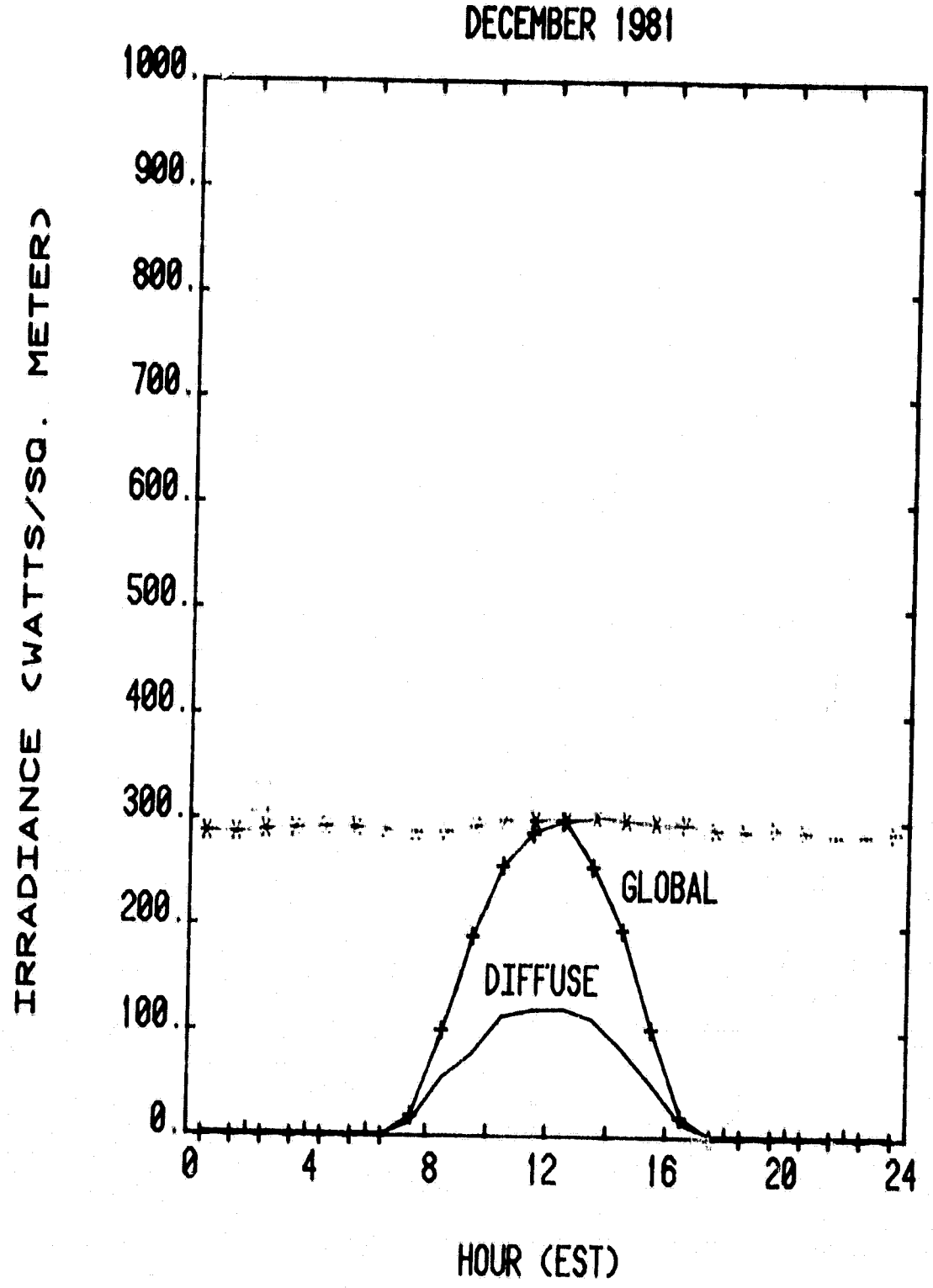

Figure 8. Hourly Average Global, Diffuse and Direct Solar Irradiances and Atmospheric (IR) Emittance for December 1981.

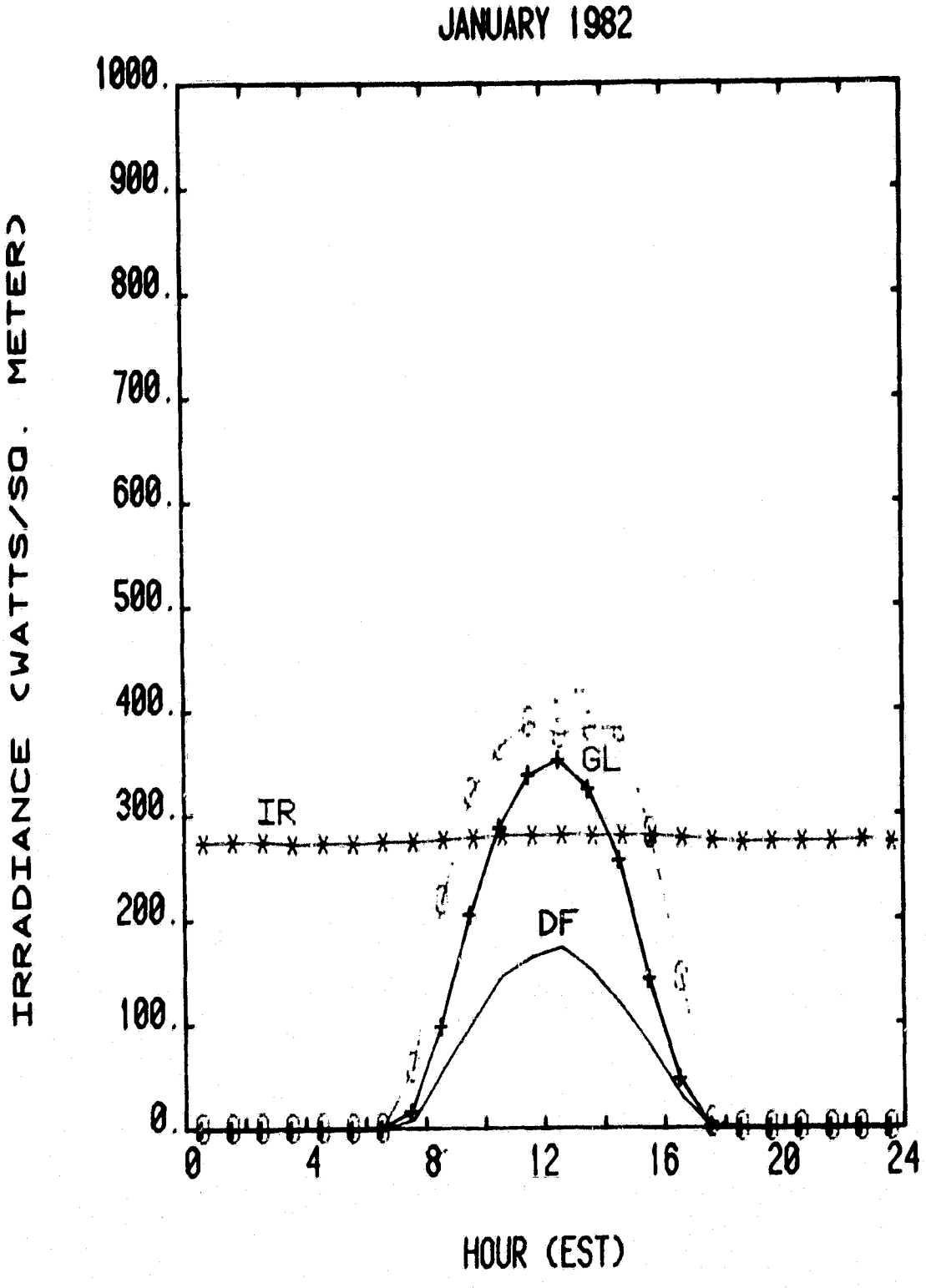

Figure 9. Hourly Average Global (GL), Diffuse (DF), and Direct (DR) Solar Irradiances and Atmospheric (IR) Emittance for January 1982.

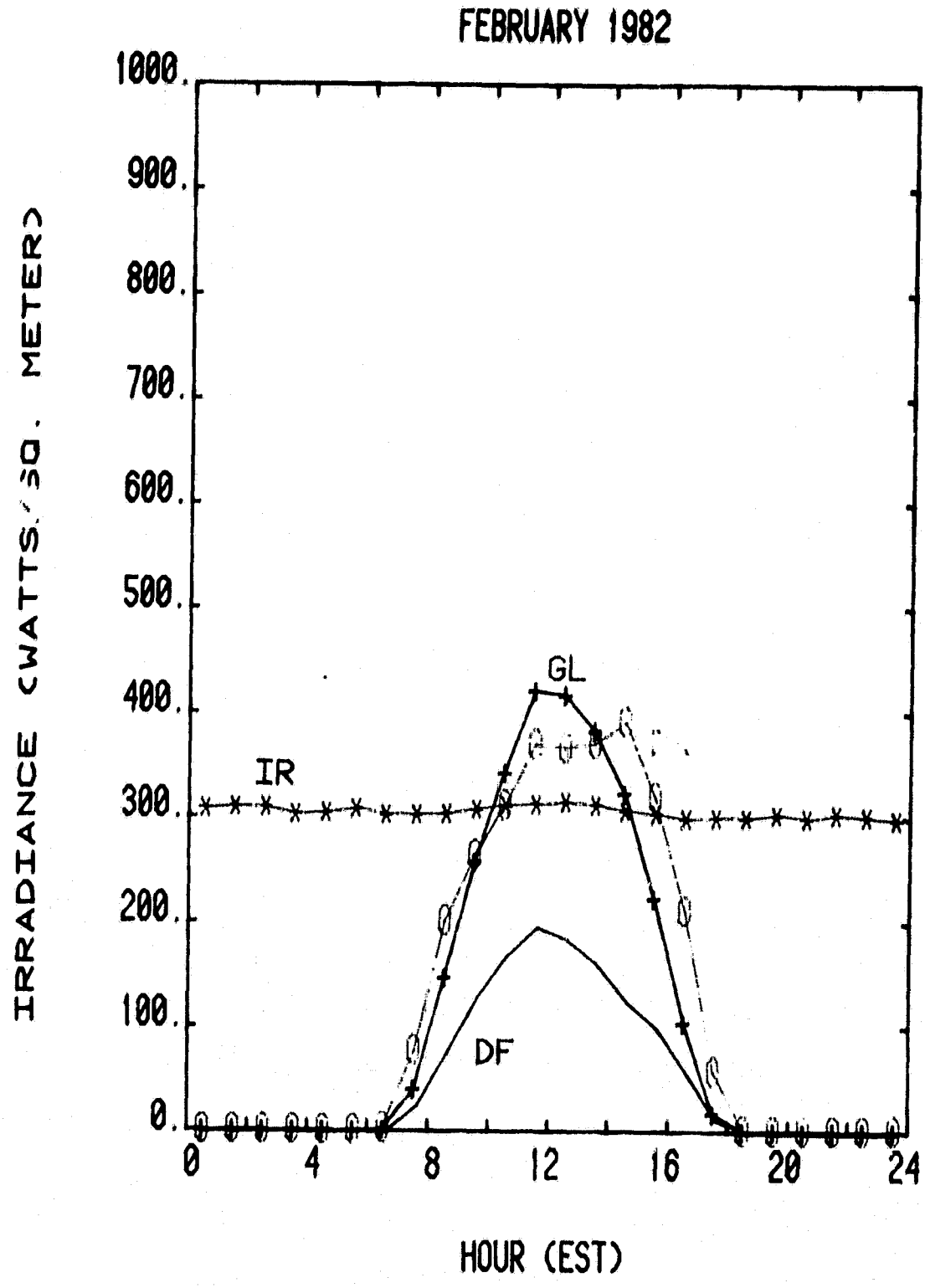

Figure 10. Hourly Average Global (GL), Diffuse (DF), and Direct (DR) Solar Irradiances and Atmospheric (IR) Emittance for February 1982.

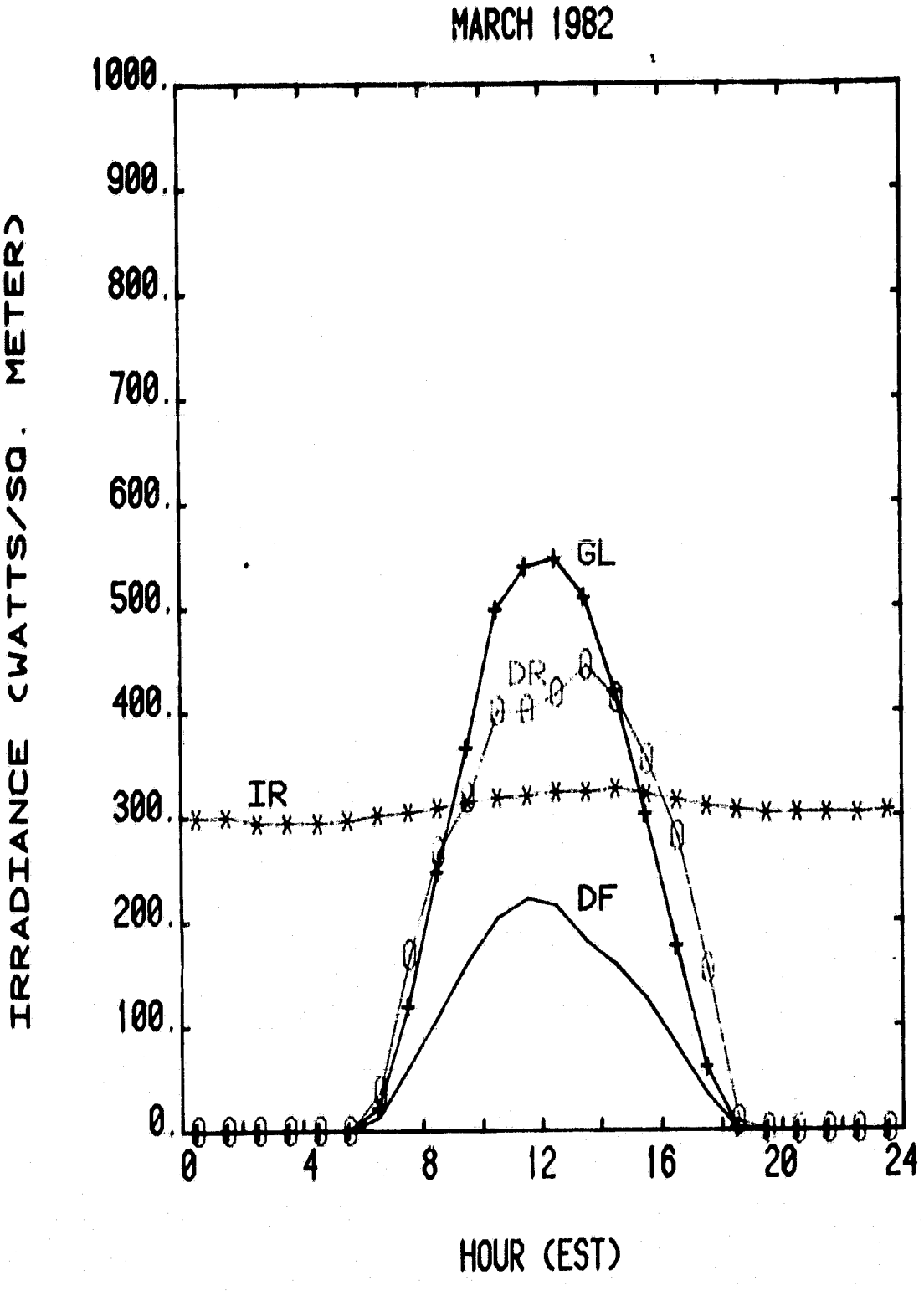

Figure 11. Hourly Average Global (GL), Diffuse (DF), and Direct (DR) Solar Irradiances and Atmospheric (IR) Emittance for March 1982.

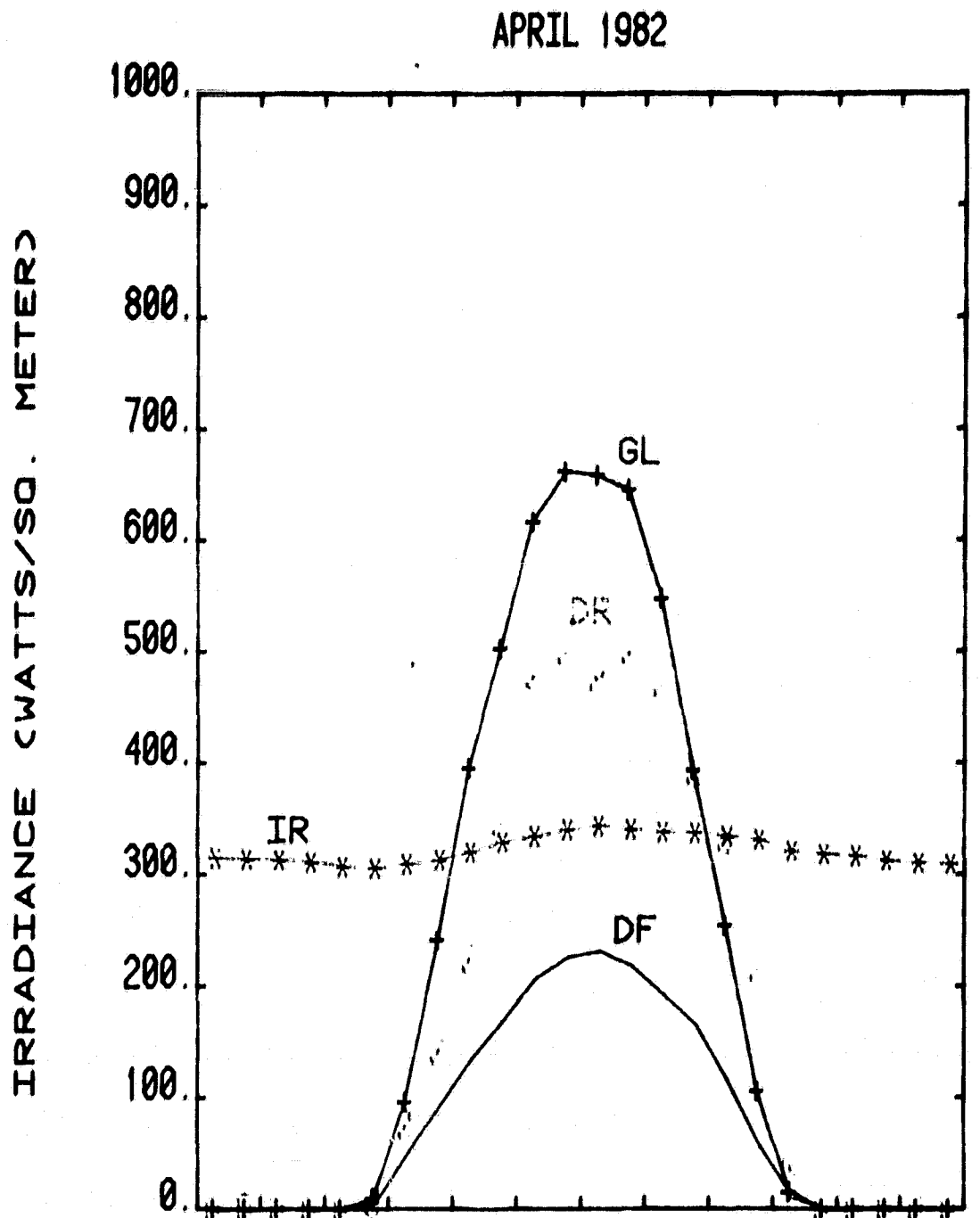

Figure 12. Hourly Average Global (GL), Diffuse (DF), and Direct (DR) Solar Irradiances and Atmospheric (IR) Emittance for April 1982.

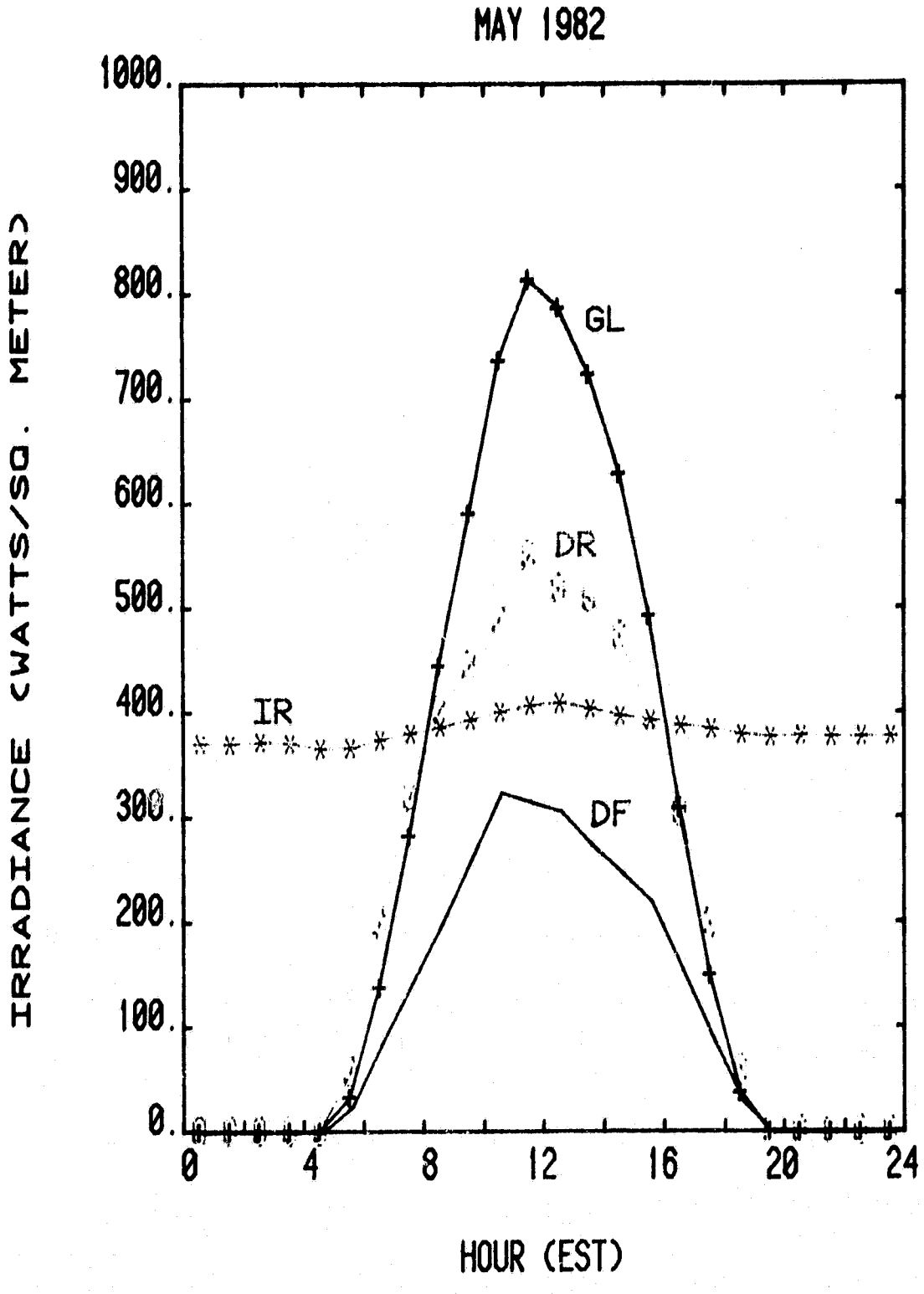

Figure 13. Hourly Average Global (GL), Diffuse (DF), and Direct (DR) Solar Irradiances and Atmospheric (IR) Emittance for May 1982.

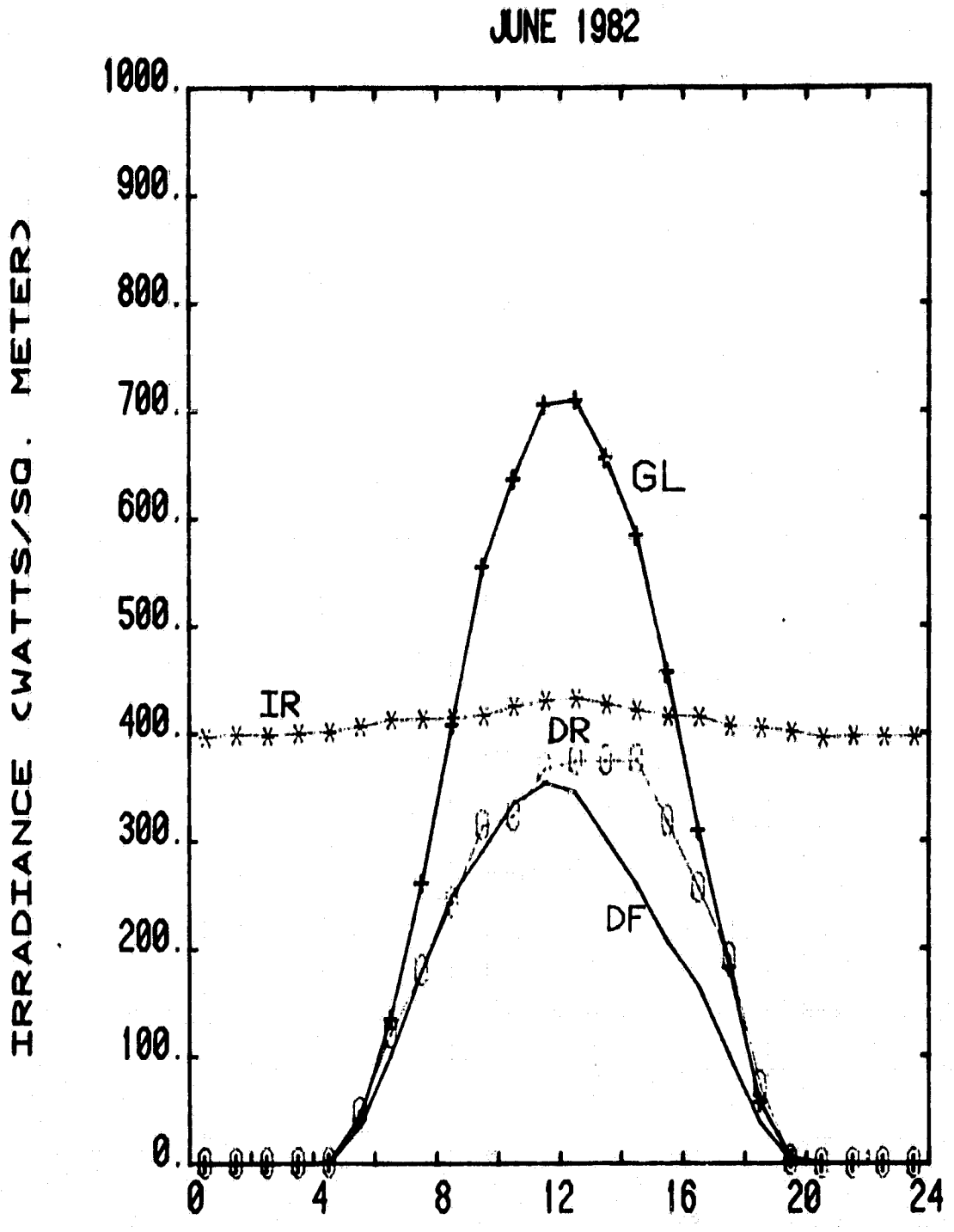

Figure 14. Hourly Average Global (GL), Diffuse (DF) and Direct (DR) Solar Irradiances and Atmospheric (IR) Emittance for June 1982.

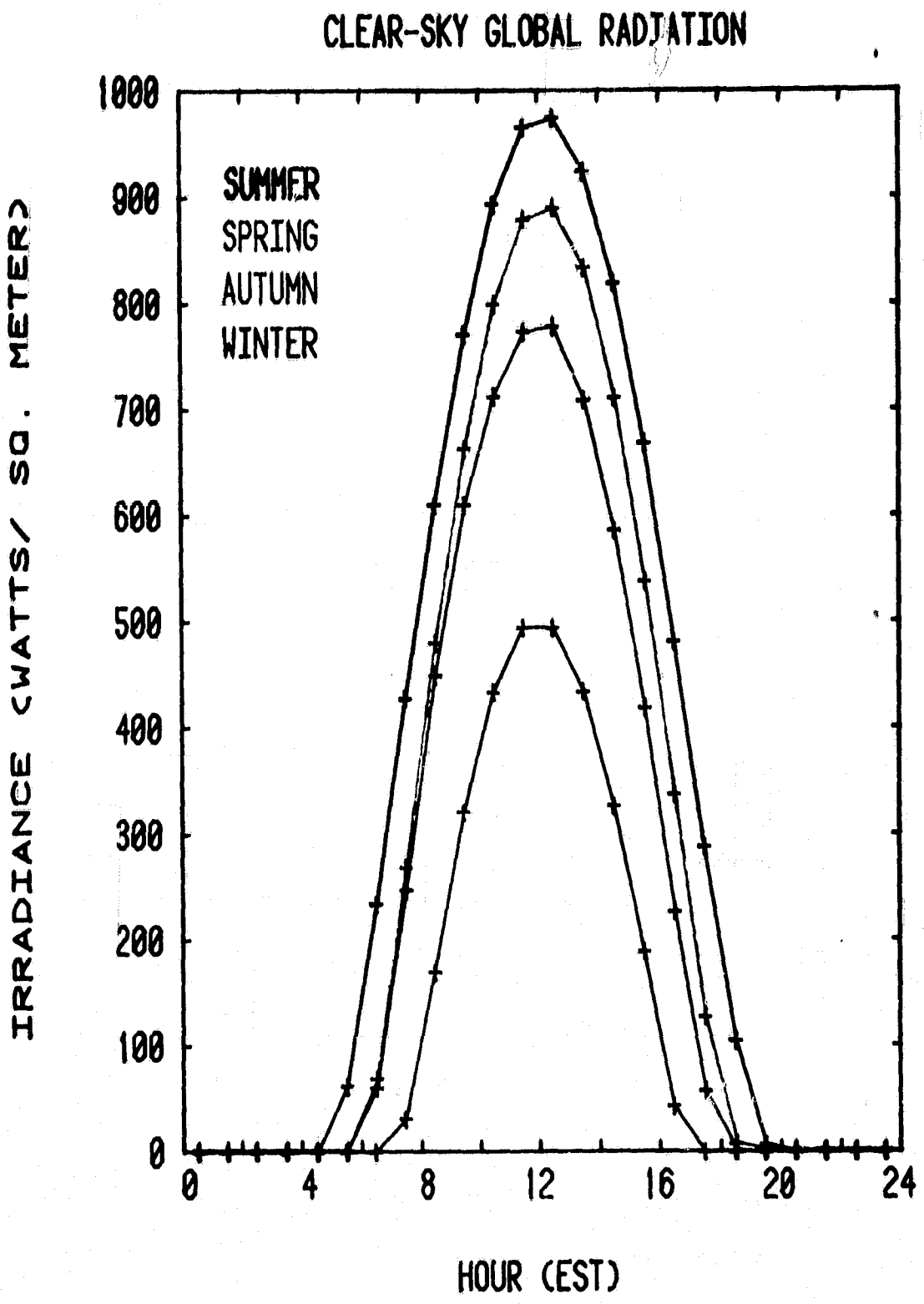

Figure 15. Seasonal Variability of Clear-Sky Global Irradiance for selected days.

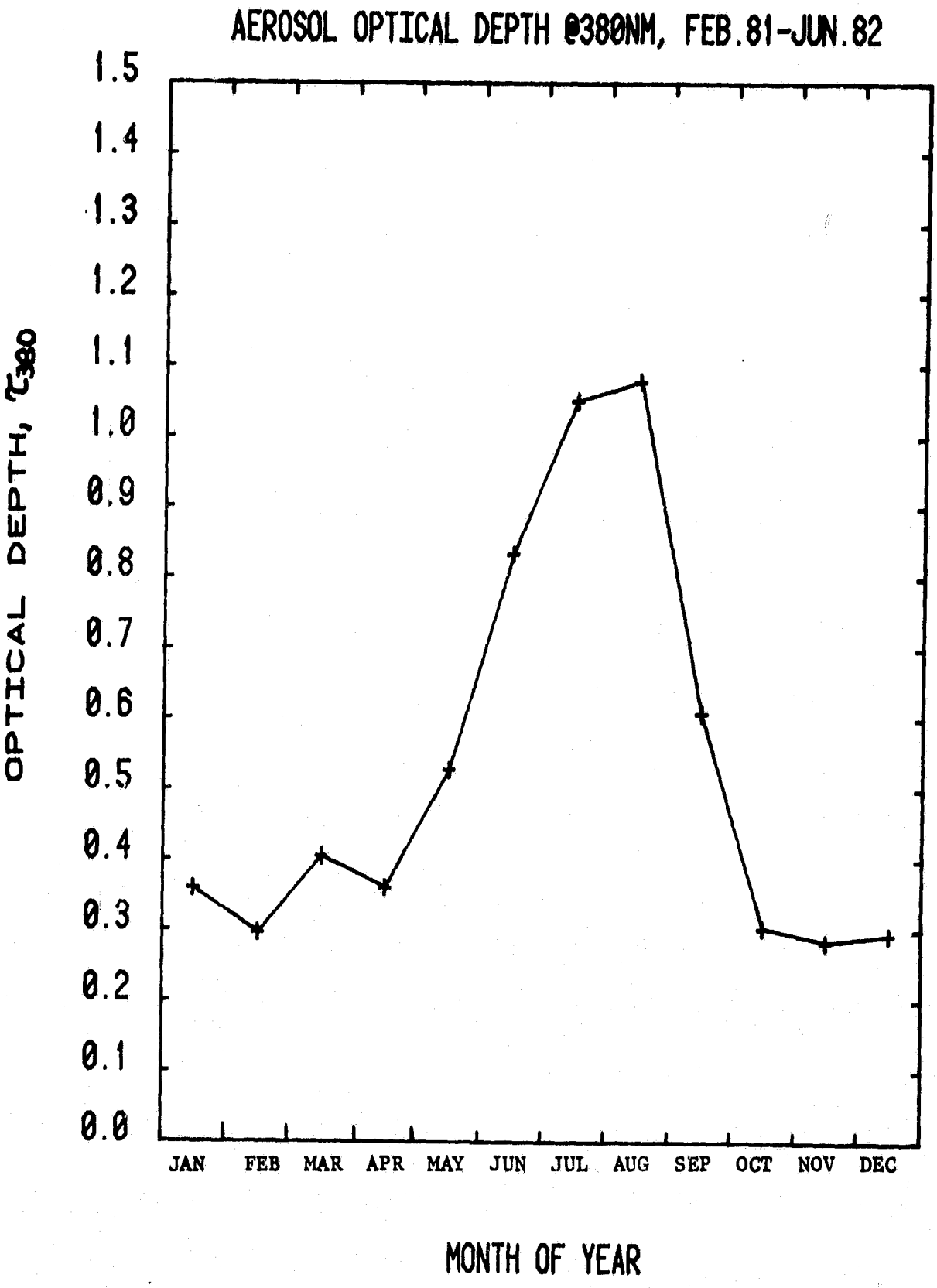

Figure 16. Monthly Average Aerosol Extinction Coefficient, or Optical Depth, at 380 nanometers for the period February 1981 through June 1982.

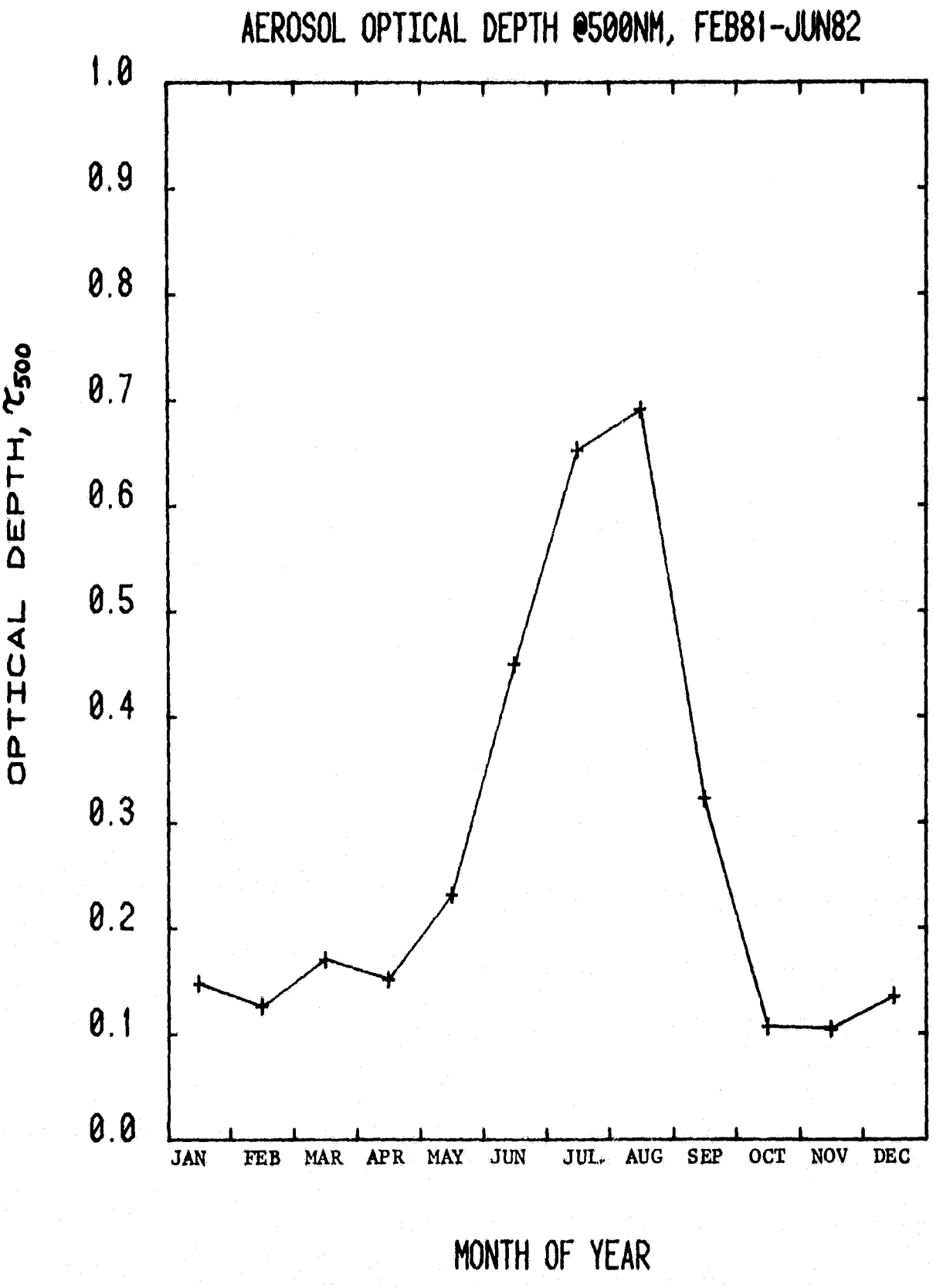

Figure 17. Monthly Average Aerosol Extinction Coefficient, or Optical Depth, at 500 nanometers for the period February 1981 through June 1982.

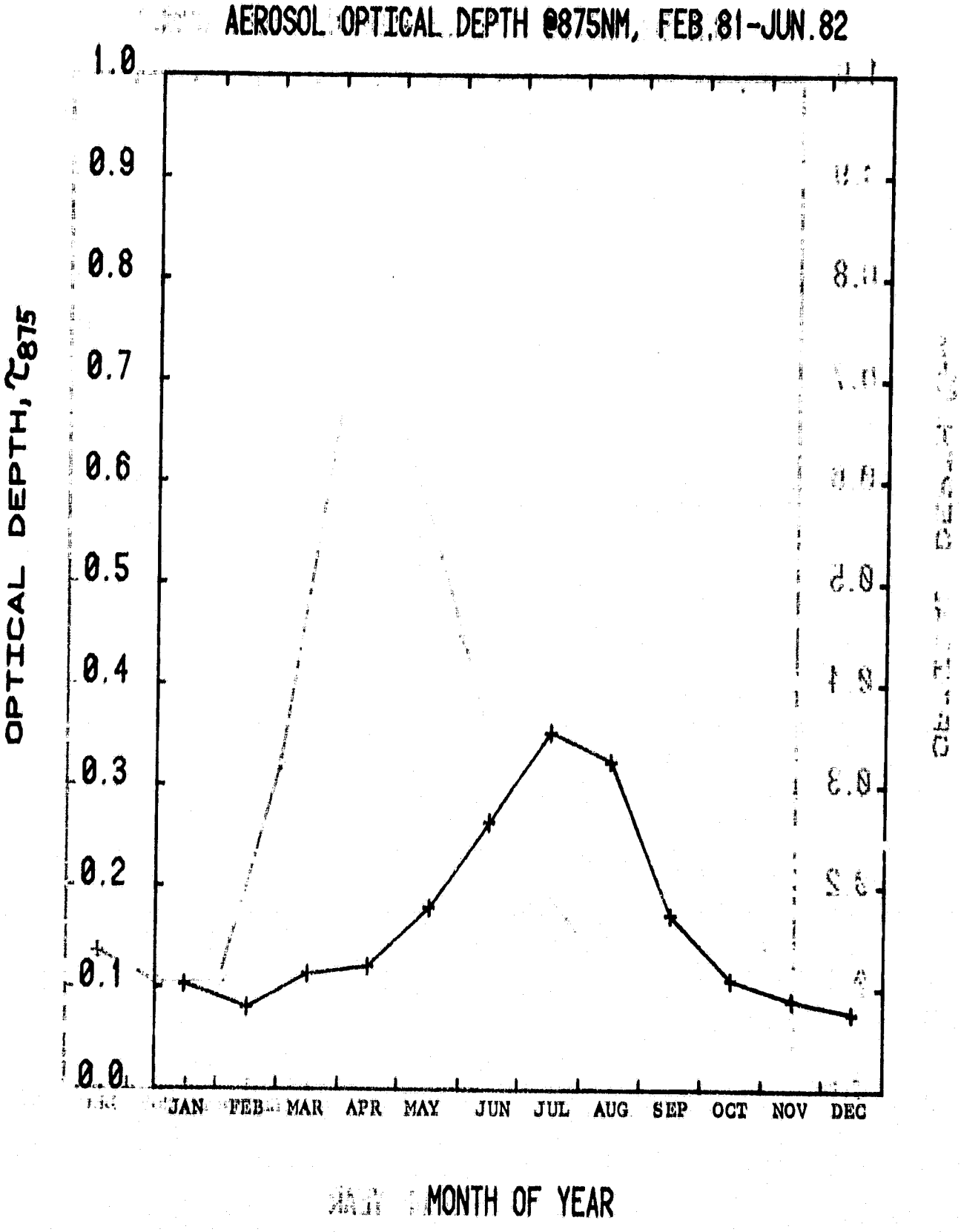

Figure 18. Monthly Average Aerosol Extinction Coefficient, or Optical Depth, at 875 nanometers for the period February 1981 through June 1982.

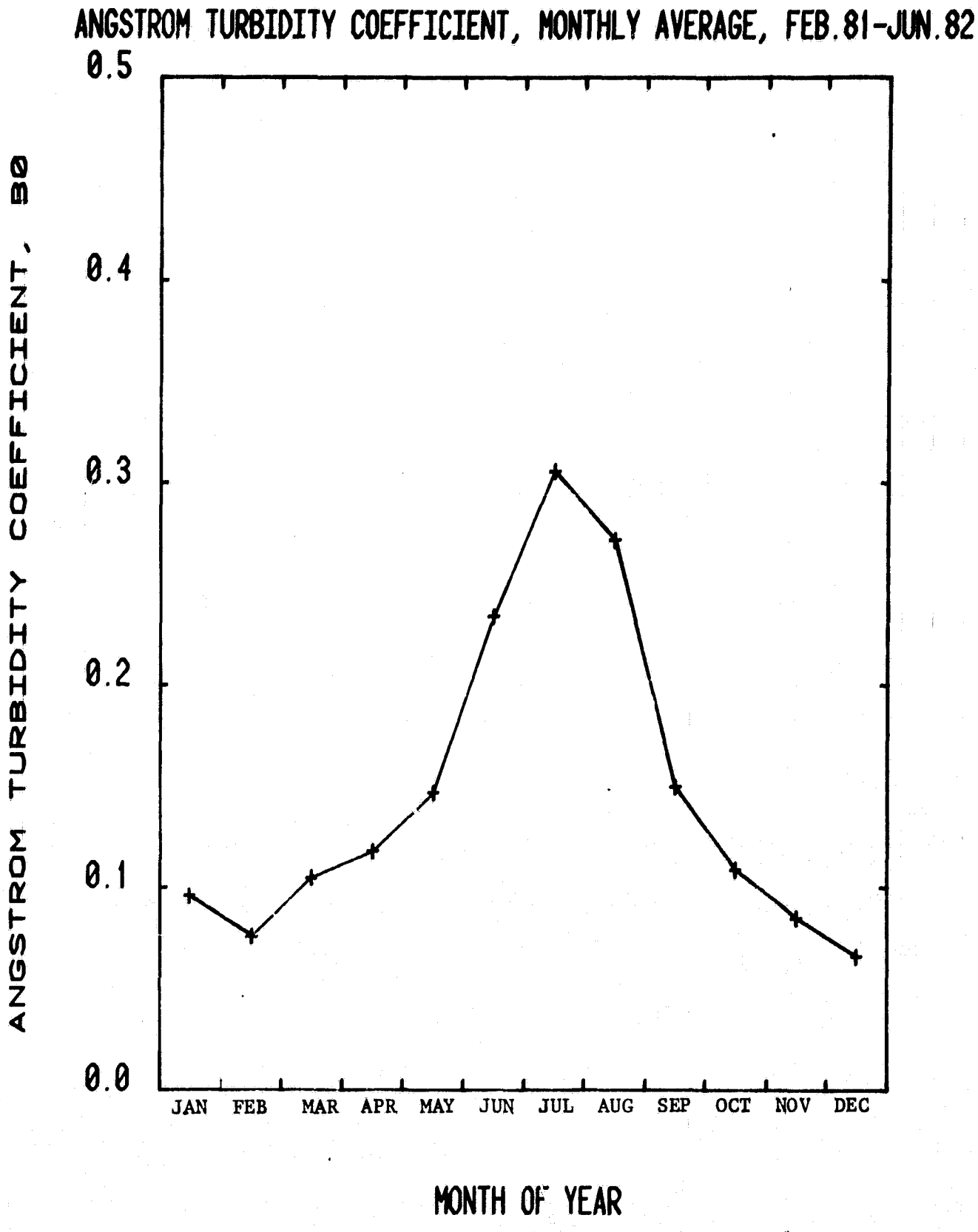

Figure 19. Monthly Average Angstrom Turbidity Coefficient, BØ, for the measurement period February 1981 through June 1982.

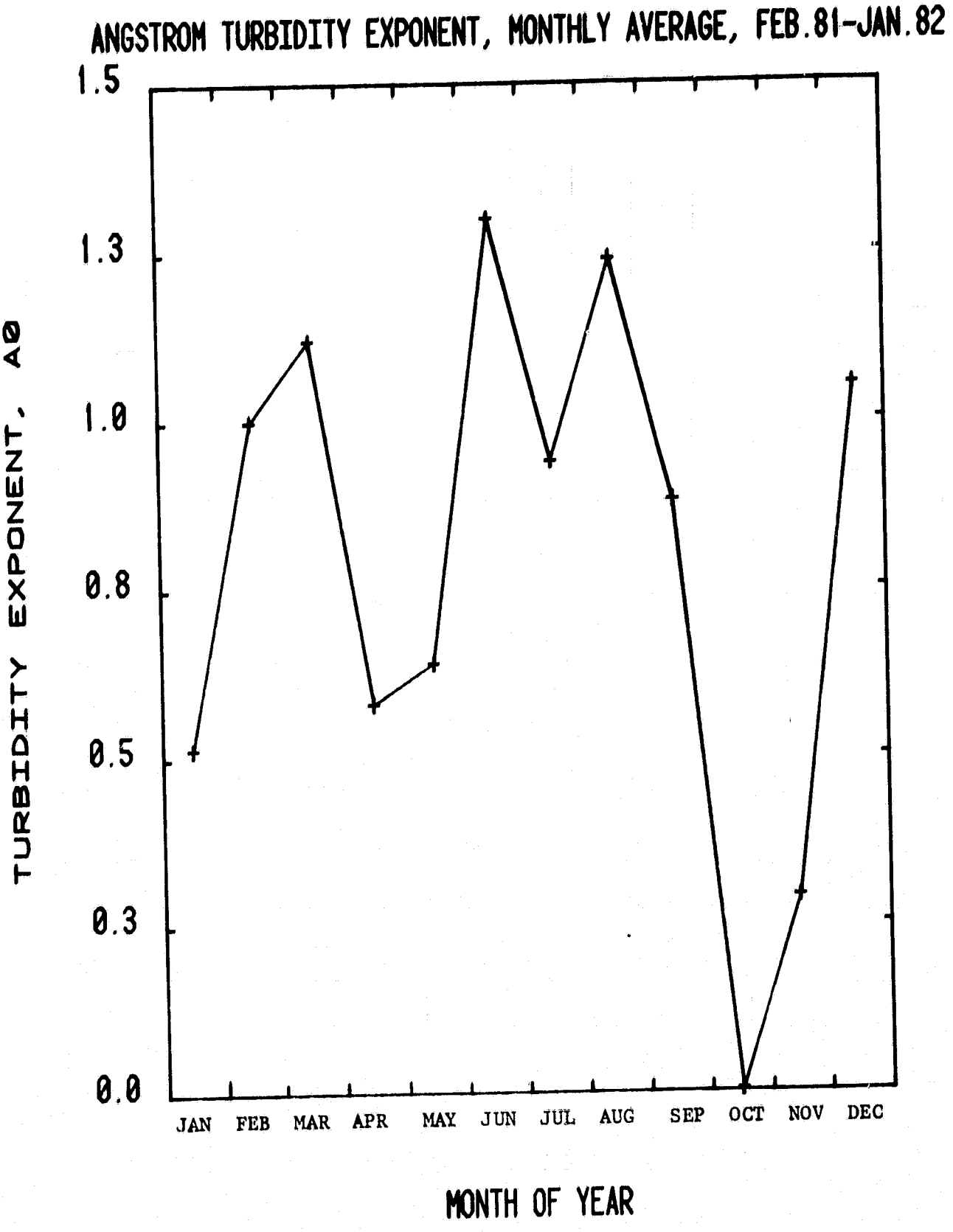

Figure 20. Monthly Average Angstrom Turbidity Wavelength Exponent, AØ, for the period February 1981 through January 1982.

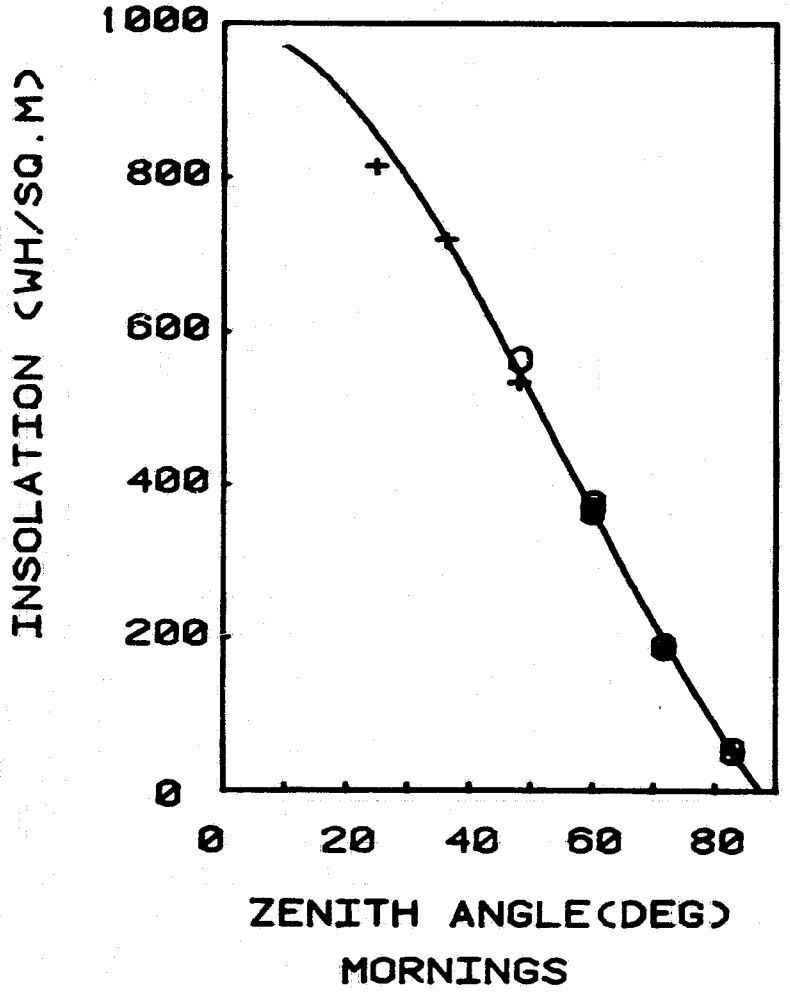

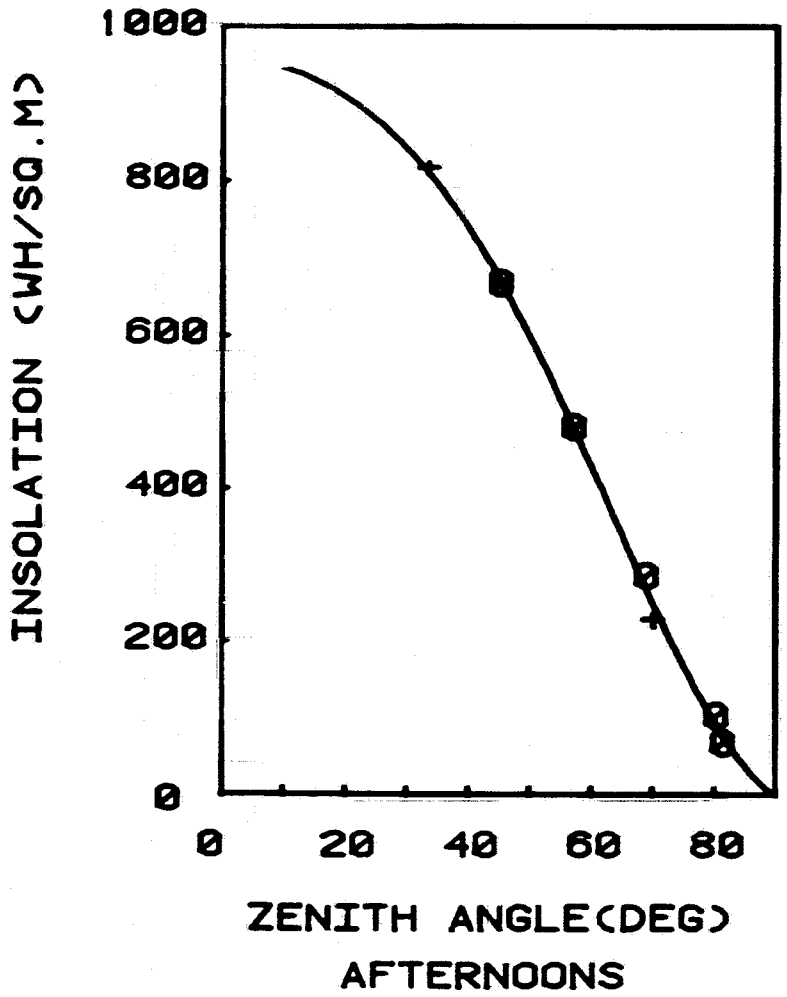

CLEAR SKY GLOBAL VS. ZENITH ANGLE
FOR THE MONTH OF JUNE 1981

O CLEAR SKY
+ NEARLY CLEAR

Figure 21

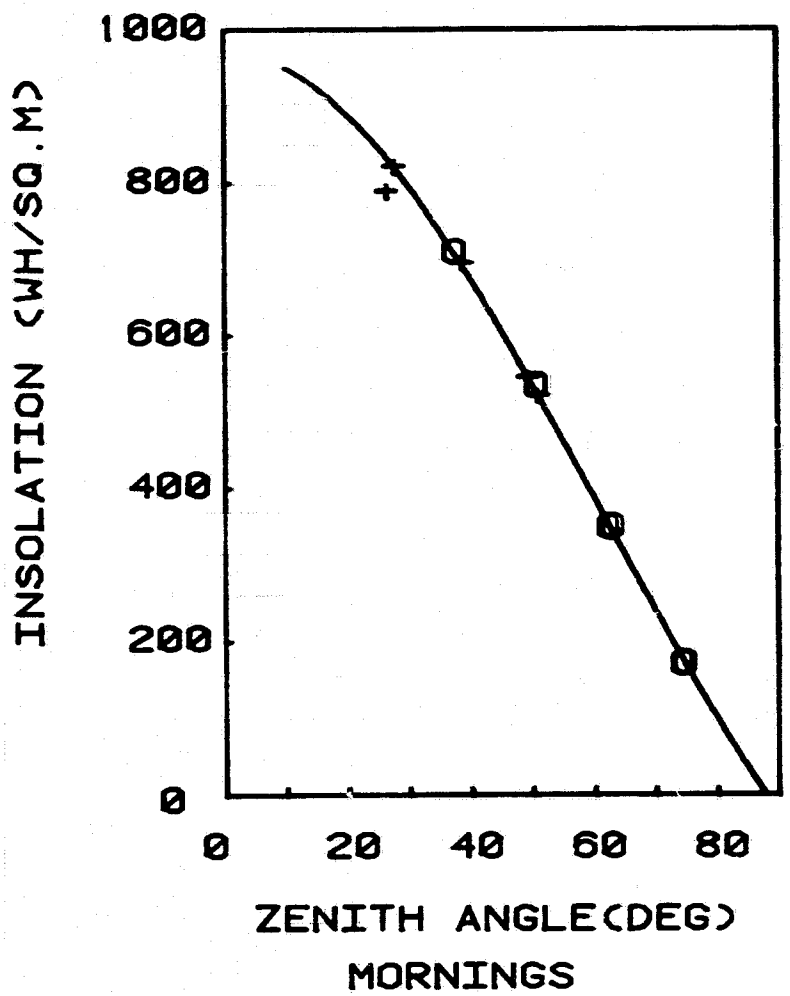

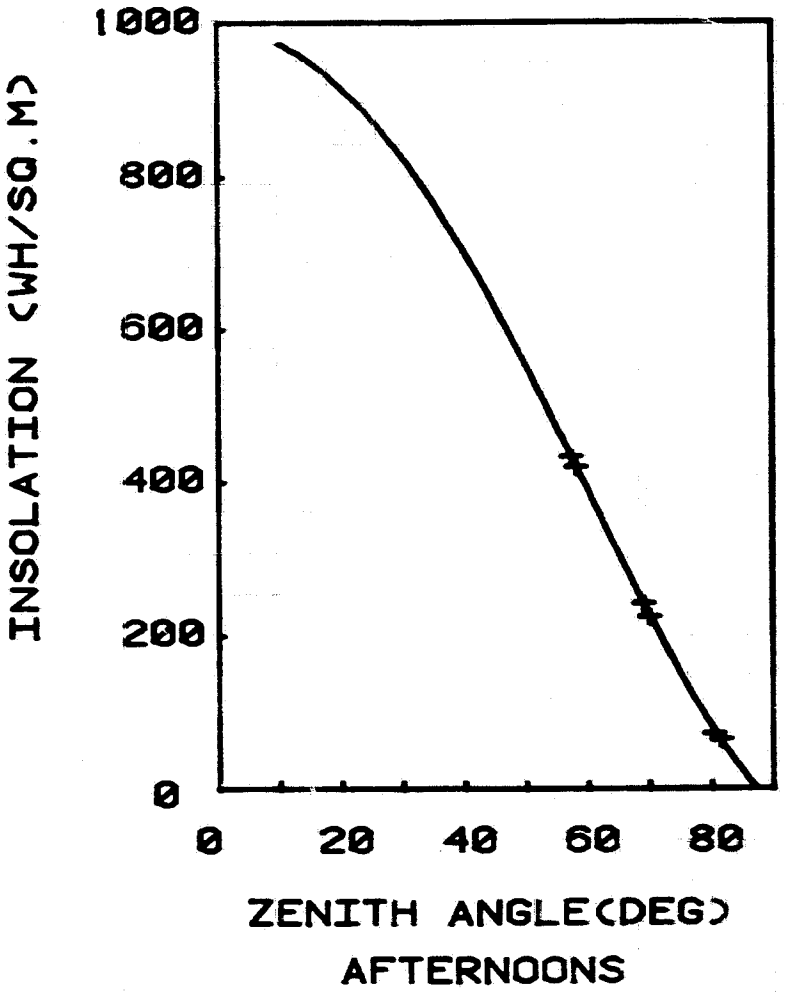

CLEAR SKY GLOBAL VS. ZENITH ANGLE
FOR THE MONTH OF JULY 1981

O CLEAR SKY
+ NEARLY CLEAR

Figure 22

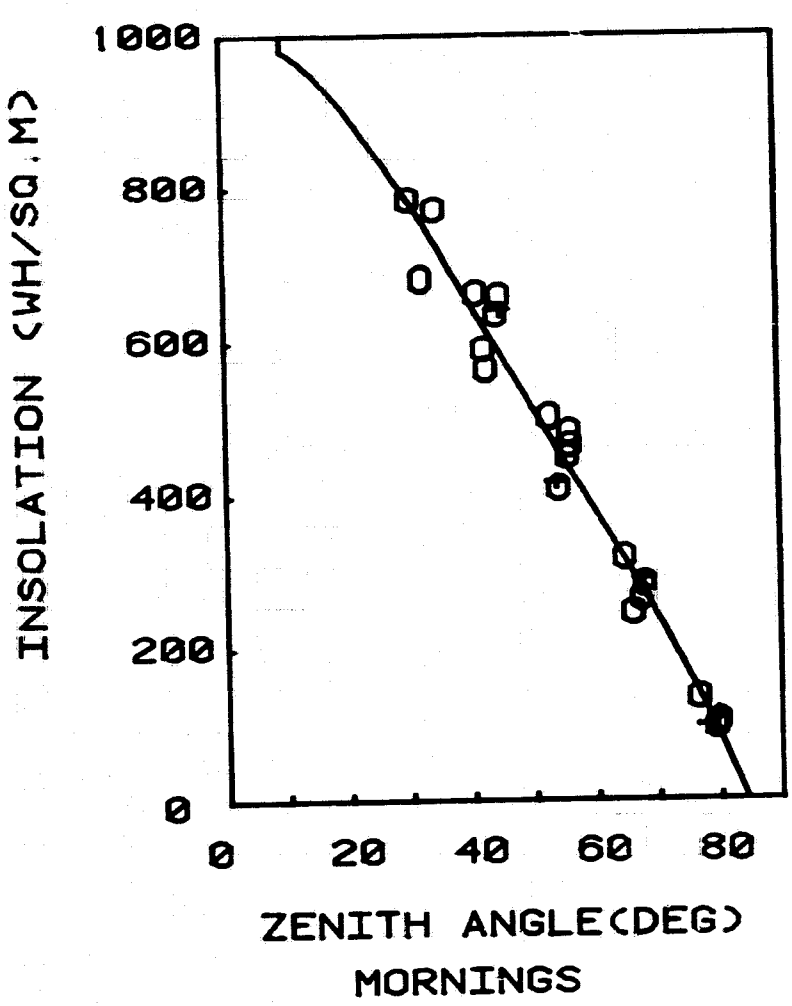

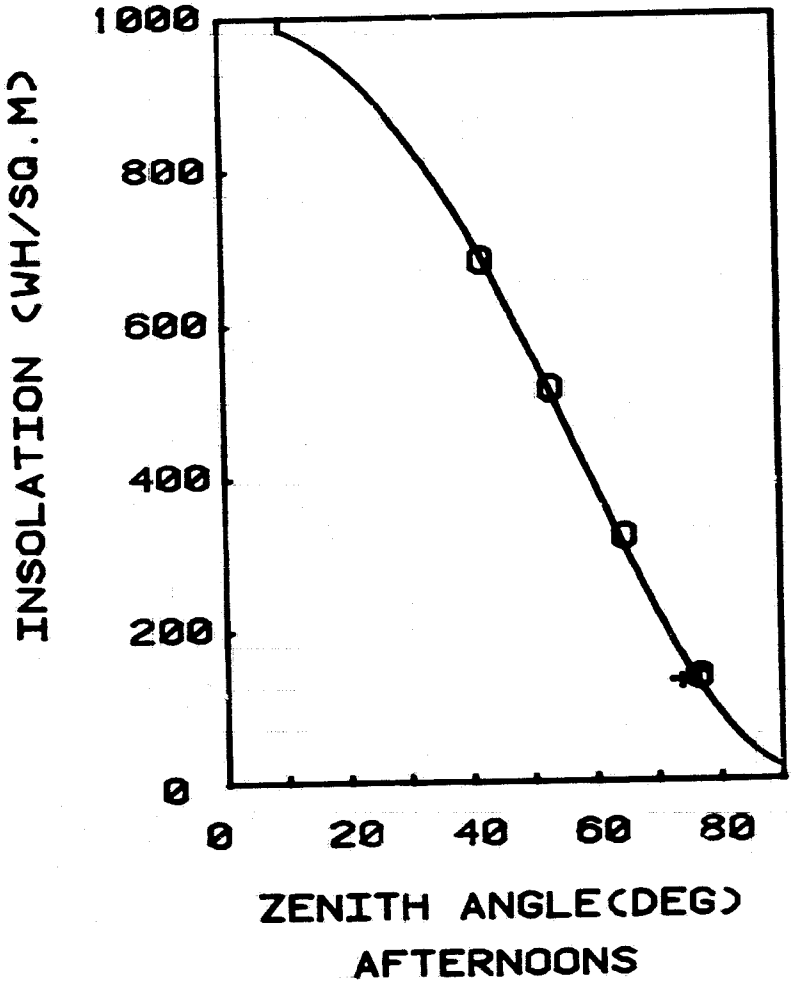

CLEAR SKY GLOBAL VS. ZENITH ANGLE
FOR THE MONTH OF AUGUST 1981

0 CLEAR SKY
+ NEARLY CLEAR

Figure 23.

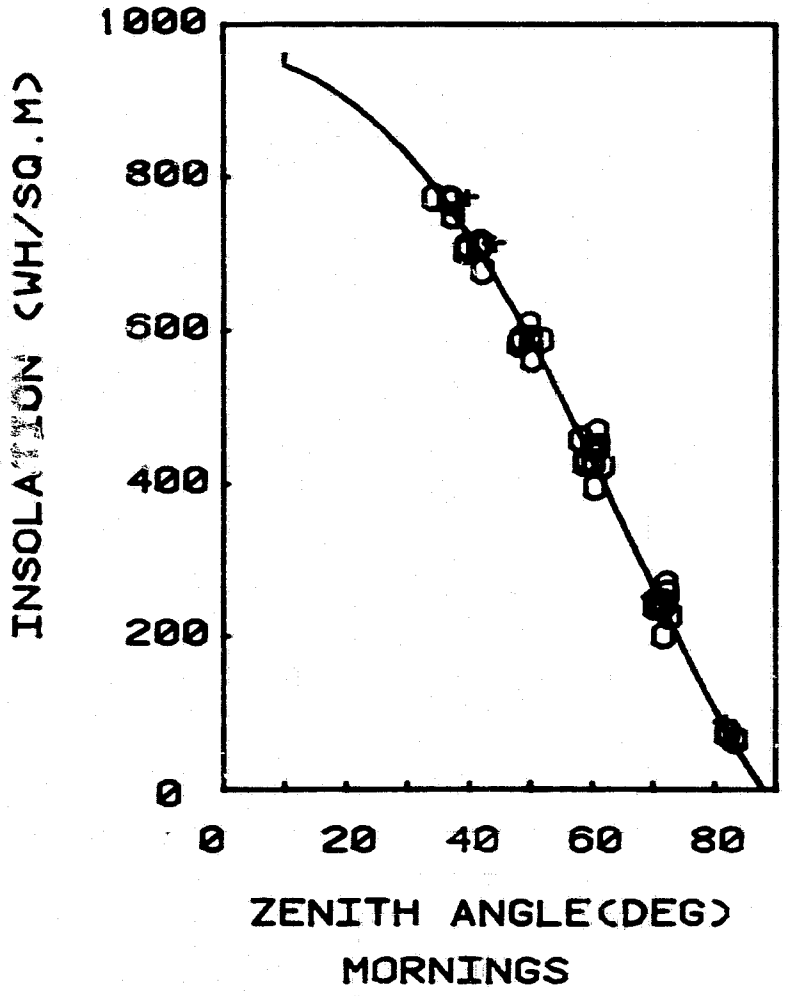

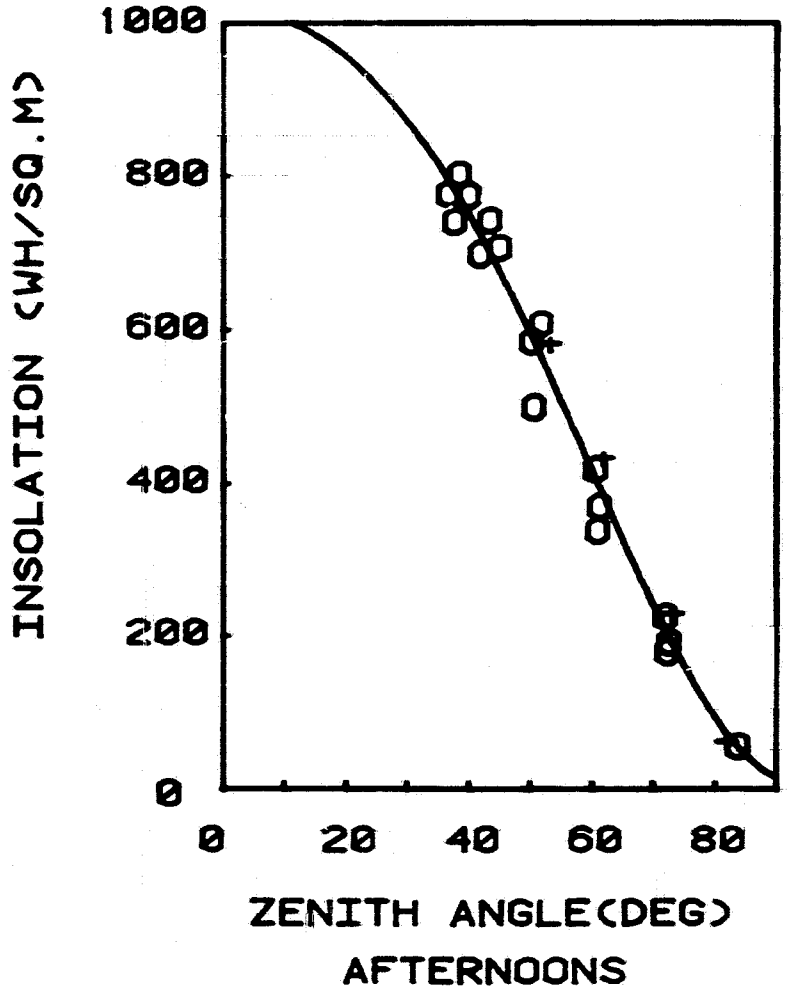

CLEAR SKY GLOBAL VS. ZENITH ANGLE
FOR THE MONTH OF SEPTEMBER 1981

O CLEAR SKY
+ NEARLY CLEAR

Figure 24

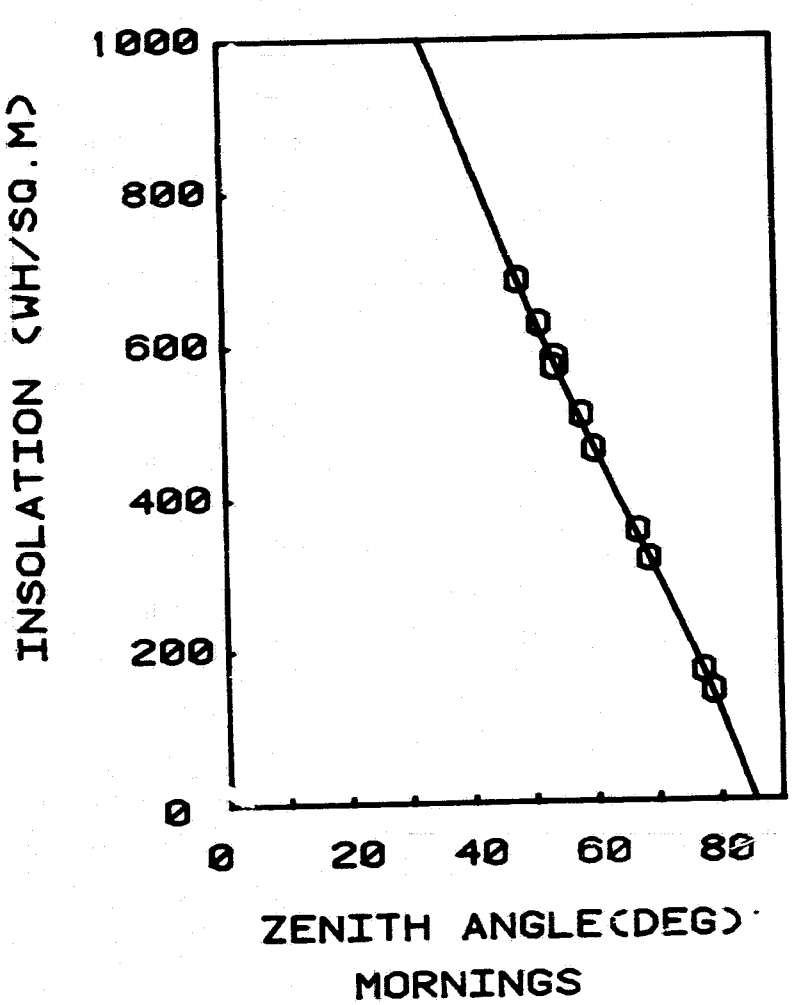

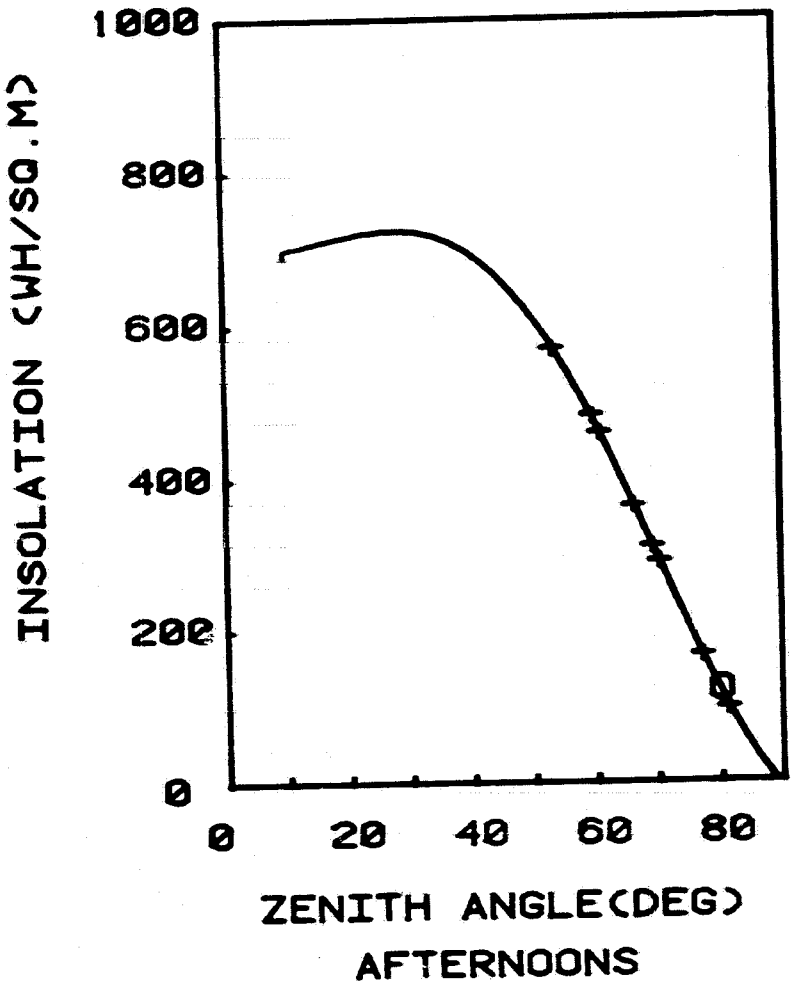

CLEAR SKY GLOBAL VS. ZENITH ANGLE
FOR THE MONTH OF OCTOBER 1981

O CLEAR SKY
+ NEARLY CLEAR

Figure 25

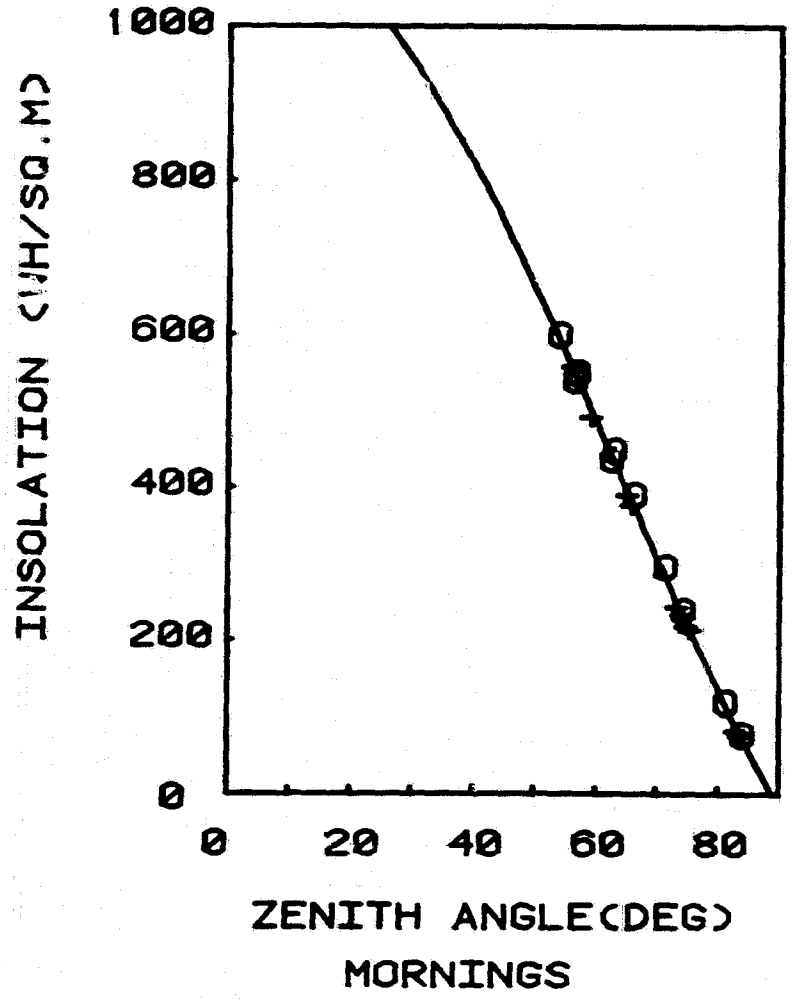

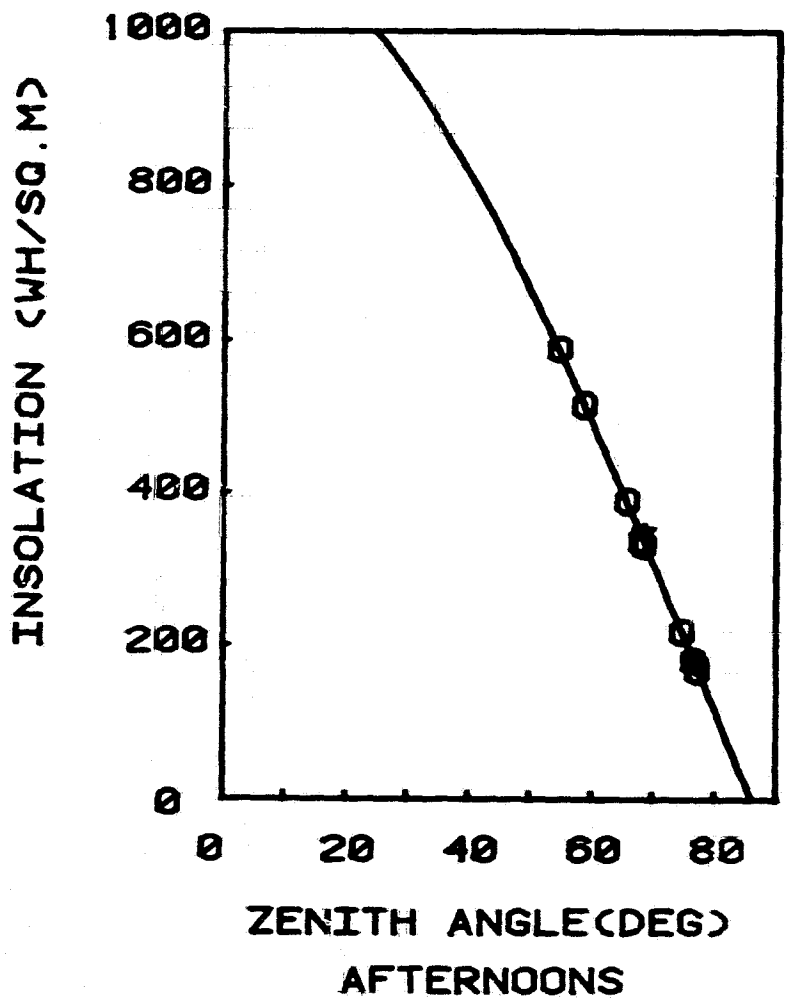

CLEAR SKY GLOBAL VS. ZENITH ANGLE
FOR THE MONTH OF NOVEMBER 1981

O CLEAR SKY
+ NEARLY CLEAR

Figure 26

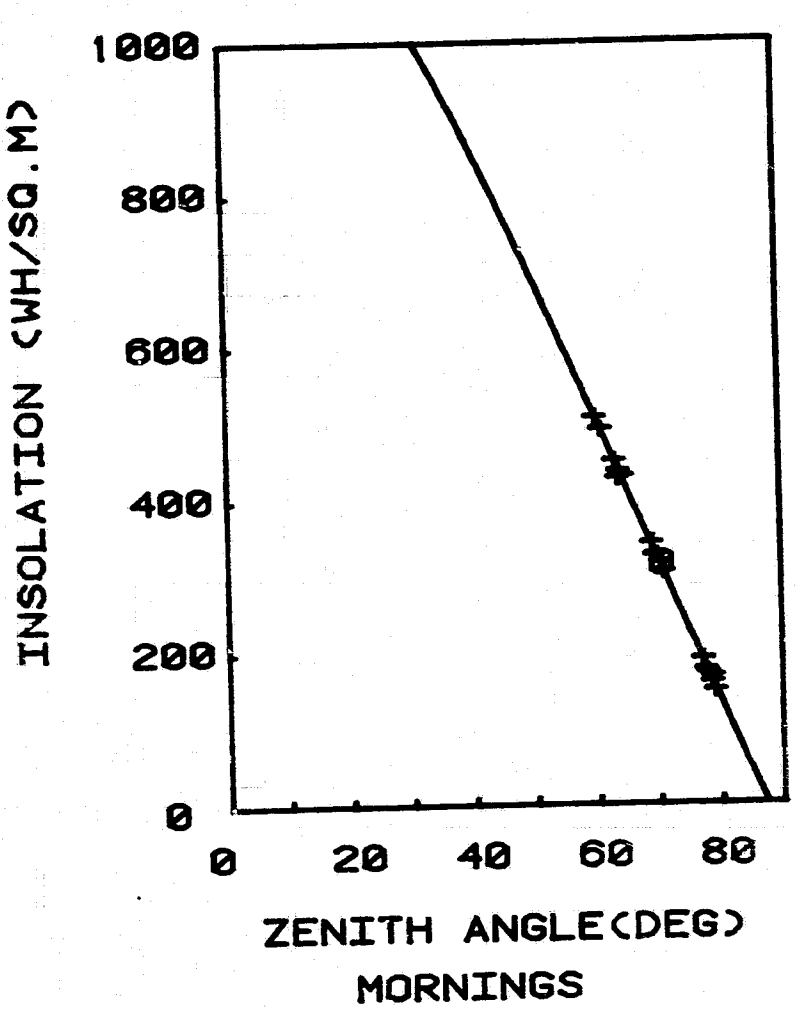

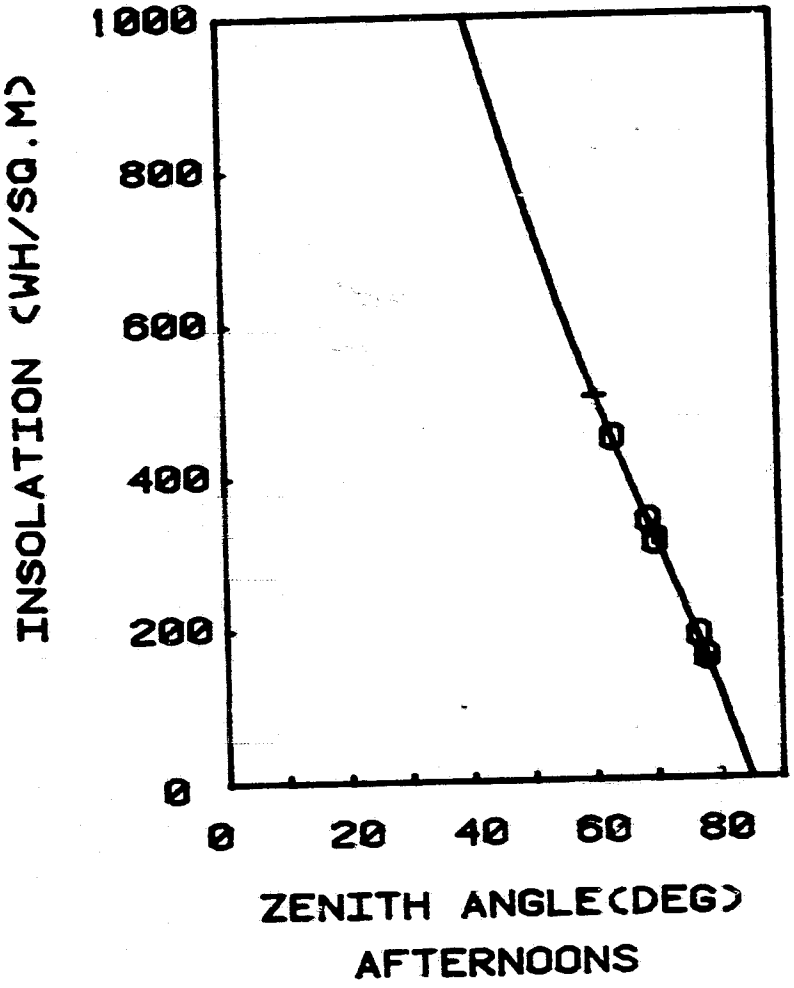

CLEAR SKY GLOBAL VS. ZENITH ANGLE
FOR THE MONTH OF DECEMBER 1981

·O CLEAR SKY
+ NEARLY CLEAR

Figure 27

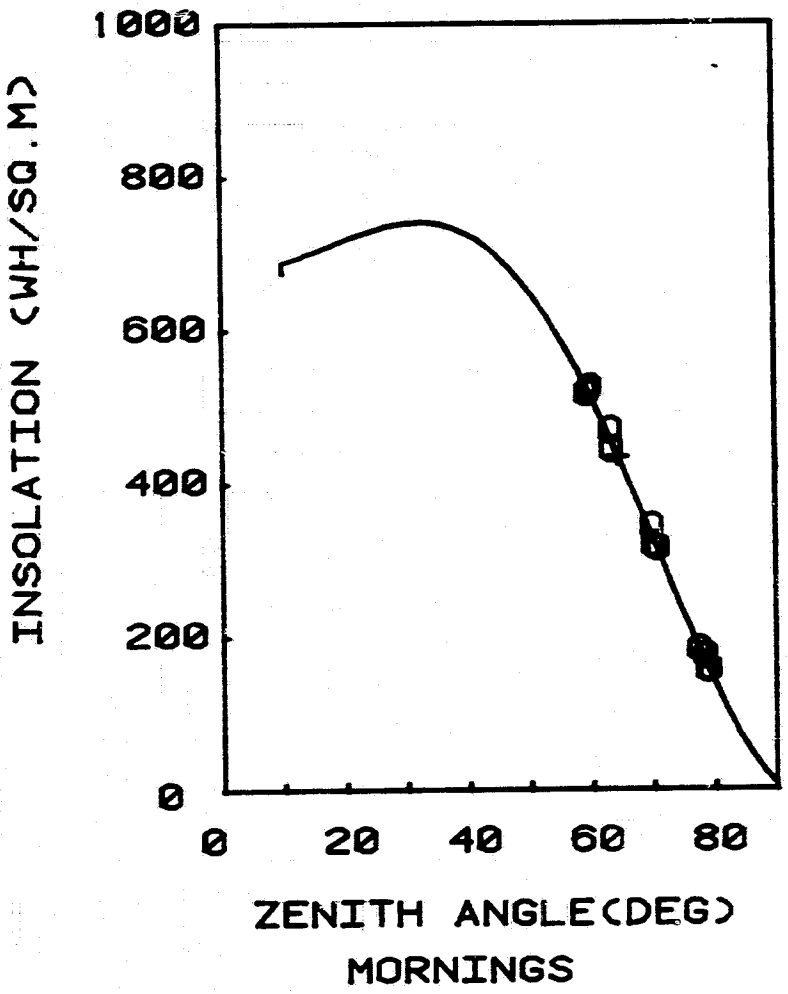

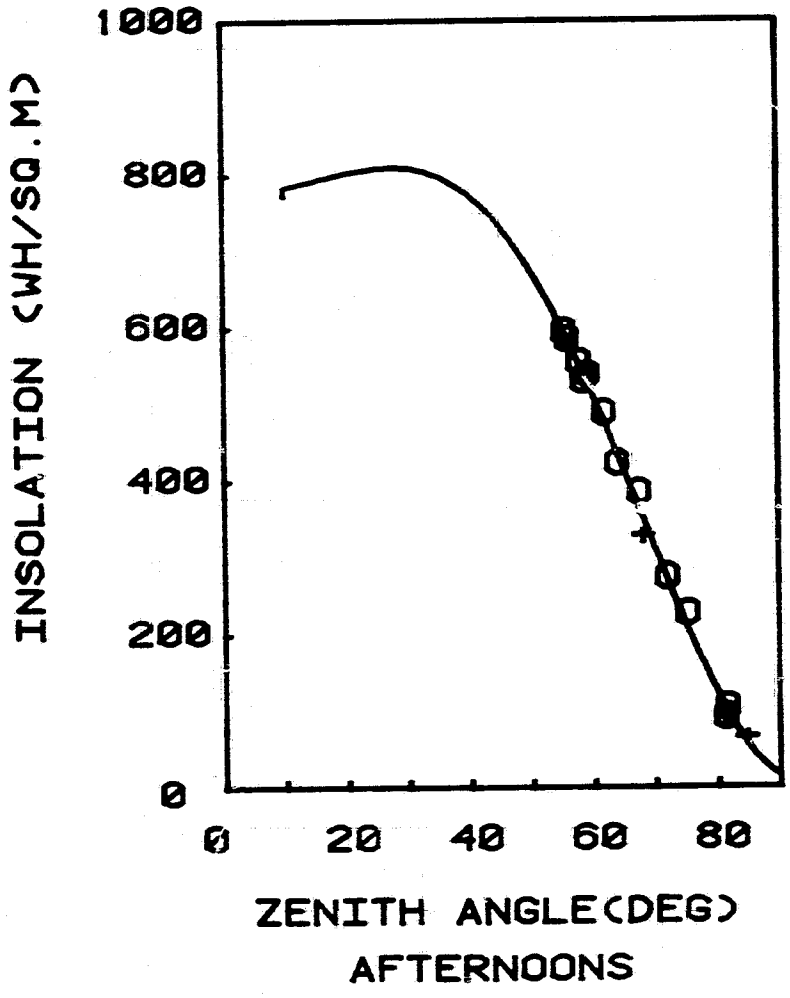

CLEAR SKY GLOBAL VS. ZENITH ANGLE
FOR THE MONTH OF JANUARY 1982

0 CLEAR SKY
+ NEARLY CLEAR

Figure 28

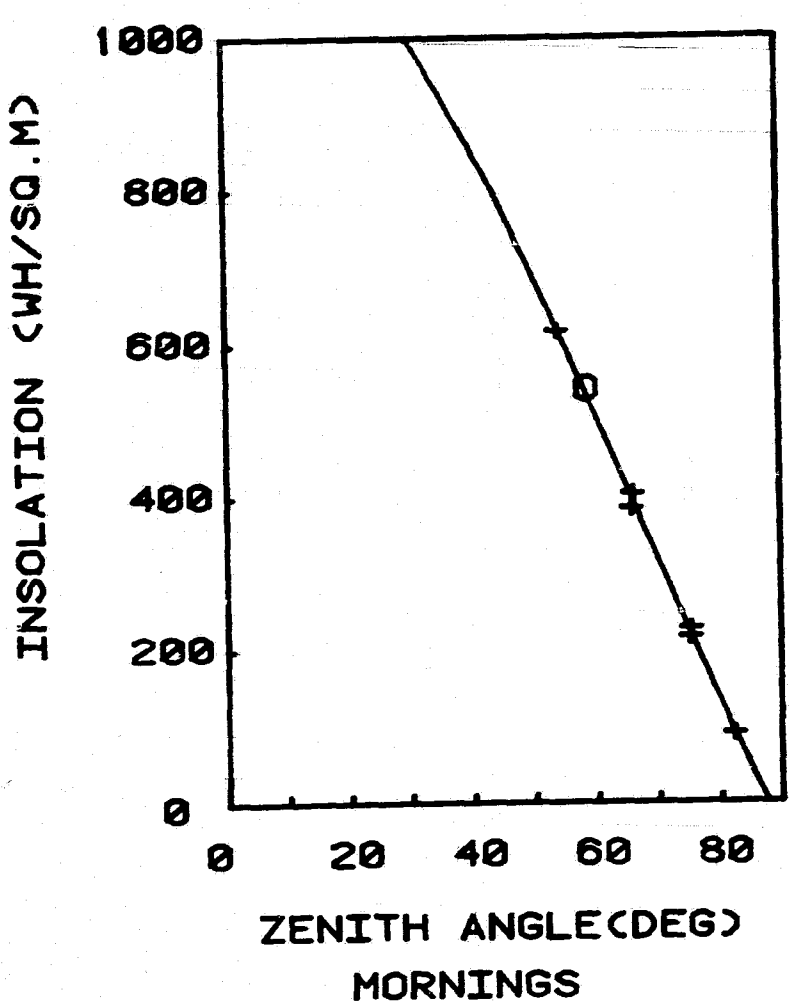

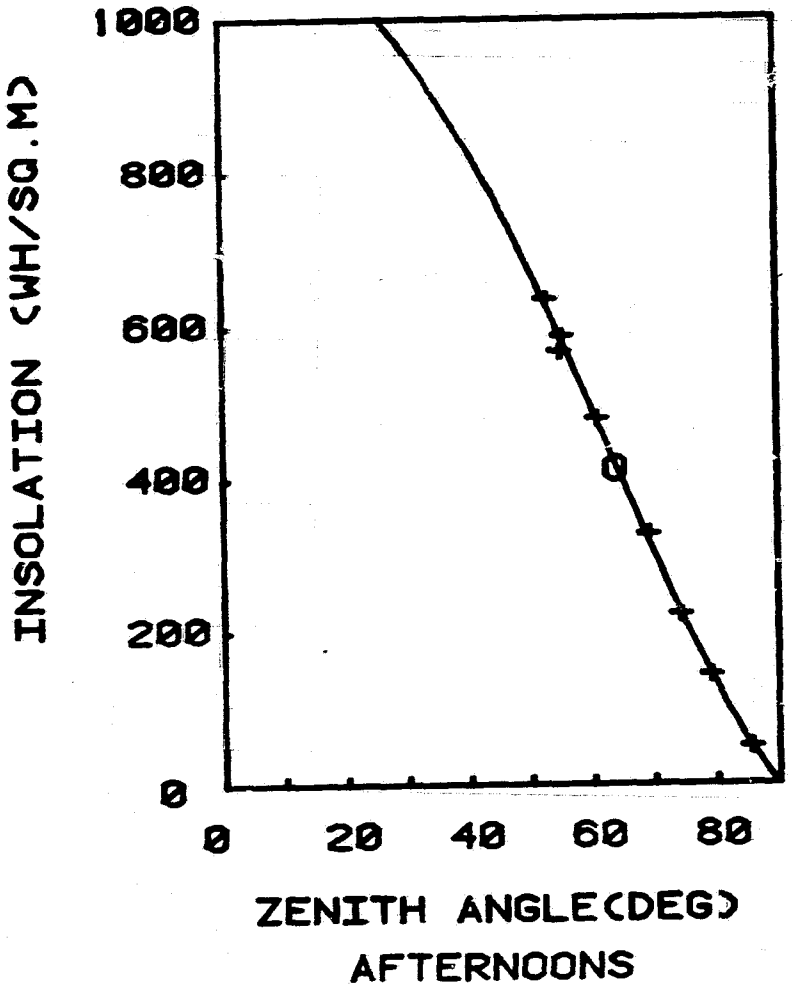

CLEAR SKY GLOBAL VS. ZENITH ANGLE
FOR THE MONTH OF FEBRUARY 1982

0 CLEAR SKY
+ NEARLY CLEAR

Figure 29

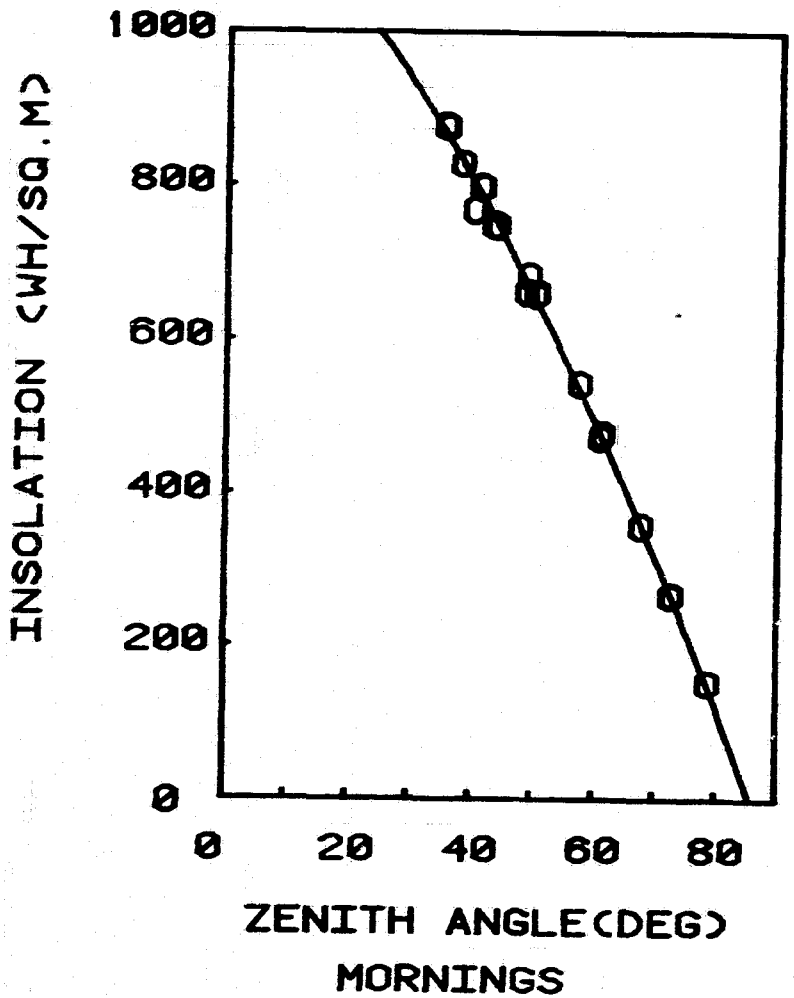

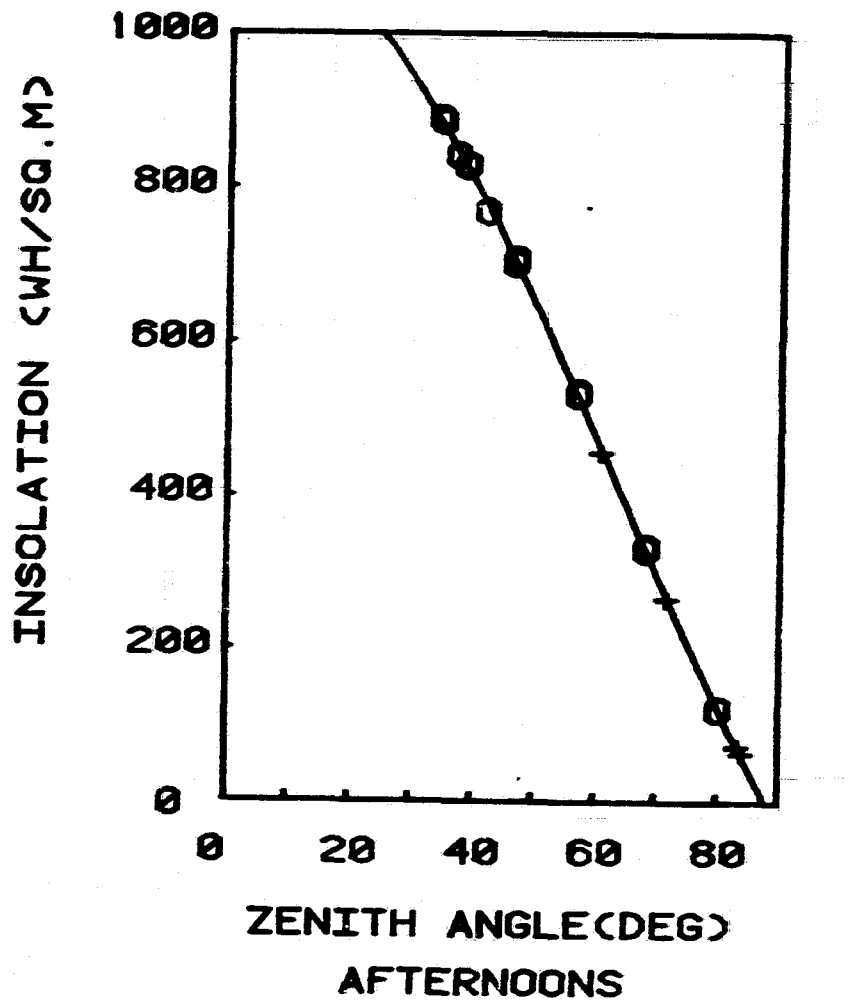

CLEAR SKY GLOBAL VS. ZENITH ANGLE
FOR THE MONTH OF MARCH 1982

O CLEAR SKY
+ NEARLY CLEAR

Figure 30

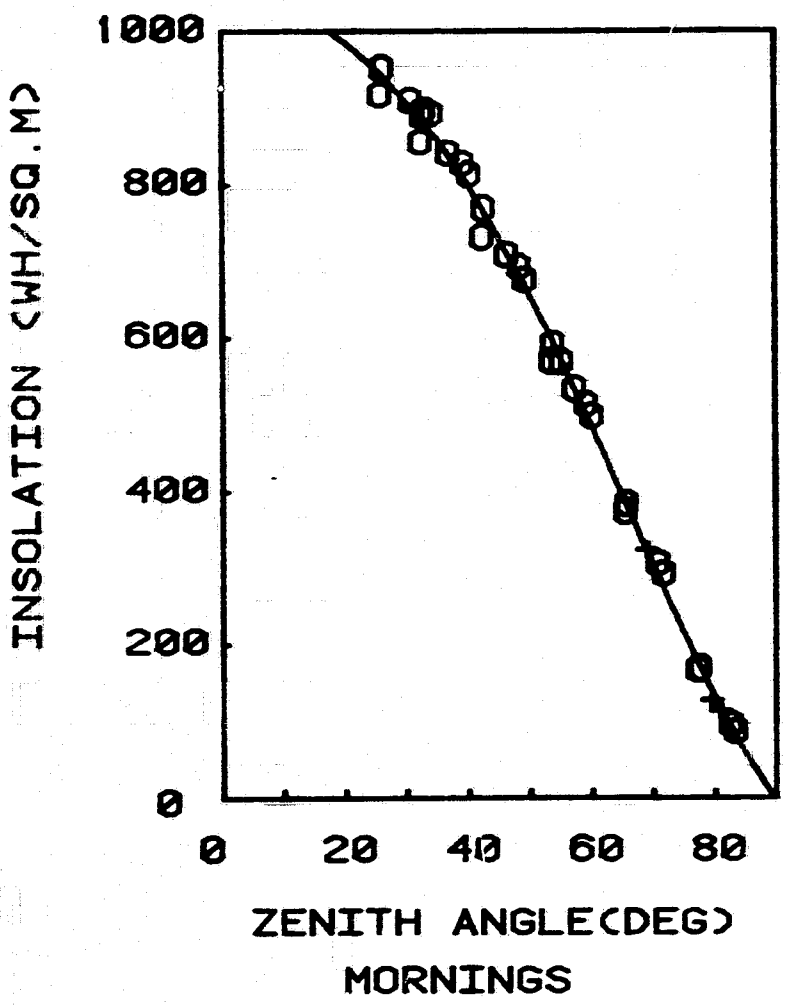

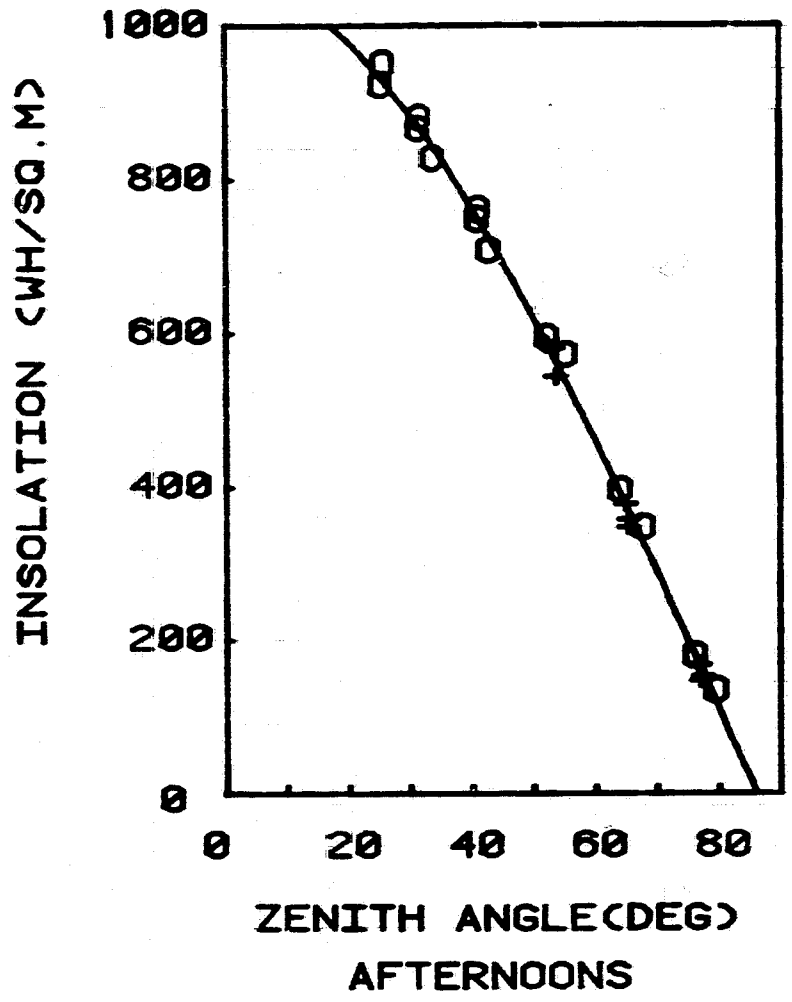

CLEAR SKY GLOBAL VS. ZENITH ANGLE
FOR THE MONTH OF APRIL 1982

O CLEAR SKY
+ NEARLY CLEAR

Figure 31

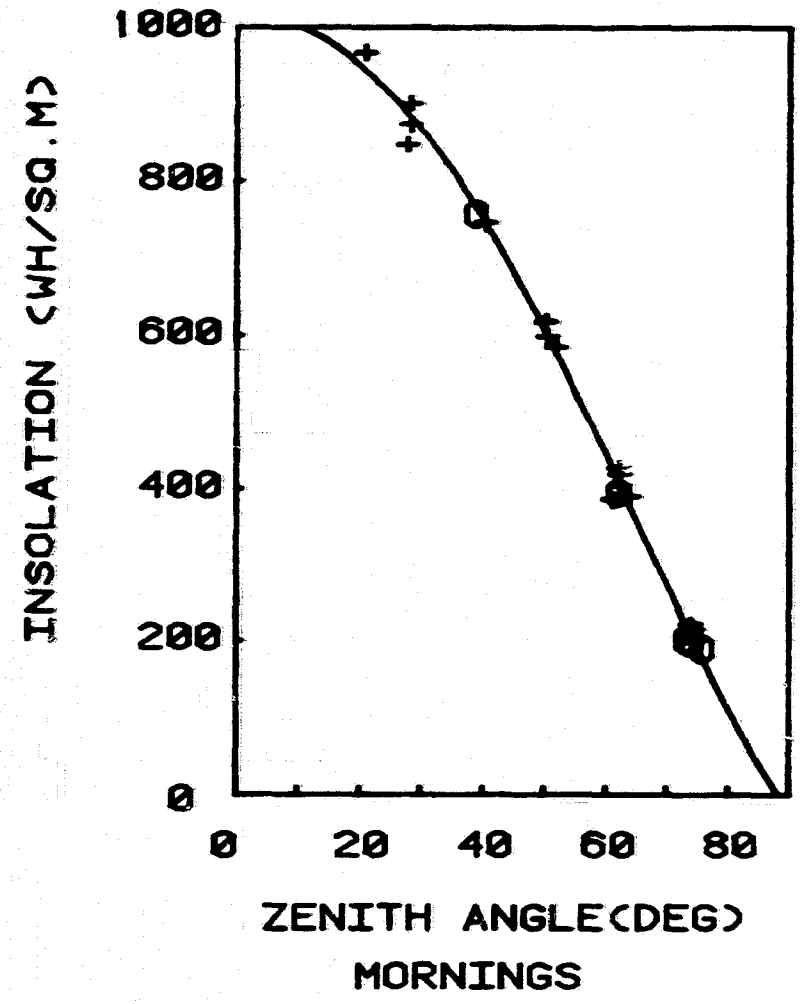

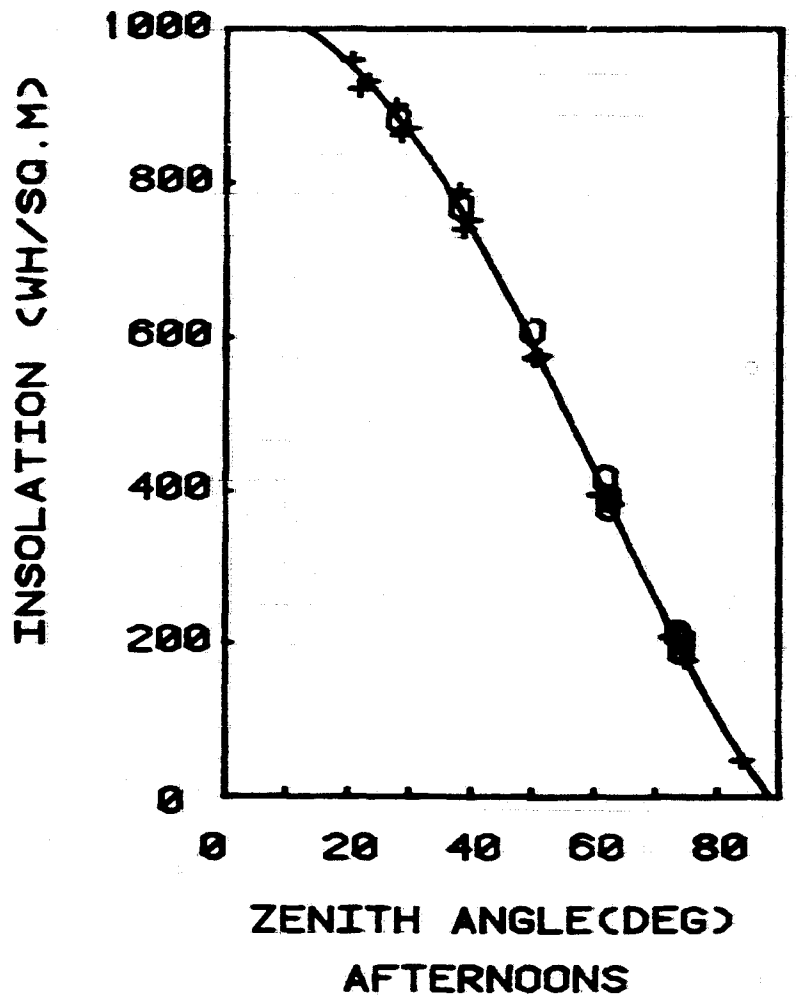

CLEAR SKY GLOBAL VS. ZENITH ANGLE
FOR THE MONTH OF MAY 1982

O CLEAR SKY
+ NEARLY CLEAR

Figure 32

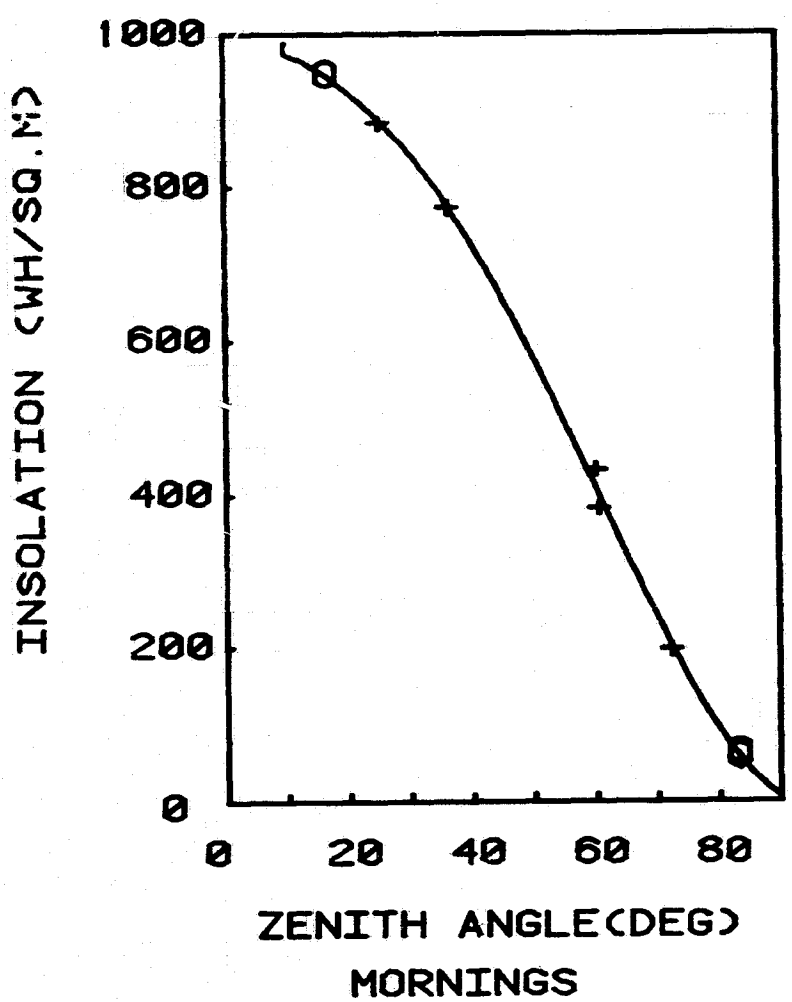

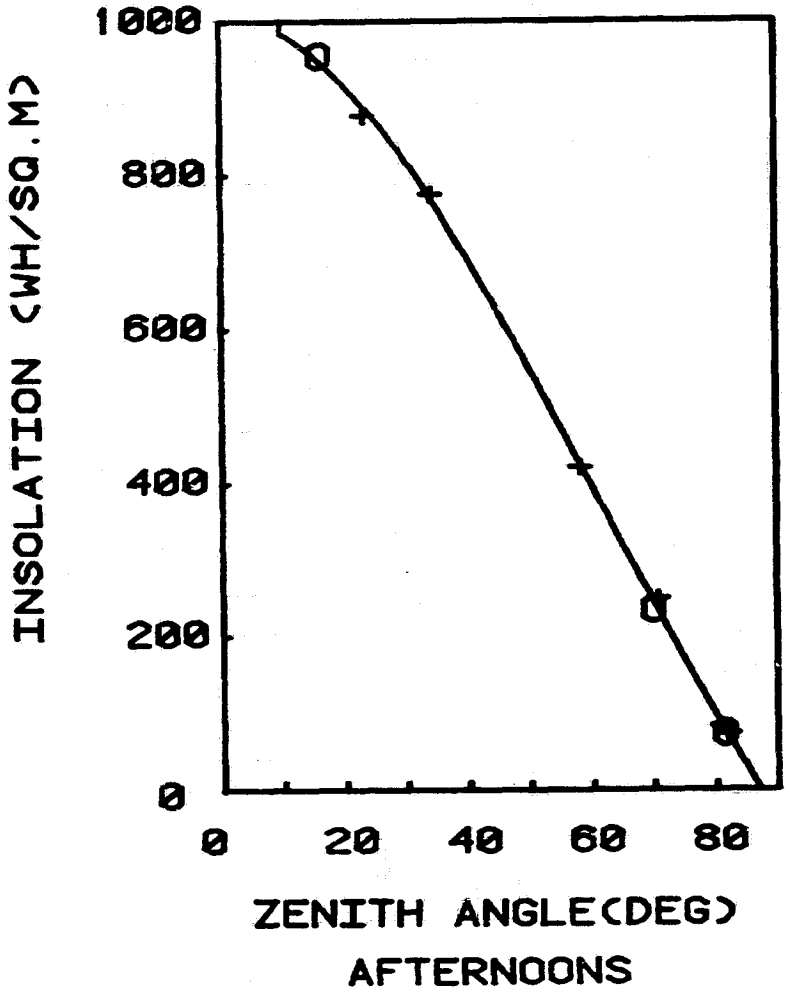

CLEAR SKY GLOBAL VS. ZENITH ANGLE
FOR THE MONTH OF JUNE 1982

O CLEAR SKY
+ NEARLY CLEAR

Figure 33

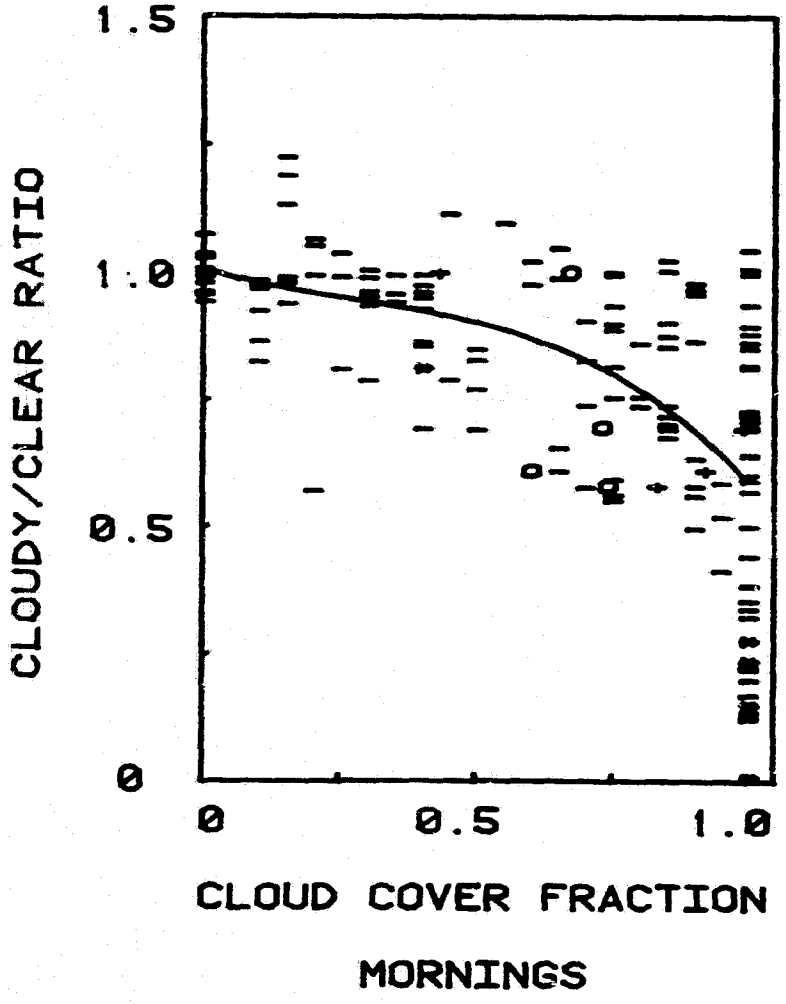

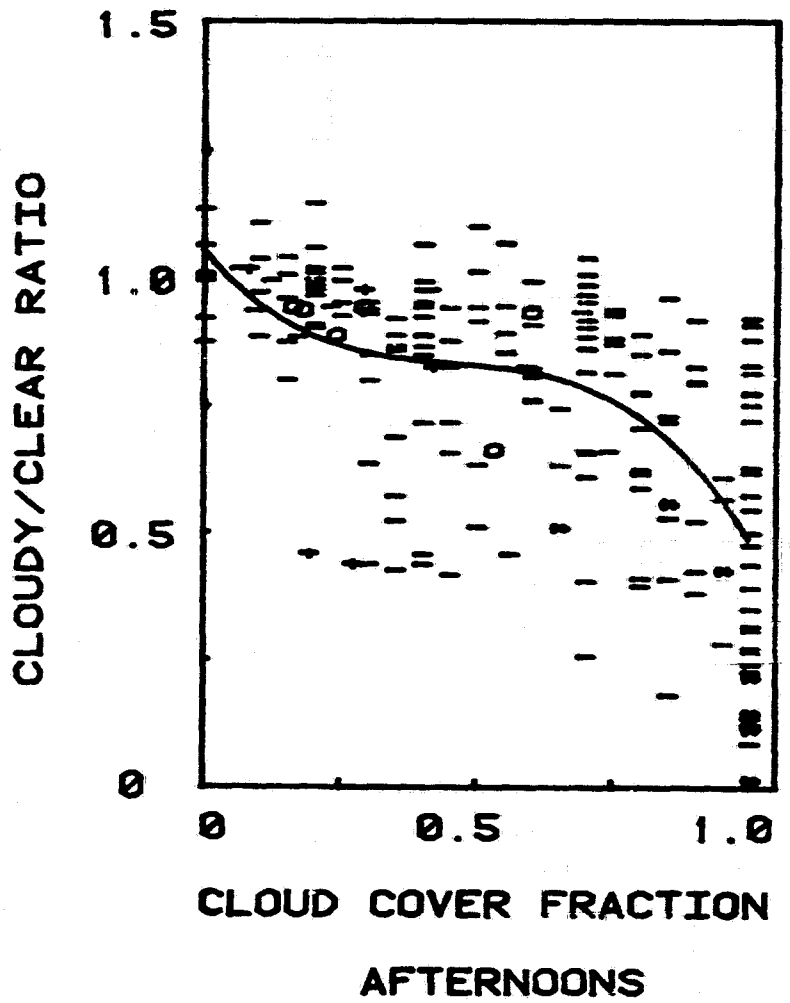

ORIGINAL PAGE IS
OF POOR QUALITY

NORM. GLOBAL VS. CLOUD COVER FRACTION
FOR THE MONTH OF JUNE 1981

–	LAFB VISUAL
O	SATELLITE PHOTO
+	WHOLE SKY PHOTO
*	PRECIPITATION

Figure 34

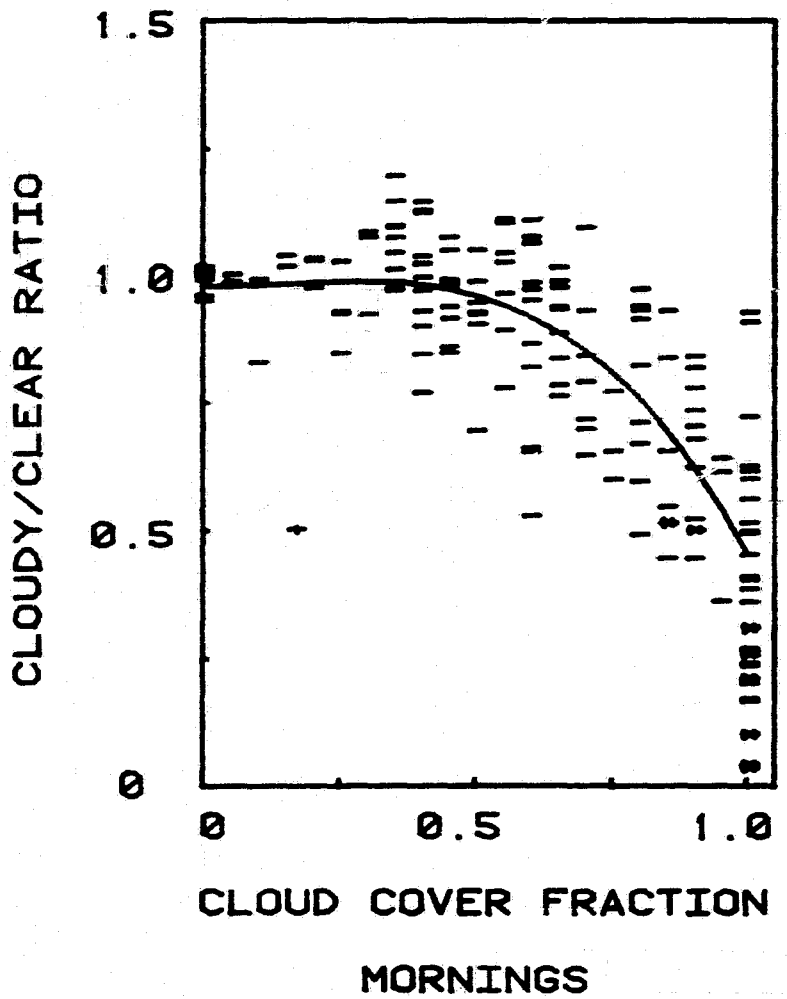

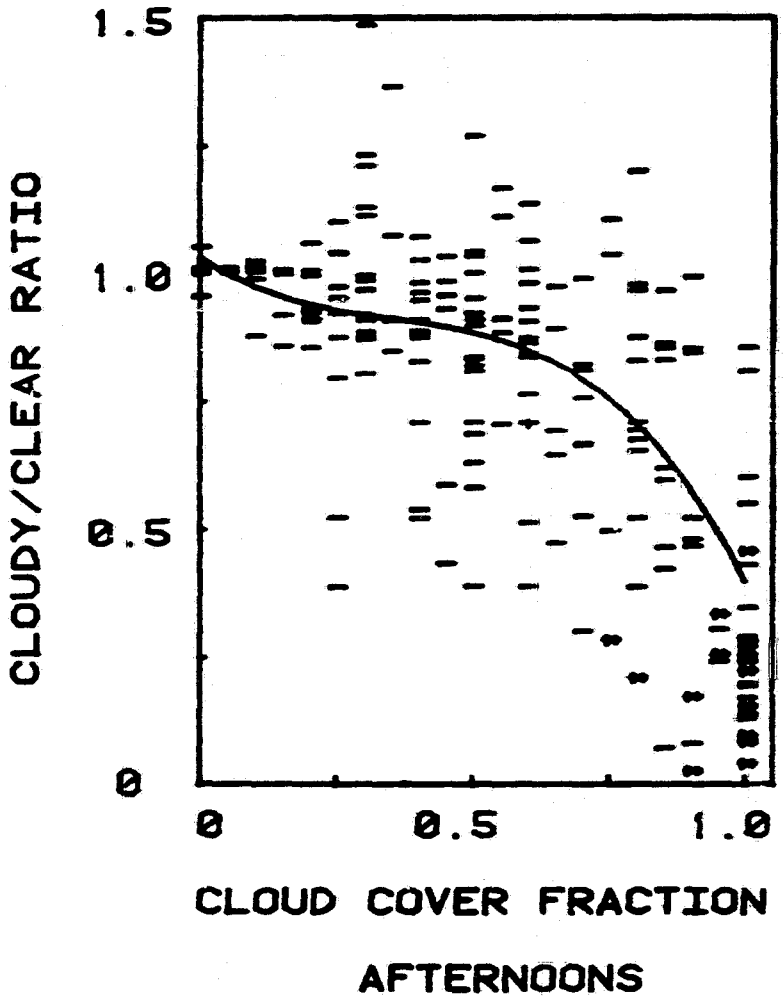

NORM. GLOBAL VS. CLOUD COVER FRACTION
FOR THE MONTH OF JULY 1981

–	LAFB VISUAL
O	SATELLITE PHOTO
+	WHOLE SKY PHOTO
*	PRECIPITATION

Figure 35

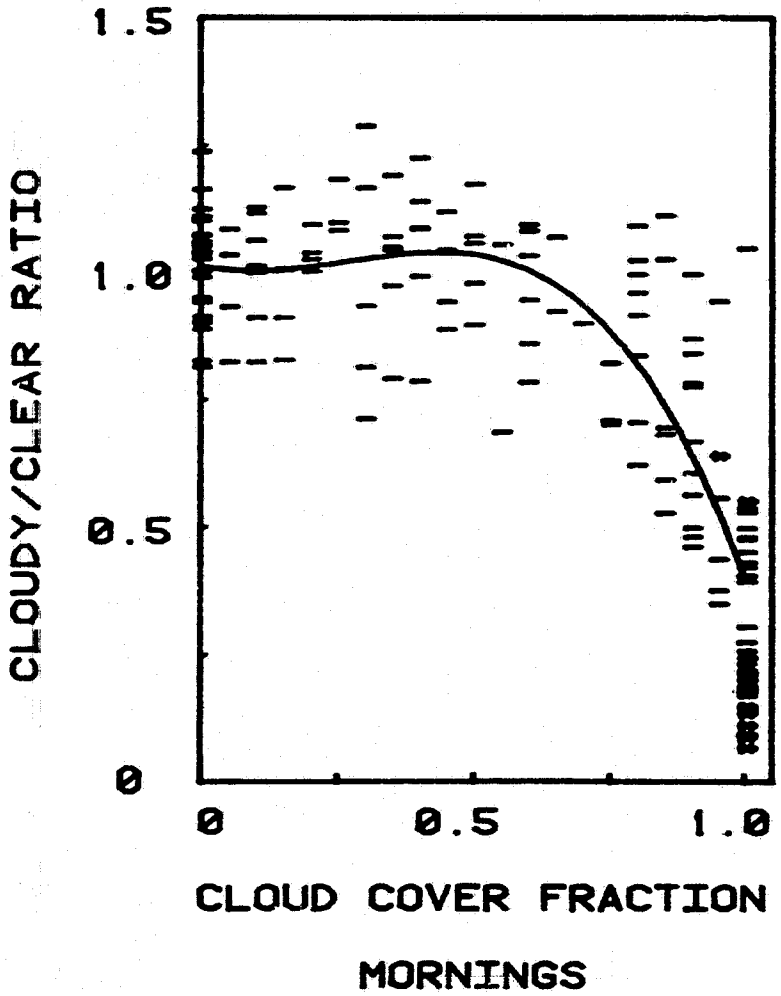

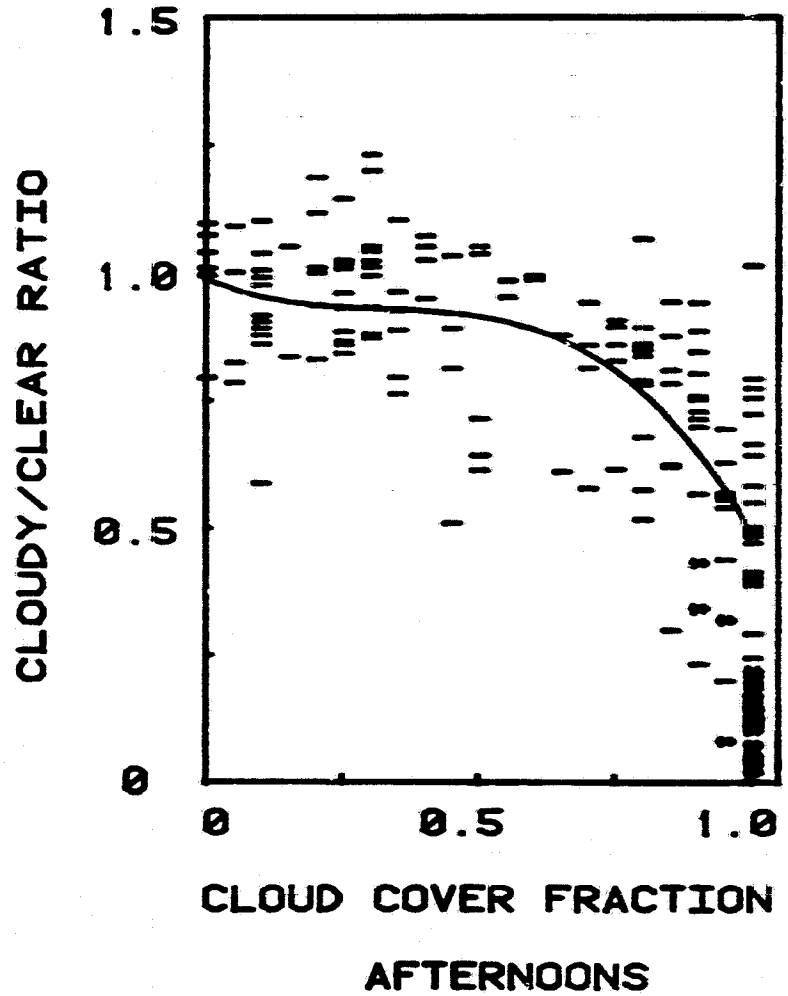

ORIGINAL PAGE IS
OF POOR QUALITY

NORM. GLOBAL VS. CLOUD COVER FRACTION
FOR THE MONTH OF AUGUST 1981

–	LAFB VISUAL
O	SATELLITE PHOTO
+	WHOLE SKY PHOTO
*	PRECIPITATION

Figure 36

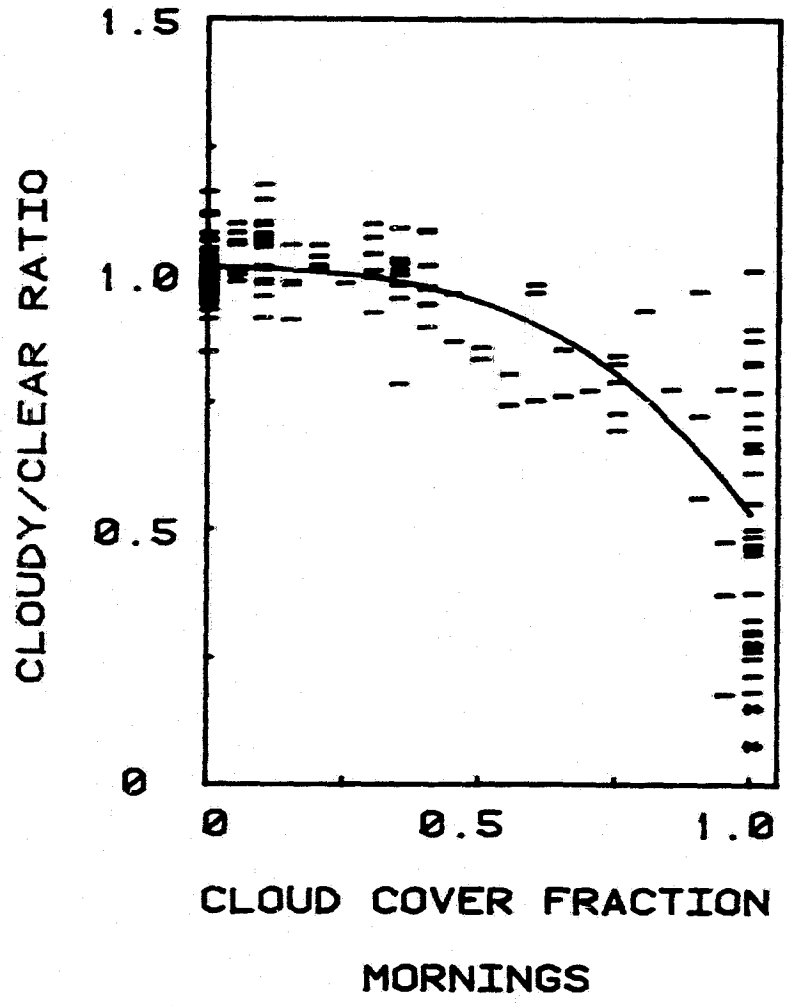

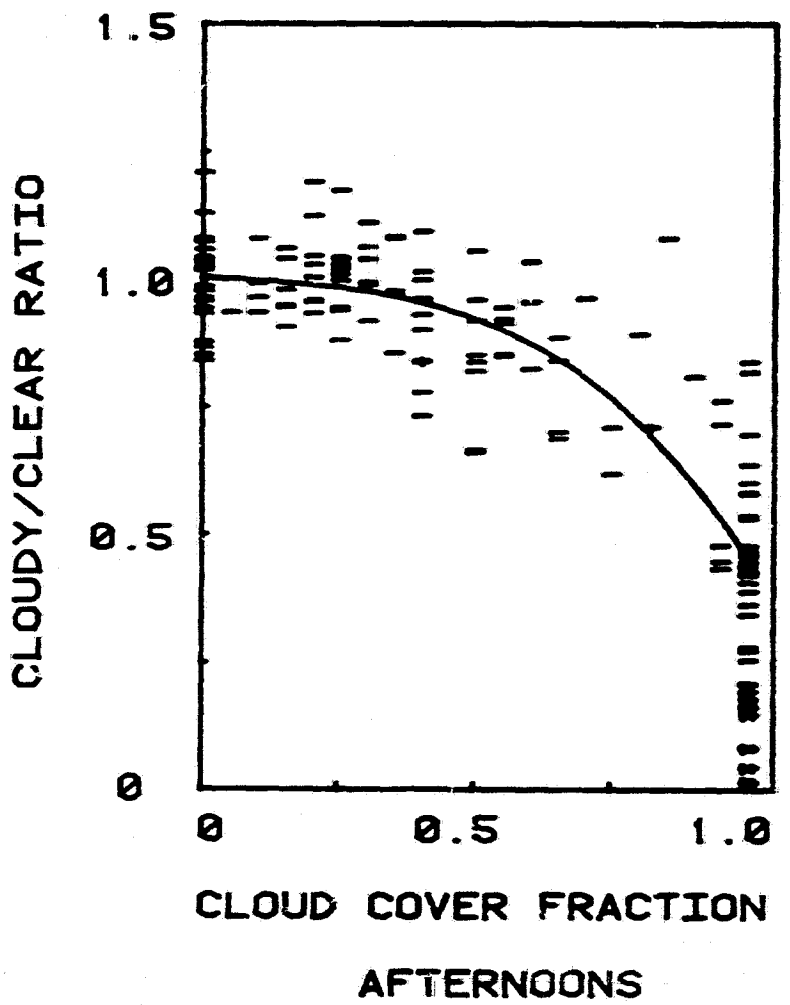

NORM. GLOBAL VS. CLOUD COVER FRACTION
FOR THE MONTH OF SEPTEMBER 1981

–	LAFB VISUAL
O	SATELLITE PHOTO
+	WHOLE SKY PHOTO
*	PRECIPITATION

Figure 37

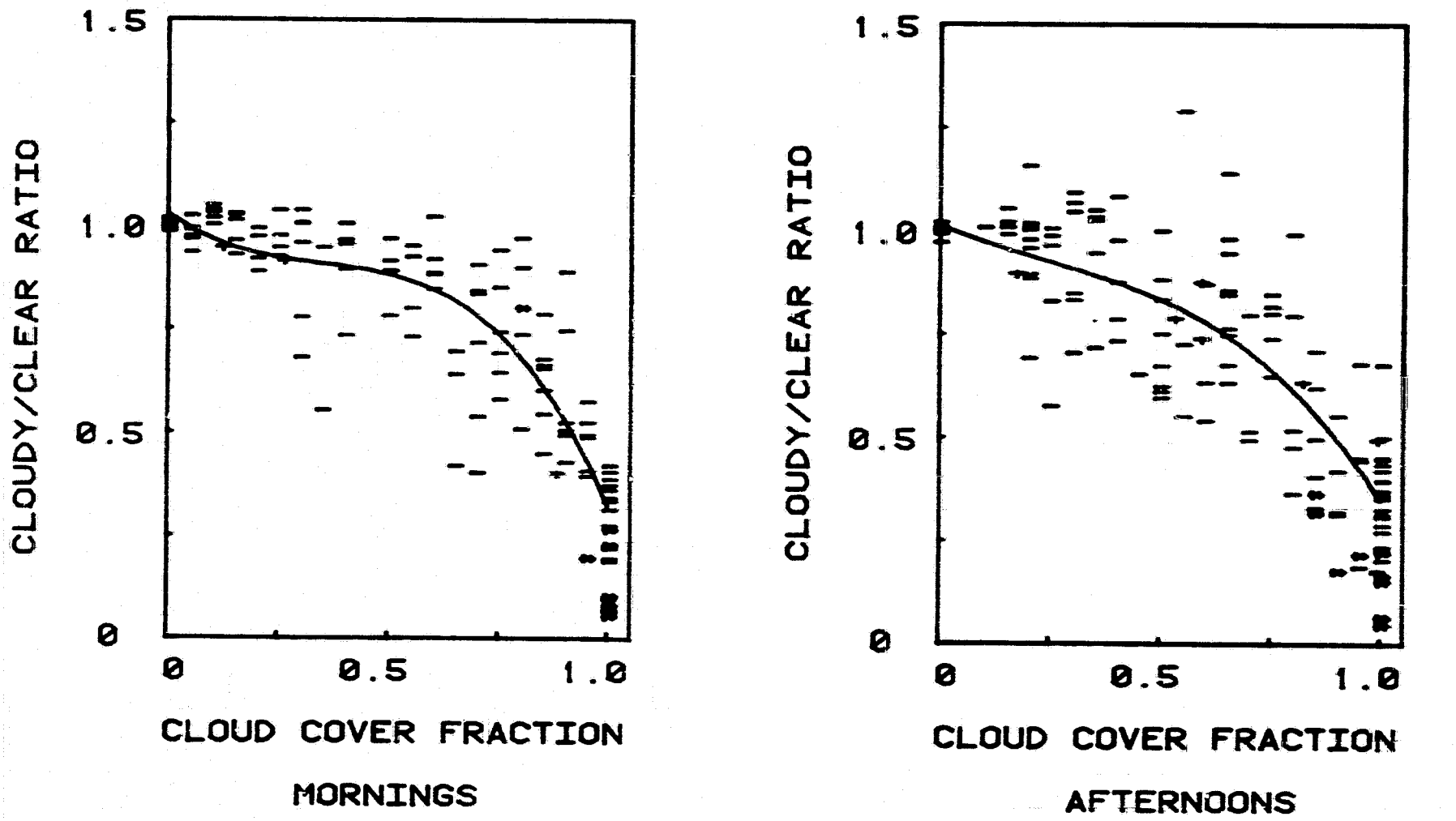

NORM. GLOBAL VS. CLOUD COVER FRACTION
FOR THE MONTH OF OCTOBER 1981

–	LAFB VISUAL
O	SATELLITE PHOTO
+	WHOLE SKY PHOTO
*	PRECIPITATION

Figure 38

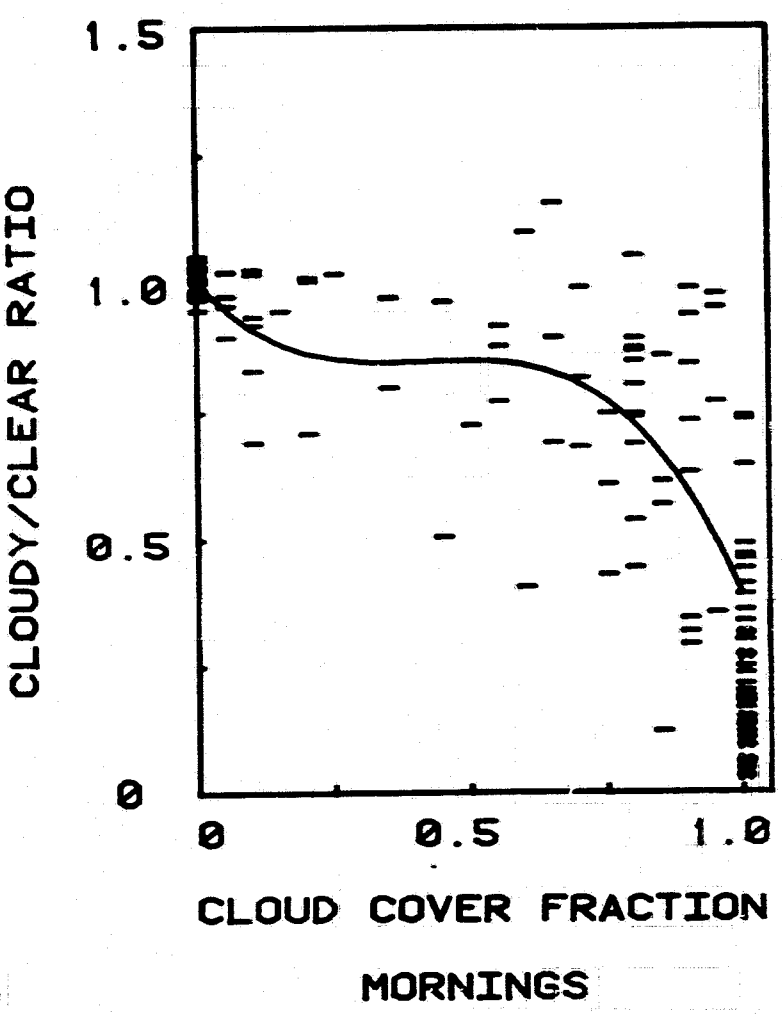

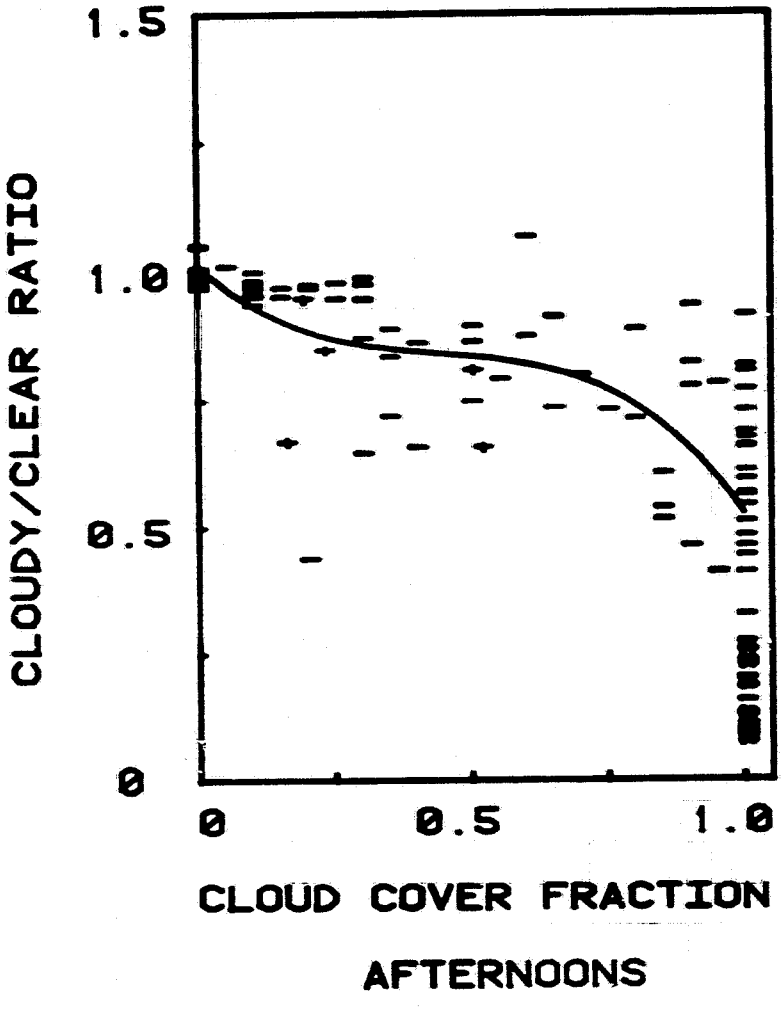

NORM. GLOBAL VS. CLOUD COVER FRACTION
FOR THE MONTH OF NOVEMBER 1981

–	LAFB VISUAL
O	SATELLITE PHOTO
+	WHOLE SKY PHOTO
*	PRECIPITATION

Figure 39

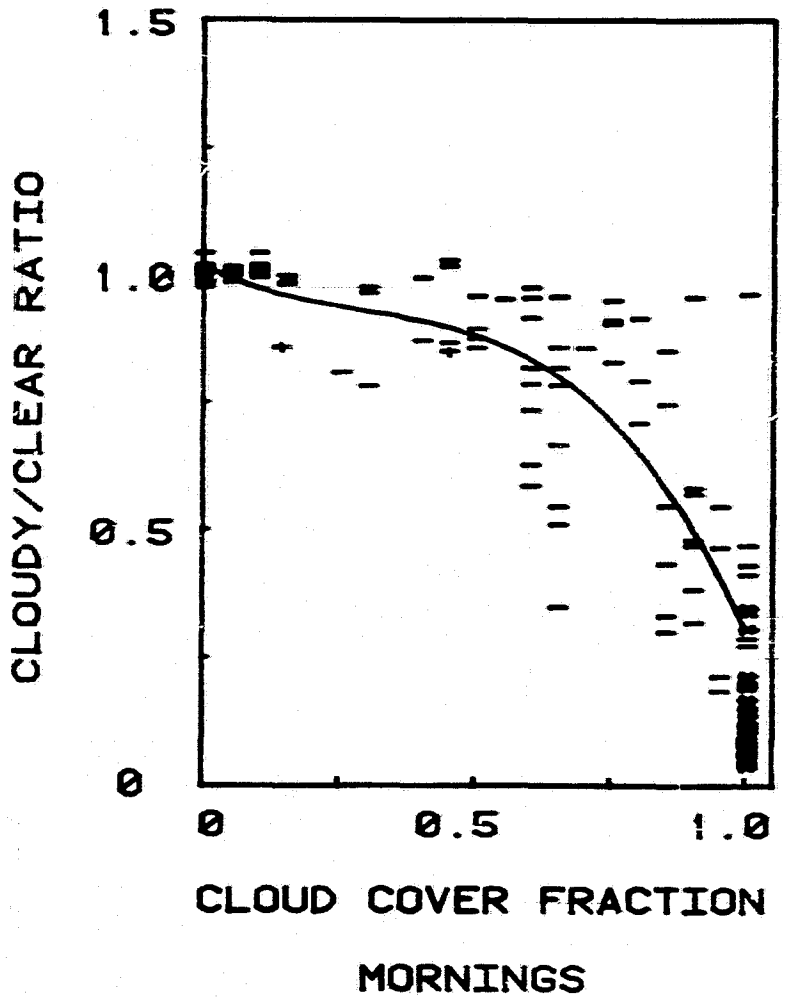

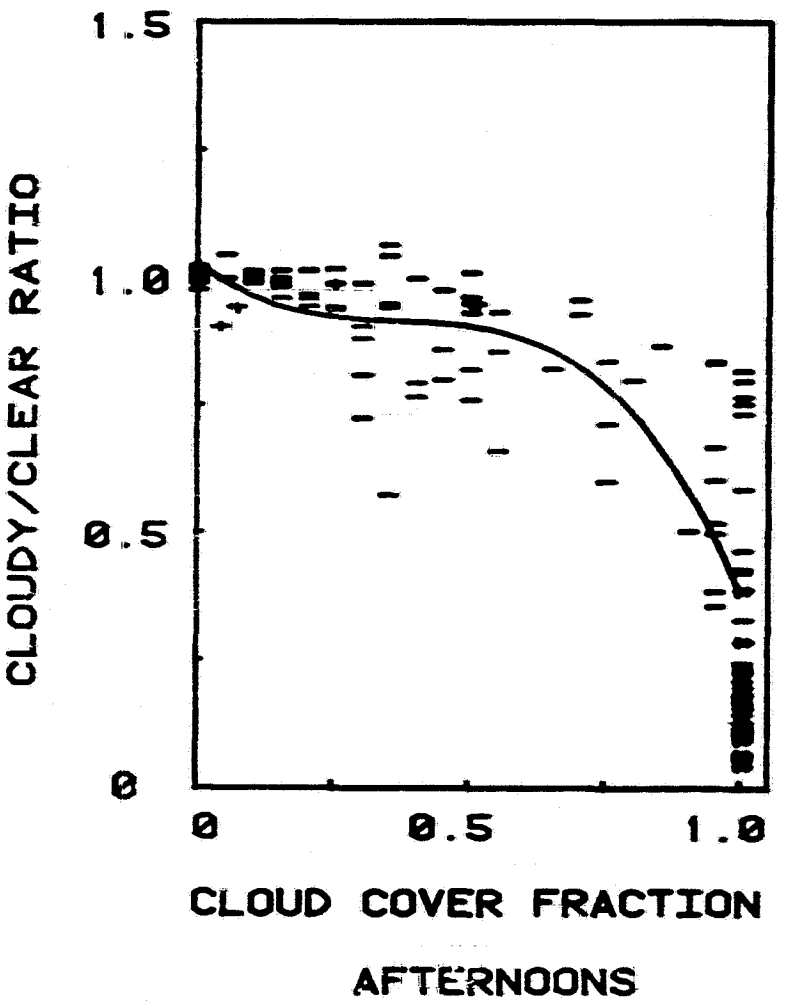

NORM. GLOBAL VS. CLOUD COVER FRACTION
FOR THE MONTH OF DECEMBER 1981

–	LAFB VISUAL
O	SATELLITE PHOTO
+	WHOLE SKY PHOTO
*	PRECIPITATION

Figure 40

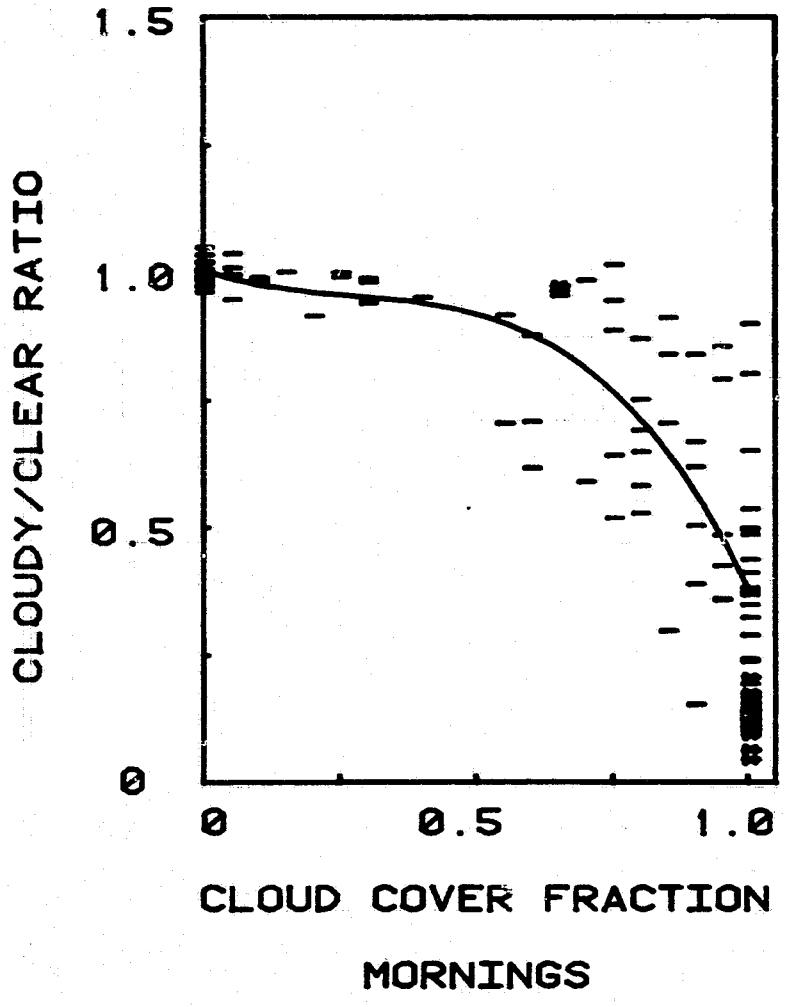

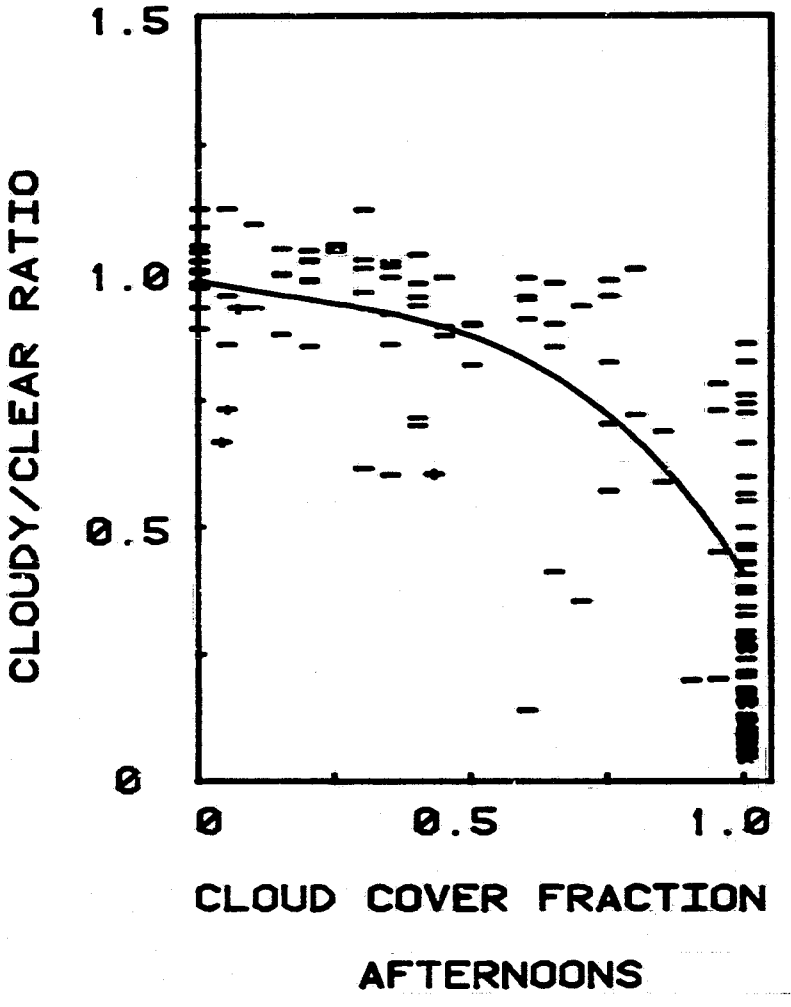

NORM. GLOBAL VS. CLOUD COVER FRACTION
FOR THE MONTH OF JANUARY 1982

–	LAFB VISUAL
O	SATELLITE PHOTO
+	WHOLE SKY PHOTO
*	PRECIPITATION

Figure 41

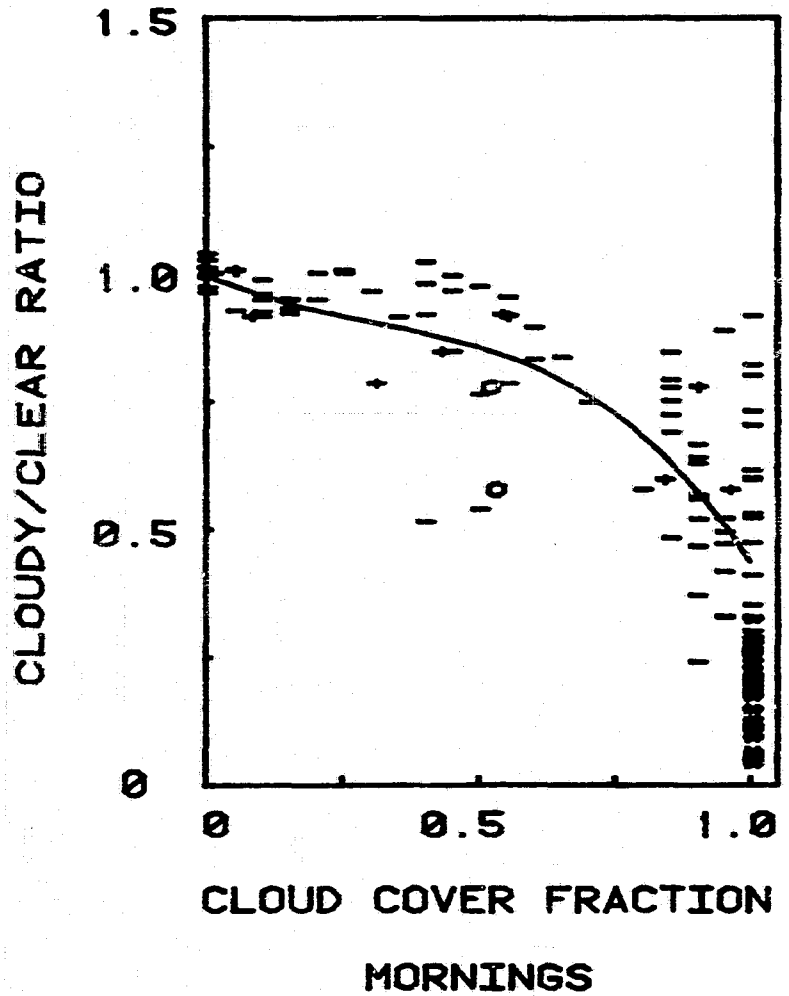

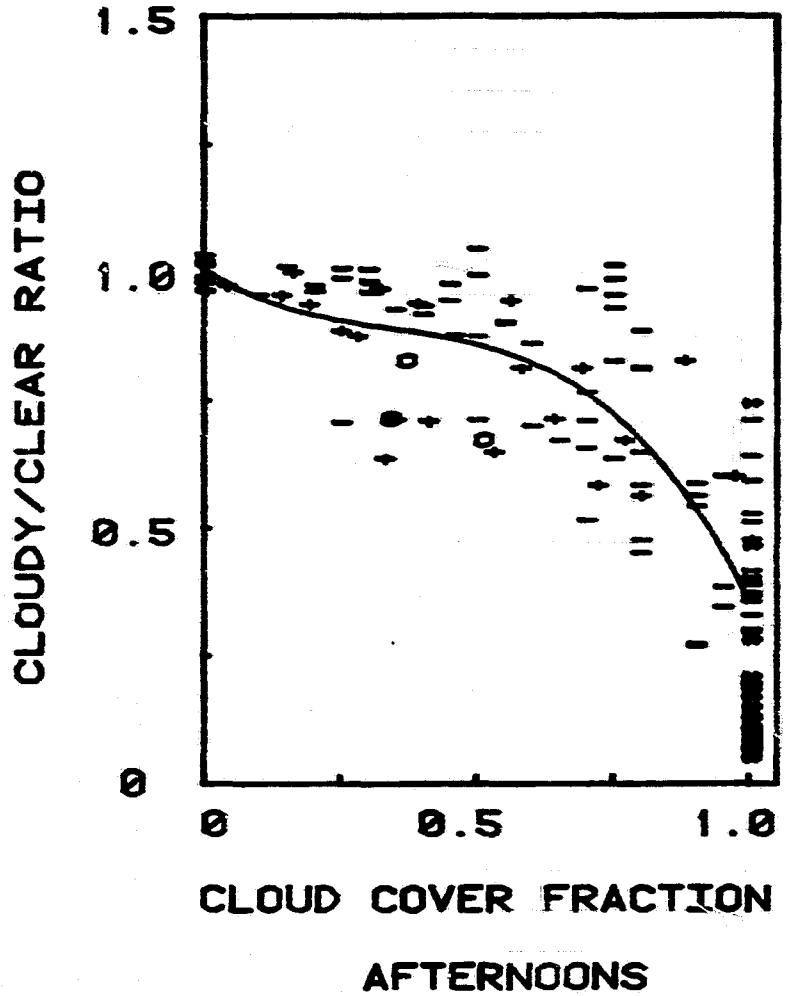

NORM. GLOBAL VS. CLOUD COVER FRACTION
FOR THE MONTH OF FEBRUARY 1982

–	LAFB VISUAL
O	SATELLITE PHOTO
+	WHOLE SKY PHOTO
*	PRECIPITATION

Figure 42

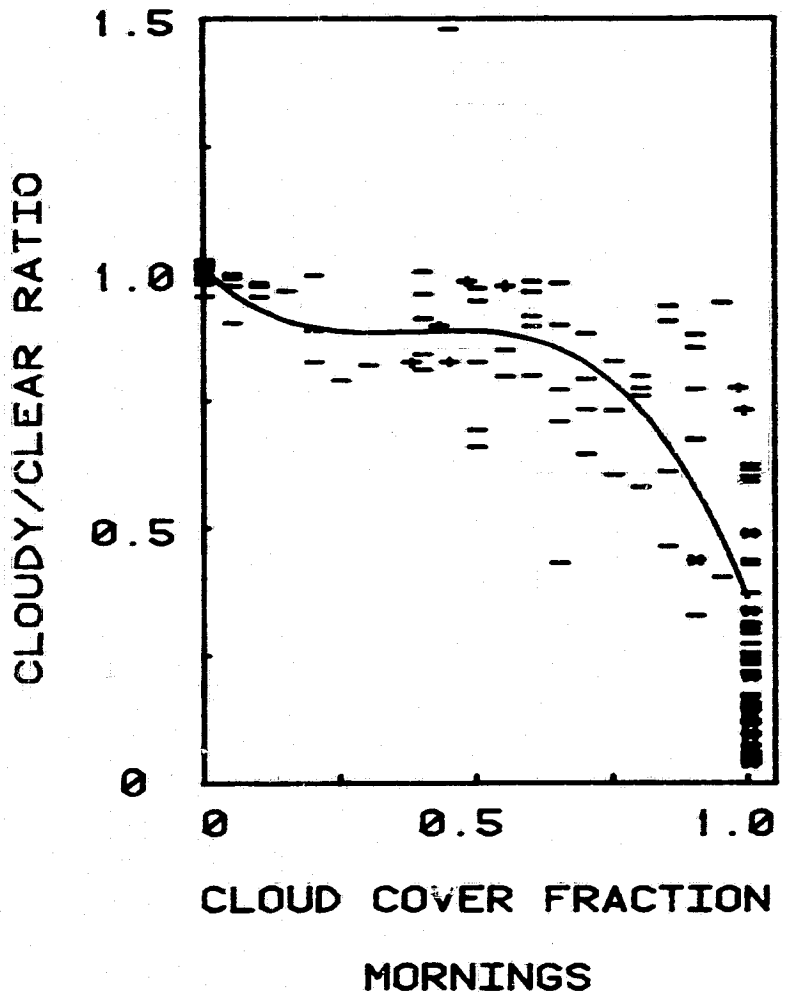

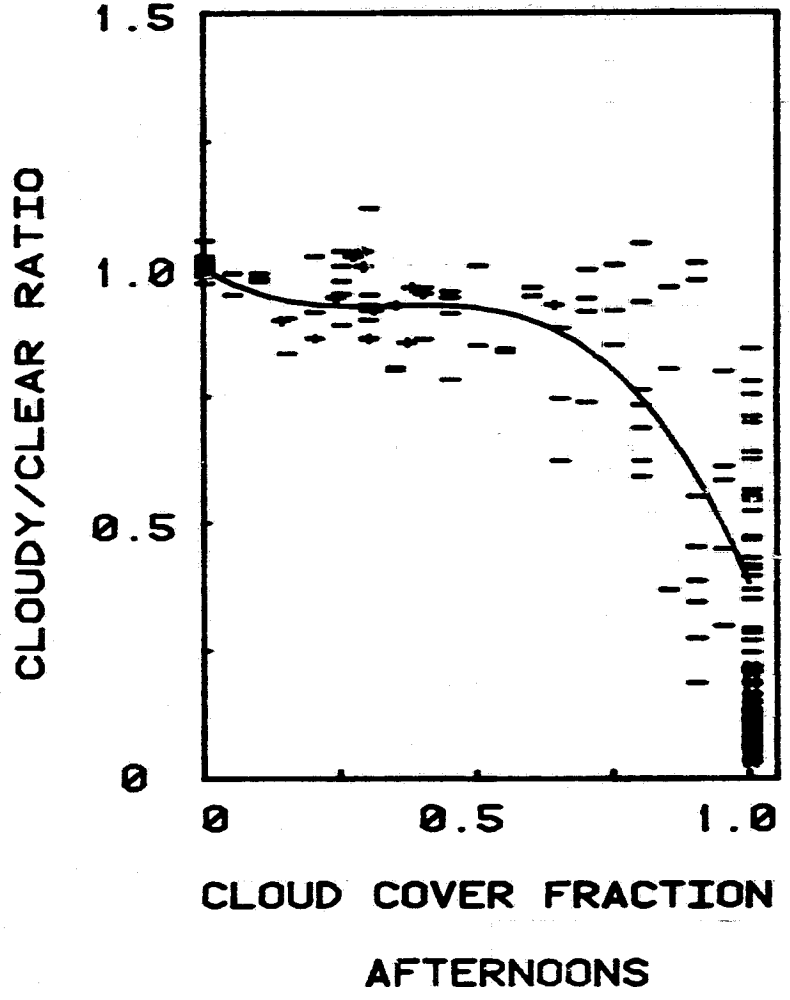

NORM. GLOBAL VS. CLOUD COVER FRACTION
FOR THE MONTH OF MARCH 1982

–	LAFB VISUAL
O	SATELLITE PHOTO
+	WHOLE SKY PHOTO
*	PRECIPITATION

Figure 43

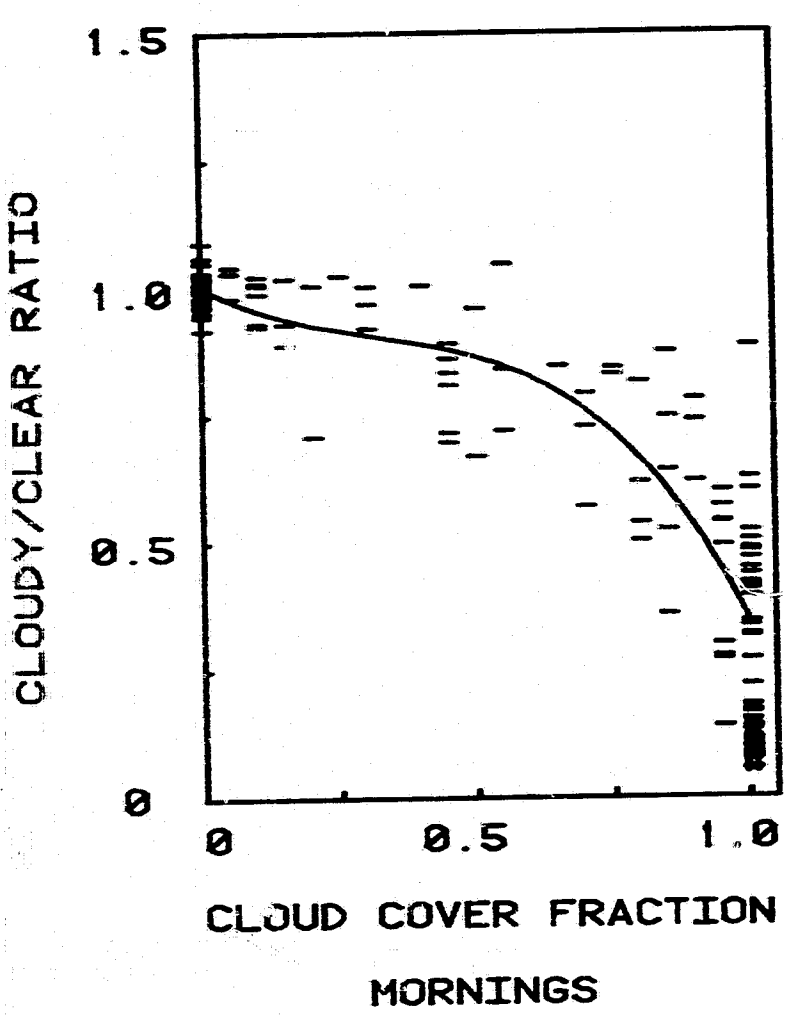

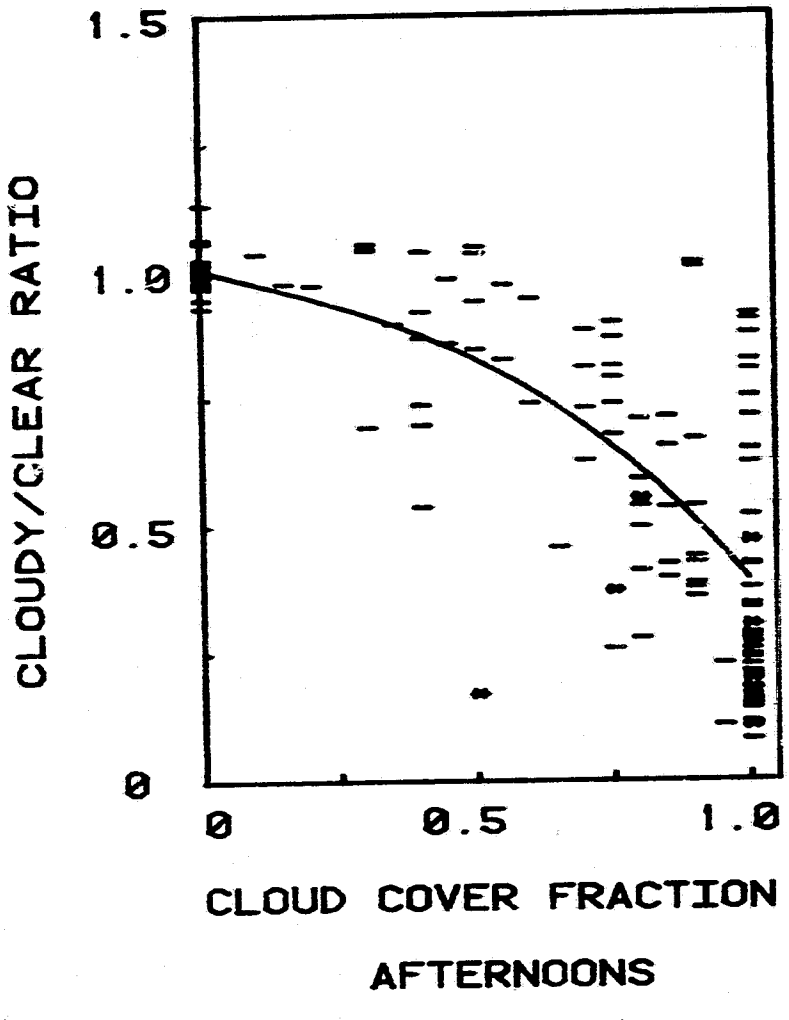

NORM. GLOBAL VS. CLOUD COVER FRACTION
FOR THE MONTH OF APRIL 1982

–	LAFB VISUAL
O	SATELLITE PHOTO
+	WHOLE SKY PHOTO
*	PRECIPITATION

Figure 44

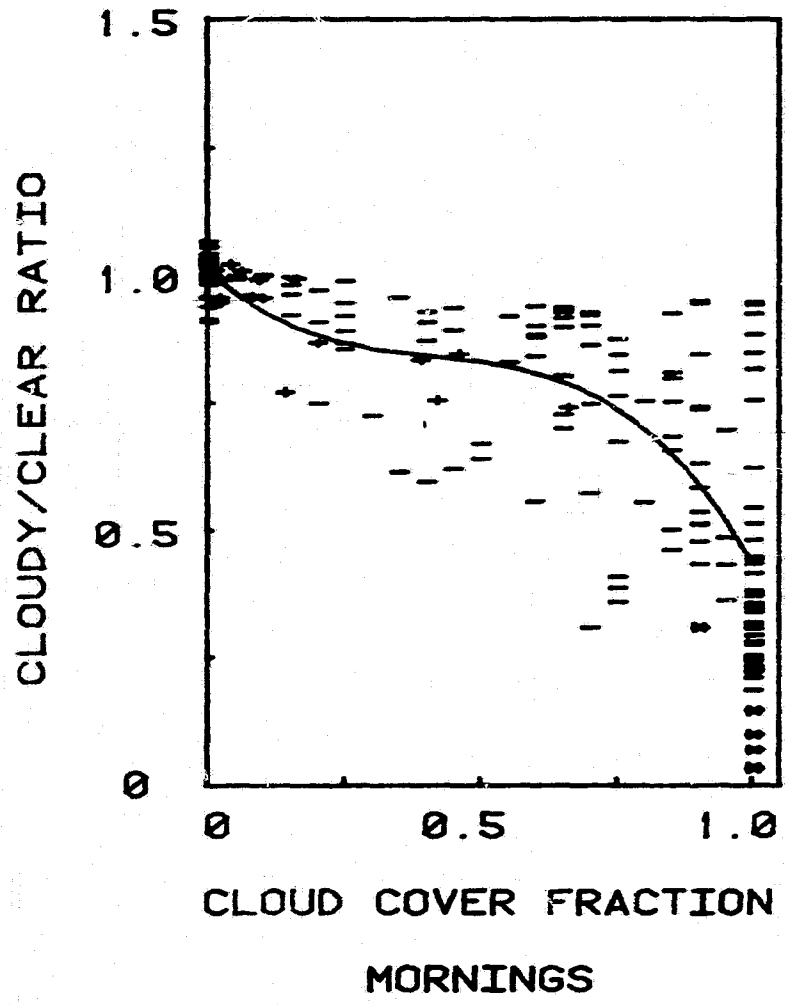

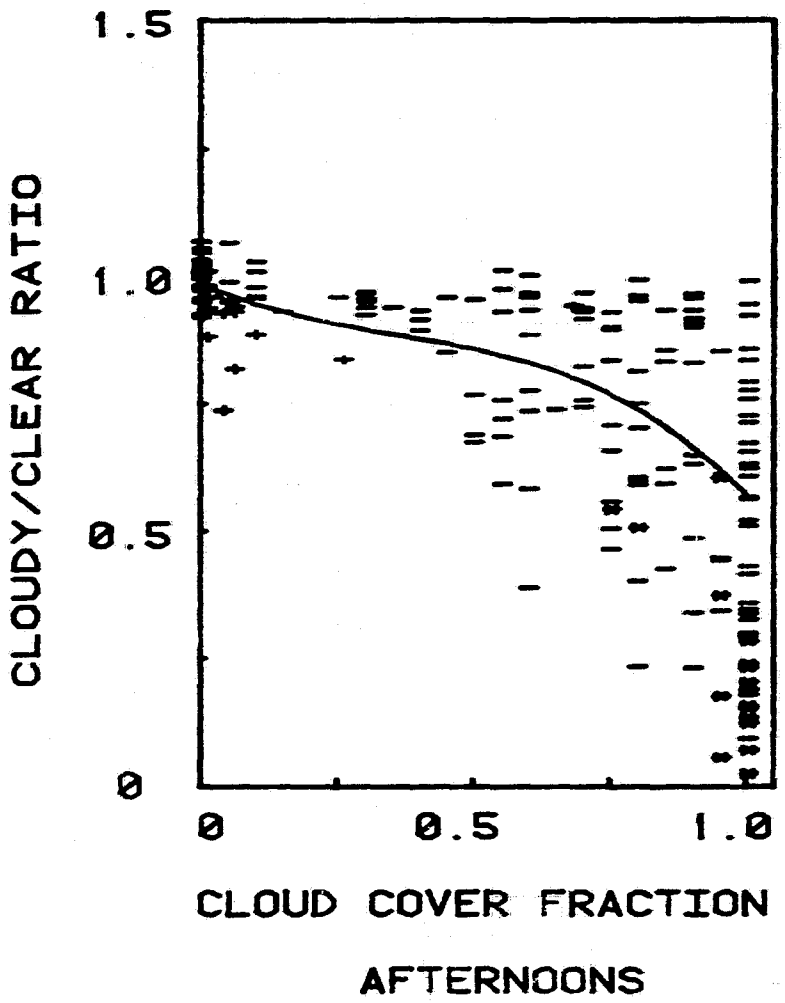

NORM. GLOBAL VS. CLOUD COVER FRACTION
FOR THE MONTH OF MAY 1982

–	LAFB VISUAL
O	SATELLITE PHOTO
+	WHOLE SKY PHOTO
*	PRECIPITATION

Figure 45

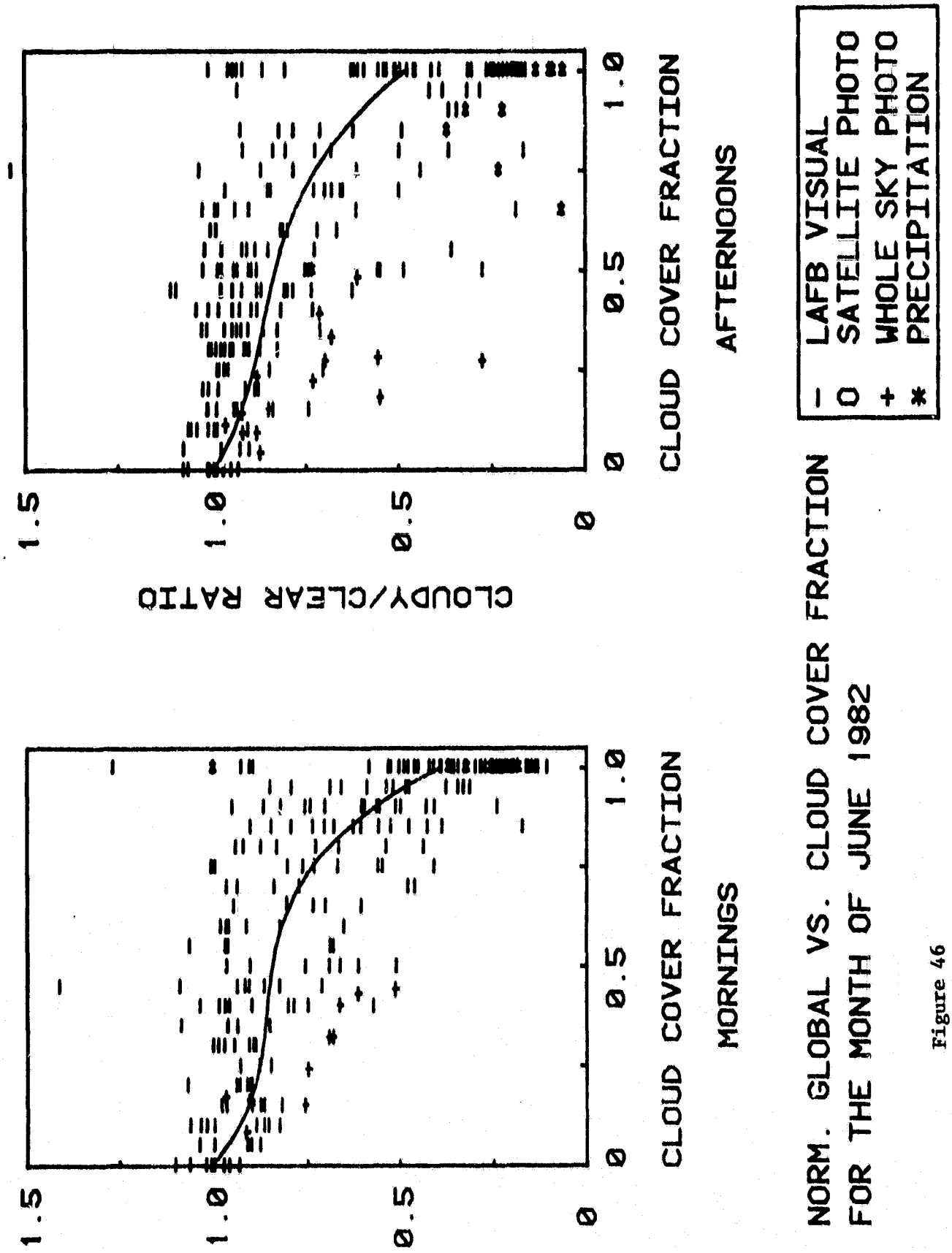

Figure 46

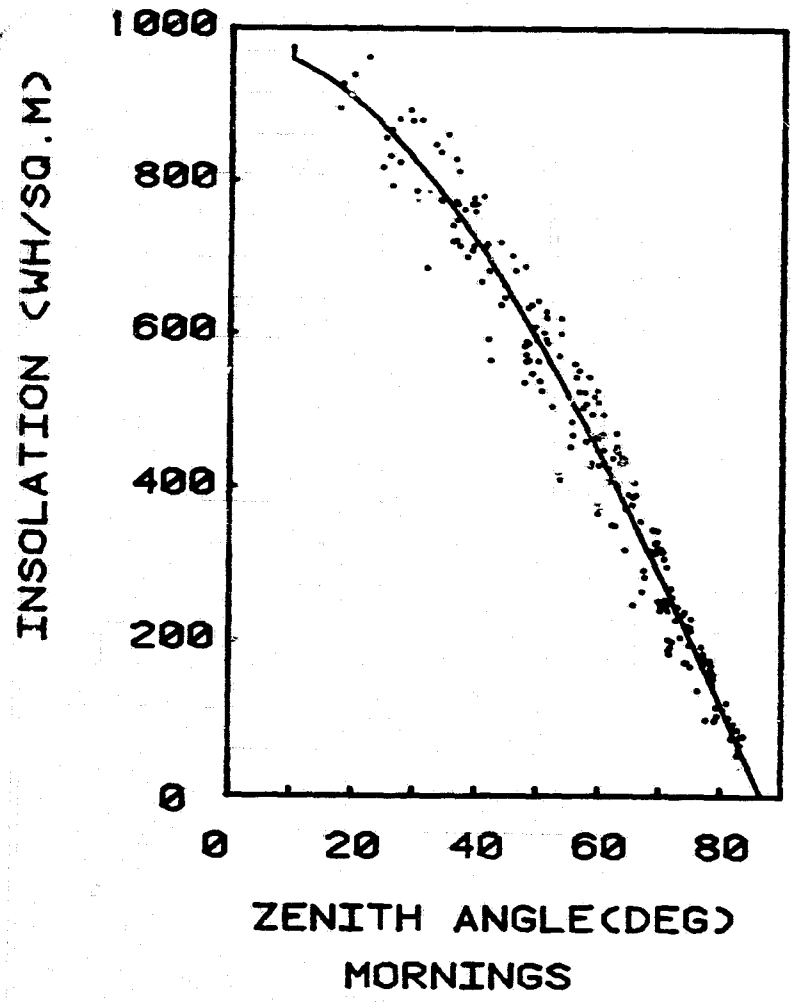

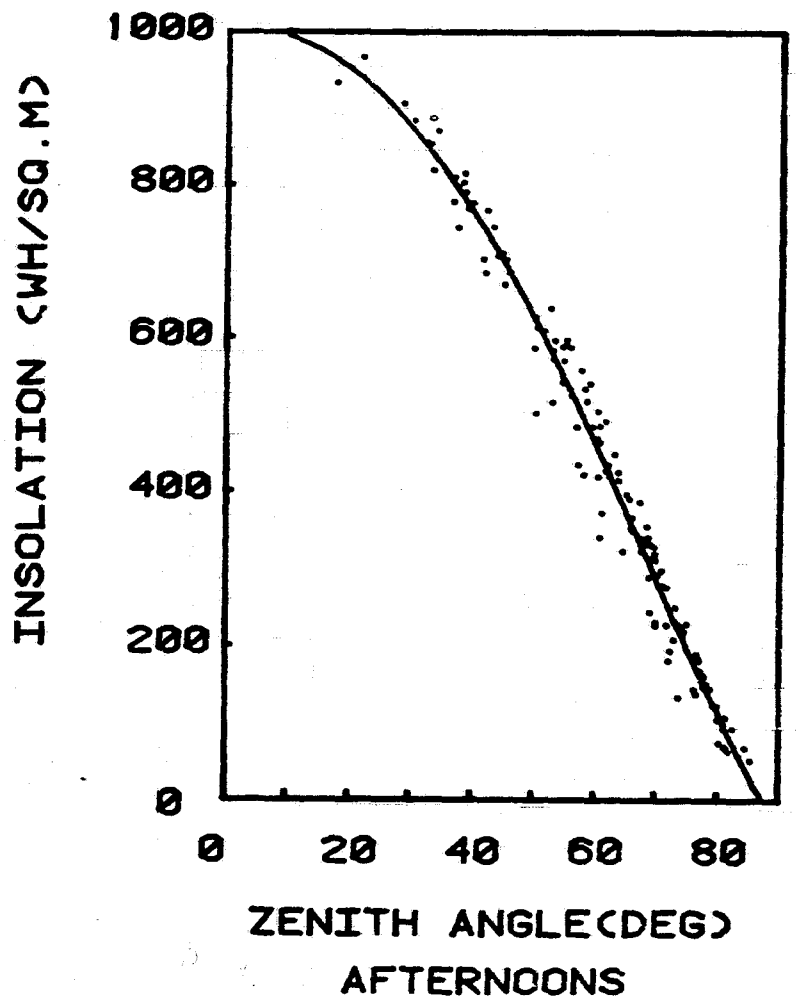

CLEAR SKY GLOBAL VS. ZENITH ANGLE
MARCH 1981 THRU FEBRUARY 1982
CLEAR & NEARLY CLEAR POINTS

Figure 47

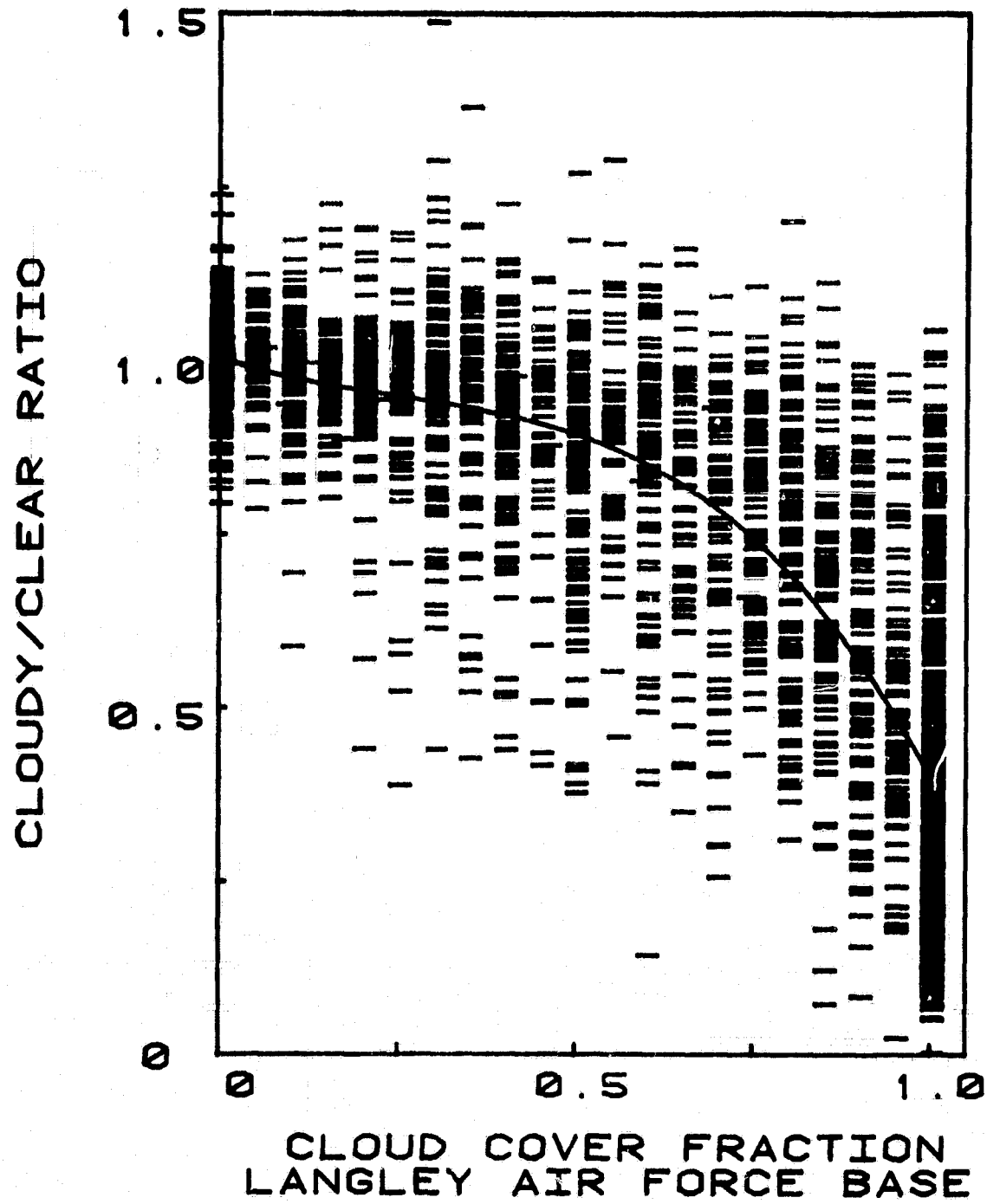

NORM. GLOBAL VS. CLOUD COVER FRACTION

MARCH 1981 THRU FEBRUARY 1982

Figure 48

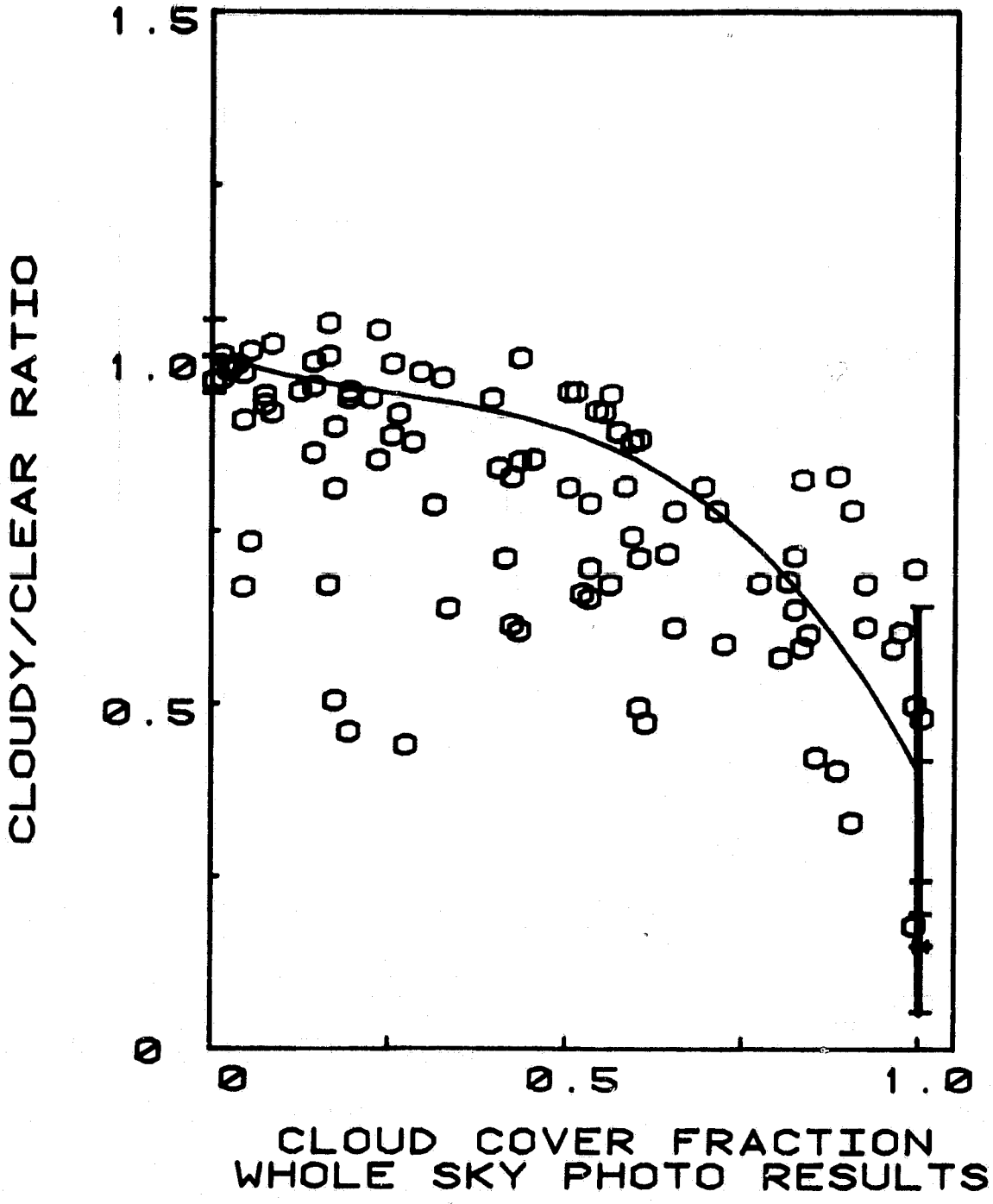

NORM. GLOBAL VS. CLOUD COVER FRACTION

MARCH 1981 THRU FEBRUARY 1982

Figure 49

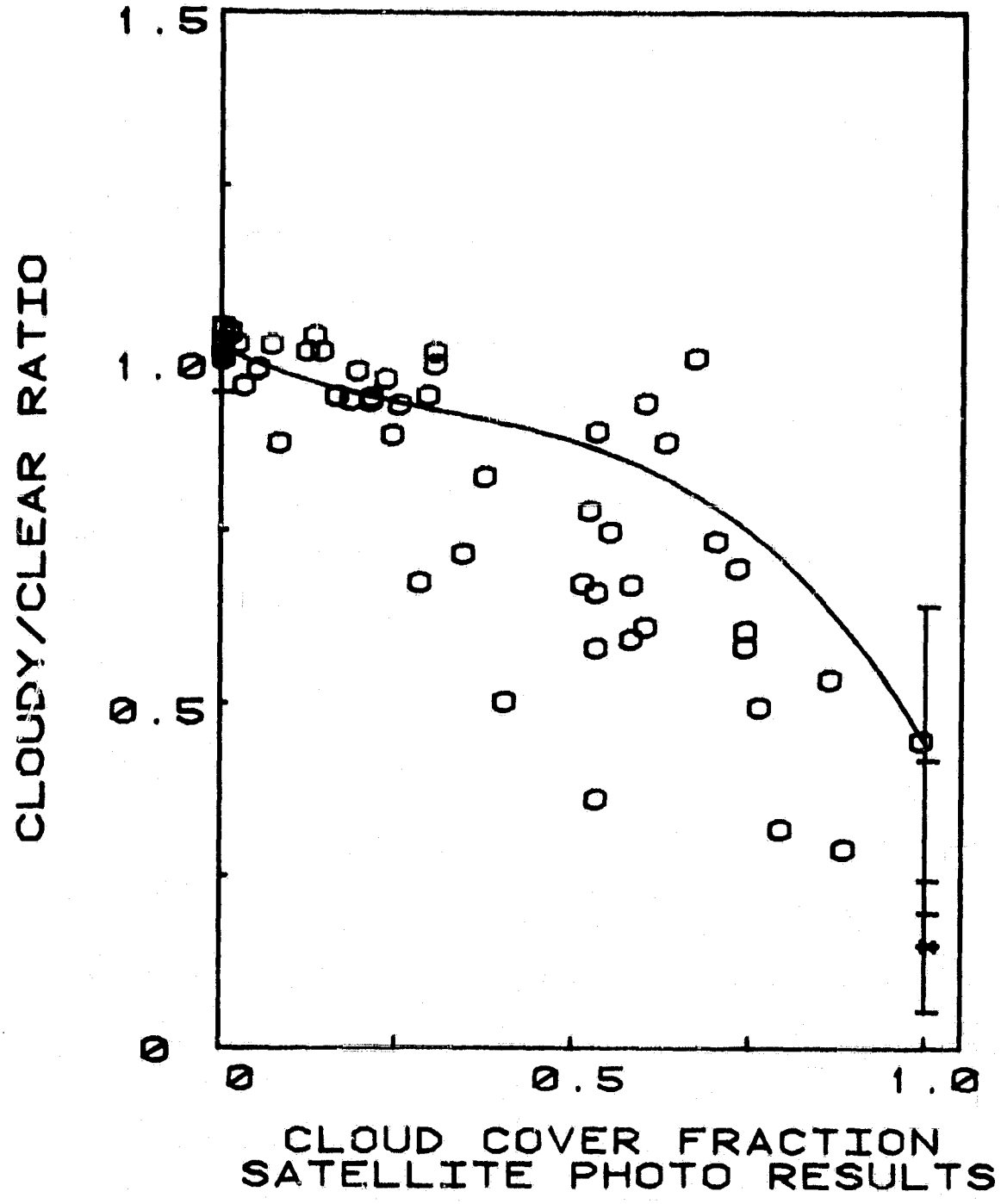

NORM. GLOBAL VS. CLOUD COVER FRACTION

MARCH 1981 THRU FEBRUARY 1982

Figure 50

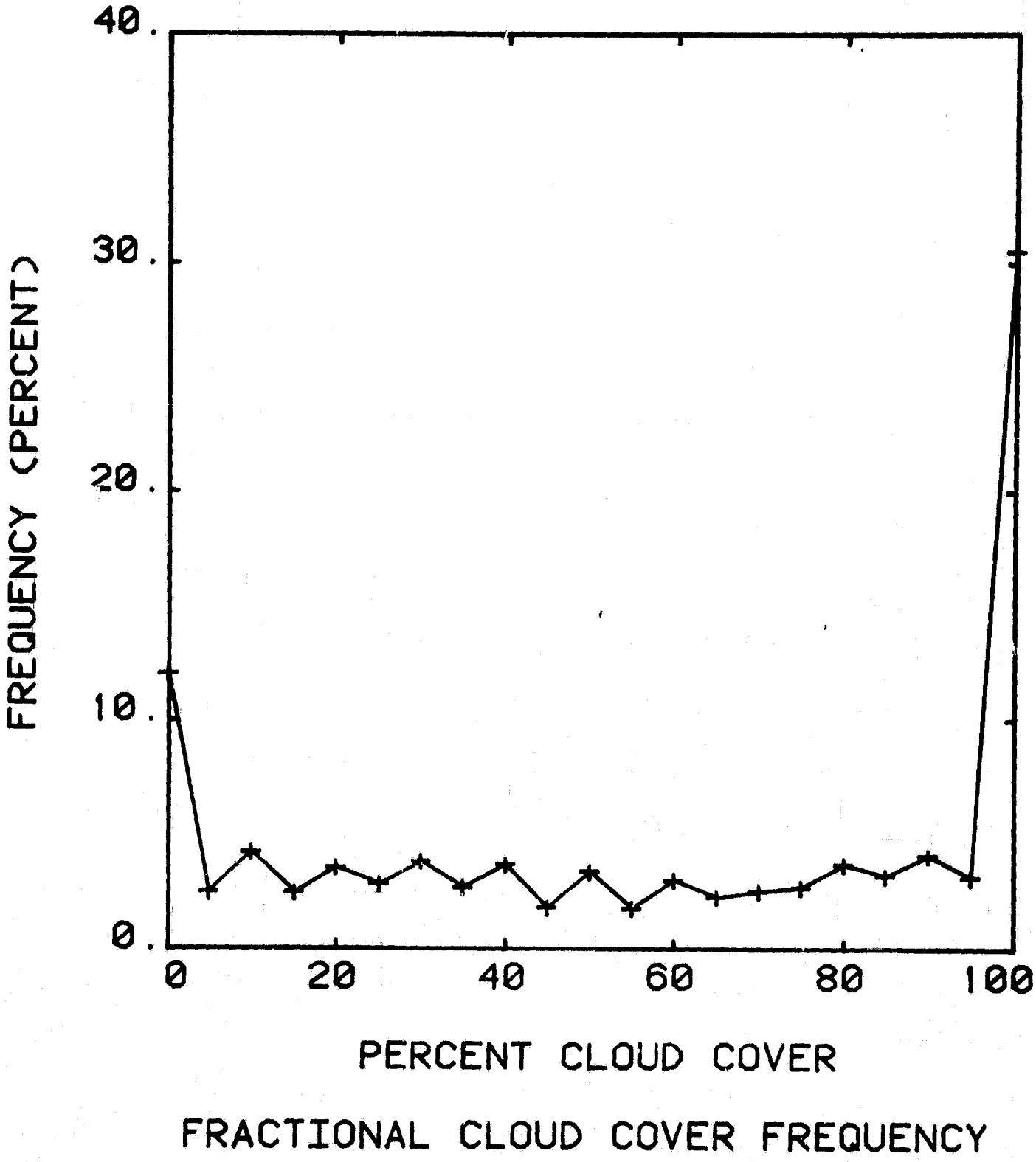

Figure 51

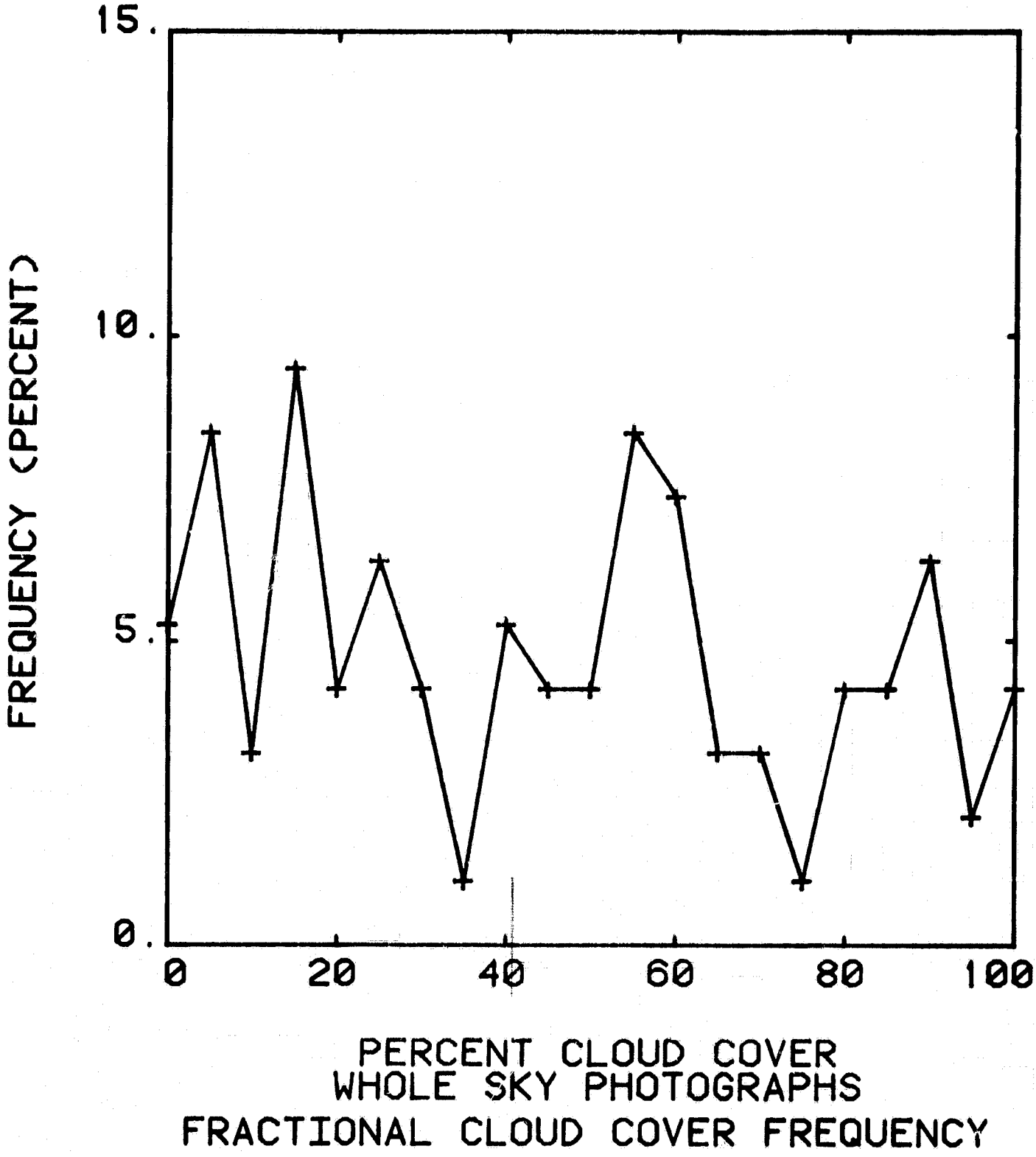

Figure 52

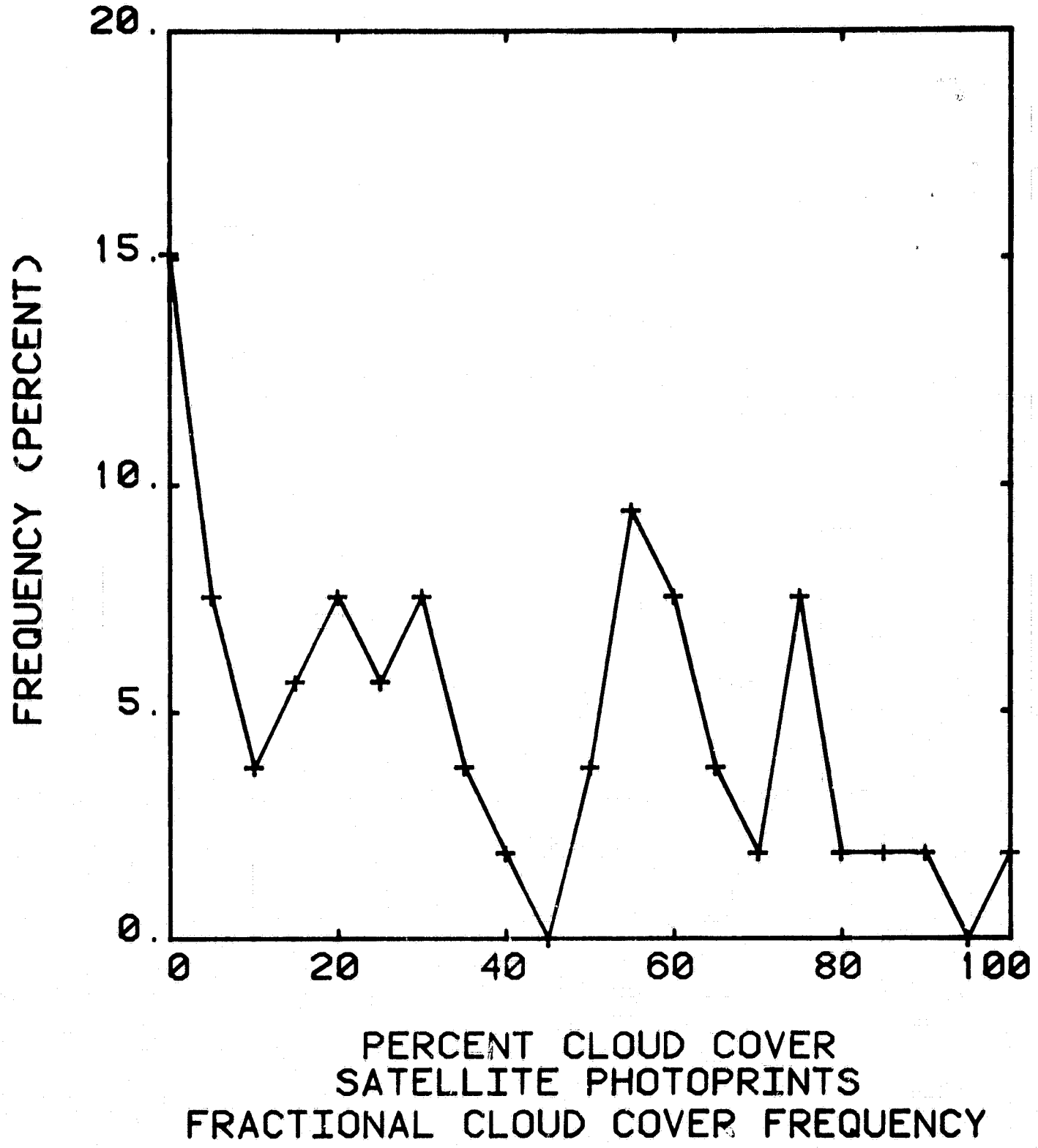

Figure 53

Figure 54 Hampton Institute Study Region and Local Meteorological Data Sources

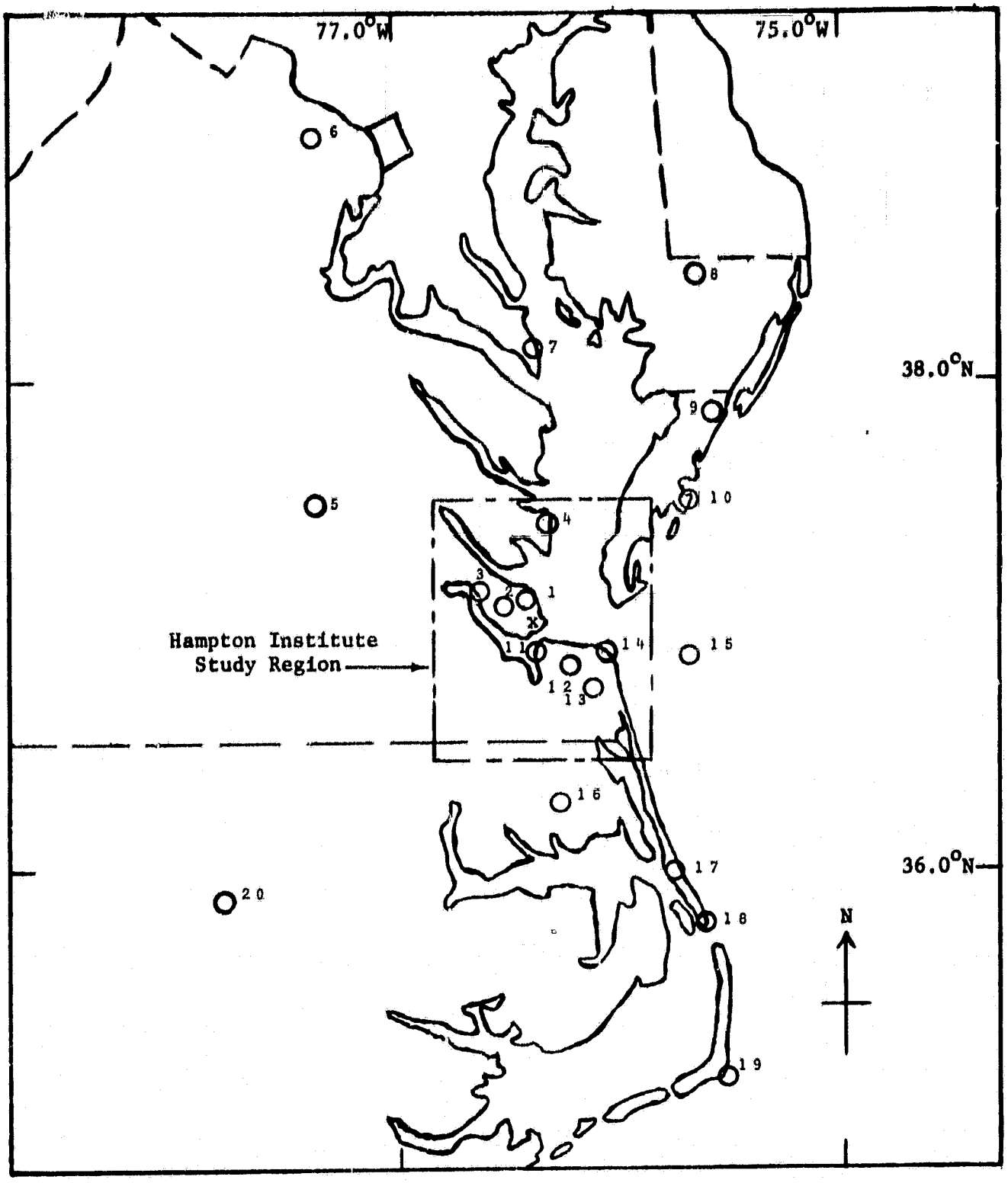

Legend

X- Hampton Institute
1- Langley A.F.B.
2- Newport News, VA
3- Fort Eustis, VA
4- Milford Haven, VA
5- Richmond, VA
6- Sterling, VA
7- Patuxent River,MD
8- Salisbury, MD
9- Wallops Island, VA
10- Paramore Beach, VA
11- Navel Air Norfolk,VA
12- Norfolk, VA
13- Oceana Navel Air, VA
14- Cape Henry, VA
15- Chesapeake Lighthouse
16- Elizabeth City, NC
17- Dare County, NC
18- Oregon Inlet, NC
19- Cape Hatteras, NC
20- Rocky Mount, NC

REFERENCES

Angström, A., 1961, "Techniques of Determining the Turbidity of the Atmosphere," Tellus XIII, 2 pp. 214-222.

Blakey, R. W., and D. D. Venable, 1982, "Computer Automation of a Solar Radiation Laboratory," Paper presented at the 39th Joint Annual Meeting of the National Institute of Science and Beta Kappa Chi Scientific Society, Washington, DC, March 17-20.

Davis, J. M., and S. K. Cox, 1981, "Regional Properties of Angular Reflectance Models," Atmospheric Science Paper No. 338, Colorado State Univ., 219 pp.

Ellis, J. S. and T. H. Vonder Haar, 1978, "Solar Radiation Reaching the Ground from Meteorological Satellite Data," Proceedings of the Third Conference on Atmospheric Radiation, June 28-30, pp. 187-189.

Griffin, T. J., D. A. Whitney, and D. D. Venable, 1982, "Development of a Solar Energy Measurement Laboratory for the Study of Insolation Variations at Hampton, Virginia," Paper presented at Virginia Academy of Science Meeting, Blacksburg, Virginia, April 20-23.

Hänel, G., 1976, "Properties of Atmospheric Particles as Functions of Relative Humidity at Thermodynamic Equilibrium with the Surrounding Air," Advances in Geophysics, 19, pp. 73-188

Kasten, T., 1966, "A New Table and Approximation Formula for the Relative Optical Air Mass," Arch. Meteorl, Geophys. Bioklimatol., B14, pp. 206-223.

Lacis, A. A. and J. E. Hansen, 1974, "A Parameterization for the Absorption of Solar Radiation in the Earth's Atmosphere," J. Atmos. Sci., 31, pp. 118-133.

Marquardt, D. W., 1963, "An Algorithm for Least-Squares Estimation of Nonlinear Parameters," J. Soc. Ind. Appl. Math., 11, pp. 431-441.

Otterman, J., S. Ungar, Y. Kaufman, and M. Podolak, 1980, "Atmospheric Effects on Radiometric Imaging from Satellites Under Low Optical Thickness Conditions," Remote Sensing of the Environment, 9, pp. 115-119.

Volz, F., 1974, "Economical Multispectral Sun Photometer for Measurements of Aerosol Extinction from 0.44 Microns to 1.6 Microns and Precipitable Water," Appl. Optics., 13(8), pp. 1732-1733.

Whitney, D. A., D. D. Venable, and T. J. Griffin, 1981, "Local Effects of Partly-Cloudy Skies on Solar and Emitted Radiation-First Annual Report," NASA Report # CR164694, NASA Acession #N81-30715, 66 pp.

Yamamoto, G., 1962, "Direct Absorption of Solar Radiation by Atmospheric Water Vapor, Carbon Dioxide and Molecular Oxygen," J. Atmos. Sci., 19, pp. 182-188.

APPENDIX I

ENVIRONMENTAL SCIENCES

DEVELOPMENT OF A SOLAR ENERGY MEASUREMENT LABORATORY FOR THE STUDY OF INSOLATION VARIATIONS AT HAMPTON, VIRGINIA. T. J. Griffin*, D. A. Whitney, and D. D. Venable. Dept. of Physics and Engineering Studies, Hampton Institute, Hampton, Virginia 23668.

The purpose of this three-year study is to investigate the cloud dependence of incident solar radiation at Hampton, Virginia. Solar irradiance at the Earth's surface is related to the extraterrestrial solar irradiance, to radiation absorbed and emitted by the atmosphere and clouds, and to radiation reflected by the Earth-atmosphere system. A ground-based measurement station has been established at Hampton Institute to monitor solar radiation, atmospheric emitted radiation, local cloud cover, and atmospheric turbidity. Continuous measurements of global, direct and diffuse solar radiation, and atmospheric infrared radiation are made and stored by computer. NOAA GOES-EAST satellite data are used to obtain albedo and cloud cover information.

Interim analyses performed on the data include monthly averages of global insolation, infrared radiation, and atmospheric turbidity. Global insolation has been correlated with fractional cloud cover from March 1, 1981 through February 1, 1982 using the ARL empirical model.

(Supported by NASA grant No. NAG-1-87)

Thomas J. Griffin

APPENDIX II

BETA KAPPA CHI
NATIONAL INSTITUTE OF SCIENCE
ABSTRACT FORM

COMPUTER AUTOMATION OF A SOLAR RADIATION LABORATORY. R. W. Blakey* and D. D. Venable,
Physics Department, Hampton Institute,
Hampton, VA 23668

A solar radiation measurement laboratory that includes two precision spectra pyranometers, a precision infrared radiometer, a normal incidence pyrheliometer and an all sky camera has been automated to allow direct computer acquisition of insolation data. Signals from the solar instruments are integrated and displayed on five digit light-emitting-diode displays. The integrated signals are transferred via a general purpose interface card to a microcomputer. We have designed, constructed and implemented hardware and software configurations that permit data acquisition, storage, transfer, and display. System reliability tests have been performed and mean time between failure and system down time have been characterized.

Abstracts must be received by FEBRUARY 1. Read instructions before typing abstract.

Indicate below the number and topic category in which your abstract might be programmed:

Category #1 14
Topic Computer Science

Category #2 _____
Topic _____

DO NOT FOLD WHEN MAILING.

Signature Rod. W. Blakey

NIS Status BKX student

Presenting Author R. W. Blakey

Address Physics Department, Hampton Institute

City Hampton State VA Zip23668

Telephone 804/727-5277 or 5788